

CONFIDENTIAL

ORNL
MASTER COPY

ORNL/ANS/INT-5/V19

~~INTERNAL USE ONLY~~

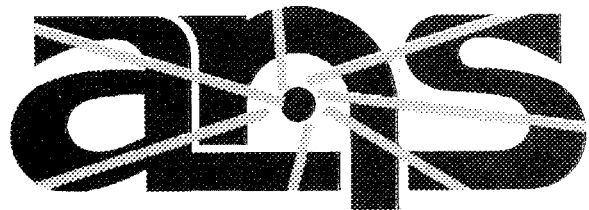
DR. D. HARRIS
11/3/88

ornl

**OAK RIDGE
NATIONAL
LABORATORY**

MARTIN MARIETTA

Monthly Progress Report for October 1989



Advanced Neutron Source

OPERATED BY
MARTIN MARIETTA ENERGY SYSTEMS, INC.
FOR THE UNITED STATES
DEPARTMENT OF ENERGY

CAUTION

This document has not been given final patent clearance and is for internal use only. If this document is to be given public release, it must be cleared through the site Technical Information Office which will see that the proper patent and technical information reviews are completed in accordance with Energy Systems Policy.

MONTHLY PROGRESS REPORT
FOR
OCTOBER 1989

Compilers:

J. A. Johnson
M. R. McBee
D. L. Selby

Contributing Authors:

R. L. Battiste	G. L. Hofman	T. L. Ryan
M. C. Billone	C. R. Hyman	J. M. Ryskamp
J. F. Carew	L. M. Jordan	W. K. Sartory
N. C. J. Chen	R. A. Lillie	H. B. Shapira
G. L. Copeland	C. R. Luttrell	J. L. Snelgrove
J. A. Crabtree	B. H. Montgomery	W. F. Swinson
F. C. Difilippo	H. A. Mook	R. P. Taleyarkhan
R. F. Domagala	W. R. Nelson	H. R. Thresh
C. C. Eberle	L. C. Oakes	C. D. West
R. R. Fullwood	R. E. Pawel	T. C. Wiencek
W. R. Gambill	F. J. Peretz	G. L. Yoder
M. L. Gildner	R. T. Primm, III	G. T. Yahr
R. M. Harrington	C. C. Queen	S. A. Zawadzki
J. B. Hayter	J. Rest	
M. Hayashi	A. E. Ruggles	

November 1989

Prepared by the
OAK RIDGE NATIONAL LABORATORY
Oak Ridge, Tennessee 37831
operated by
MARTIN MARIETTA ENERGY SYSTEMS, INC.
for the
U.S. DEPARTMENT OF ENERGY
under Contract No. DE-AC05-84OR21400

Internal Correspondence

MARTIN MARIETTA ENERGY SYSTEMS, INC.

November 28, 1989

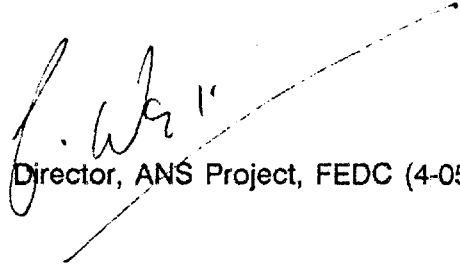
Distribution

Monthly Progress Report for October 1989

The attached monthly reports are unedited, unreviewed, timely reports of work done. In some cases, the work is incomplete or preliminary. In others, problems are identified that will, presumably, be resolved in later reports. I ask you, therefore, to be cautious in using this information; it has not been given patent clearance and is intended as a means of internal communication. If you have any questions or reactions to any of the results reported, you could contact the author directly.

Some items described in our monthly reports may be patentable, which is why I have been asked to remind you of the "warning" paragraph on the cover of this report, and of the sub-contract terms relating to such material.

Your Monthly Progress Report contributions should be submitted to James A. Johnson, FEDC Bldg, MS-8218. However, if you are using the U.S. mail services, please note that our mailing address is Advanced Neutron Source Project, Oak Ridge National Laboratory, FEDC, MS-8218, P. O. Box 2009, Oak Ridge, TN 37831-8218. Your reports are due to James by the 10th of the month, and reports received after that date *will not* be included in the Monthly Progress Report.



Colin D. West, Director, ANS Project, FEDC (4-0558)

:MRM

Attachments

PROJECT HIGHLIGHTS FOR OCTOBER 1989

BUSINESS

A Site and Facility Planning Workshop was held October 18-19 to identify and evaluate various user facility requirements (see Attachment 22). A short course on Research Reactor Design Methods and Some Benchmarks was presented by Herbert Reutler and Alfred Stroemich (Interatom) on October 23-25 to provide project staff with information from other high efficiency research reactor design projects.

TECHNICAL

WBS 1.1.1 - Reactor Core Development

- a) During October more MCNP calculations were performed further characterized the ANS core characteristics (see Attachment 1).
- b) The reactivity effect of voiding has been examined for various conditions (see Attachment 1). It should be noted that a small but positive voiding effect was identified for the gap region between the upper core and the core pressure boundary tube. This effect was confirmed by 1-D transport calculations at ORNL.
- c) An evaluation of the effect of using multiple thermal groups in the neutronics calculations has been performed (see Attachment 2).
- d) Preliminary single-phase heat transfer correlations for decay heat removal analysis have now been proposed (see Attachment 3).
- e) The thermal hydraulic performances of various power distributions produced from different PS2 core fuel gradings have been examined (see Attachment 4). It appears that even with the high peaking factors of our present configuration, we are not too far from conditions which we would consider to be acceptable.
- f) The effect of Xe on several parameters has been examined (see Attachment 5).

WBS 1.1.3 - ANS Corrosion Test Loop

- a) CTEST Nos. 15 and 16 were completed during the month of October (see Attachment 7).
- b) Data are now available on film growths for CTEST Nos. 14, 15, and 16 (see Attachment 7).
- c) A preliminary relationship between oxide growth rate and inlet temperature under certain circumstances has been identified (see Attachment 8).

WBS 1.1.7 - Structural Analysis

- a) A series of analyses was performed to examine the impact that increasing the core central hole size would have on the fuel plate's critical velocity limitation (see Attachment 9).

WBS 1.1.8 - Cold Source Development

- a) New estimates of the liquid fraction for the ANS cold source conditions have been obtained (see Attachment 10).

WBS 1.1.9 - Instrument Development

- a) The ANISN detector shielding calculations have been completed (see Attachment 12).
- b) The seventh issue of TRans is now available (see Attachment 12).

WBS 1.1.11 - Neutron Transport and Shielding

- a) New calculations of neutron and gamma fluxes have been obtained using a highly biased quadrature for various positions in a beam tube (see Attachment 13). It should be noted that these calculations were performed for a radial beam tube configuration looking at the fuel. Therefore, the gamma and fast neutron fluxes are not at all what we expect to see for the no-line-of-sight beam tube geometry.

WBS 1.1.12 - Instrumentation and Controls

- a) Dynamic model calculations have been performed to define expected power overshoots associated with reactivity transients (see Attachment 14).

WBS 1.2.5 - Quality Assurance

- a) The ANS Quality Assurance Plan has been revised to address comments from DOE-ORO and to reflect recent ORNL organization changes (see Attachment 19).
- b) A Key Activity Review of the PS2 Reference Core Development has been initiated (see Attachment 19).

WBS 1.3 - Reactor Systems Development

- a) Two refueling system approaches are being considered (see Attachment 21).

ATTACHMENTS

- 1 INEL Monthly Progress Report, by J. M. Ryskamp, et al.
- 2 Reactor Physics Studies, by R. T. Primm, III
- 3 Heat Removal Monthly Progress Report, by W. R. Gambill
- 4 Steady-State Thermal Hydraulic Code Analysis, by N. C. J. Chen, W. R. Nelson, and G. L. Yoder; Thermal Hydraulic Correlation Selection, by A. E. Ruggles
- 5 Control and Core Developments, by F. C. Difilippo
- 6 Fuel Development and Evaluation, by G. L. Copeland; Management/Experiment Design, by J. L. Snelgrove; Fuel Development and Fabrication, by R. F. Domagala, T. C. Wiencek, and H. R. Thresh; and Analytical Modeling, by J. Rest, G. L. Hofman, M. C. Billone, and S. A. Zawadzki
- 7 Corrosion Test Loop Monthly Progress Report, by R. E. Pawel, et al.
- 8 A Relationship (Under Certain Limited Operating Conditions) Between Oxide Growth Rate and Inlet Temperature, by J. A. Crabtree, B. H. Montgomery, R. E. Pawel, C. D. West, and G. L. Yoder
- 9 Flow Test of a Single Involute Epoxy Plate, by R. L. Battiste, W. F. Swinson, and G. T. Yahr; Studies to Support Conceptual Core Design Committee, by G. T. Yahr and C. R. Luttrell; and Analytical Prediction of Involute Plate Hydraulic Instability, by W. K. Sartory
- 10 Cold Source Thermal-Hydraulic Monthly Progress Report, by T. L. Ryan; and Thermal-Hydraulic Experimental Facilities and Thermal-Hydraulics Modeling, by C. C. Eberle
- 11 Design Calculations for the ANS Cold Source, by R. A. Lillie
- 12 Monthly Progress Report on Neutron Science Tasks, by J. B. Hayter; Detector Shielding, by J. F. Carew; and Neutron Polarizer Development, by H. A. Mook
- 13 Energy and Angular Dependent of Particle Fluxes in a Radial Beam Tube, by M. Hayashi
- 14 Instrumentation and Controls Monthly Progress Report, by L. C. Oakes, et al.
- 15 Safety Activities Monthly Progress Report, by R. M. Harrington
- 16 Transient Thermal Analysis Task Monthly Progress Report, by G. L. Yoder; RELAP5 Model Development and Review, by N. C. J. Chen; and Decay Heat Removal, by N. C. J. Chen and G. L. Yoder
- 17 Probabilistic Risk Assessment for ANS, by R. R. Fullwood

- 18 Severe Accident Analysis Program Report, by R. P. Taleyarkhan and C. R. Hyman
- 19 Quality Assurance Monthly Progress Report, by M. L. Gildner and L. M. Jordan
- 20 Design Activities Monthly Progress Report, by F. J. Peretz
- 21 Reactor Systems Design Monthly Progress Report, by C. C. Queen
- 22 Balance-of-Plant Site and Facility Planning Monthly Progress Report, by H. B. Shapira



Mickie R. McBee, FEDC, MS-8218 (6-5429)

ADVANCED NEUTRON SOURCE
IDAHO NATIONAL ENGINEERING LABORATORY
MONTHLY REPORT FOR OCTOBER 1989

J. M. Ryskamp and E. L. Redmond II
FTS 583-9533 or (208) 526-9533

1.1.01.01.03 MCNP Modeling of the ANS

During October more MCNP calculations were performed to further characterize the ANS. Table I lists some of the runs performed as well as a few of the runs presented in the September monthly. The core multiplication factor and its standard deviation are given for each run. The run number is also listed for future reference.

TABLE 1. MCNP AND PDQ CALCULATIONS PERFORMED IN SEPTEMBER AND OCTOBER 1989

<u>Run</u>	<u>Description</u>	<u>Core Multiplication Factor</u>
DD470	PDQ-7 calculation of graded fuel core model without boron in the fuel end caps.	1.2994
DD478	PDQ-7 calculation of graded fuel core model containing boron in the fuel end caps. Homogenized hafnium was present in the central hole to the core midplane.	1.0301
ANS34	MCNP calculation of graded fuel core model without boron in the fuel end caps. The D_2O $S(\alpha, \beta)$ library used was evaluated at 400 K.	1.2742 ± 0.0032^a
ANS38	MCNP calculation of graded fuel core model containing boron in the fuel end caps. The D_2O $S(\alpha, \beta)$ thermal library used was evaluated at 400 K.	1.1368 ± 0.0040
ANS39	MCNP calculation of graded fuel core model containing boron in the fuel end caps. The D_2O $S(\alpha, \beta)$ thermal library used was evaluated at 300 K.	1.1205 ± 0.0045
ANS43	MCNP calculation of graded fuel core model containing boron in the fuel end caps. There was no $S(\alpha, \beta)$ thermal library used in this calculation.	1.1343 ± 0.0033

TABLE 1. (Continued)

Run	Description	Core Multiplication Factor
ANS53	MCNP calculation of graded fuel core model containing boron in the fuel end caps. There was no $S(\alpha, \beta)$ thermal library used in this calculation. The free gas temperature used was 300 K for all liquid except the D_2O above the fuel elements which was 350 K. The free gas temperature of the fuel and all Al6061 was 350 K.	1.1232 ± 0.0033
ANS50	MCNP calculation of graded fuel core model containing boron in the fuel end caps. All four control rods were inserted to core mid-plane. The D_2O $S(\alpha, \beta)$ thermal library used was evaluated at 300 K.	1.0036 ± 0.0040
ANS45	MCNP calculation of graded fuel core model containing boron in the fuel end caps. The D_2O $S(\alpha, \beta)$ thermal library used was evaluated at 300K. All four control rods are at the fully removed position (100 mm above the top element).	1.1162 ± 0.0040
ANS36	MCNP calculation of graded fuel core model containing boron in the fuel end caps. The D_2O $S(\alpha, \beta)$ thermal library used was evaluated at 300 K. All four control rods were fully inserted in the central hole.	0.9014 ± 0.0032
ANS46	MCNP calculation of graded fuel core model containing boron in the fuel end caps. All eight safety rods were fully inserted. The D_2O $S(\alpha, \beta)$ thermal library used was evaluated at 300 K.	0.8568 ± 0.0030
ANS48	MCNP calculation of graded fuel core model containing boron in the fuel end caps. Four voided beam tubes were modeled. No $S(\alpha, \beta)$ thermal library was used. The temperatures used for the free gas treatment were the same as ANS43.	1.1302 ± 0.0033

^a The statistical uncertainties reported with all MCNP calculations represent one standard deviation.

Thermal Neutron Flux Calculation for Control Rods Inserted

An MCNP model containing control rods inserted to core midplane was run. Incorporated into this model was a reasonably fine segmentation of the D₂O reflector for flux mapping purposes. Figure 1 shows the axial thermal neutron flux profile as calculated by MCNP and PDQ. Both axial profiles shown contain the peak thermal neutron flux as calculated by the respective codes. The MCNP profile presented was calculated between 34.05 cm and 36.55 cm from the core centerline. The PDQ profile occurs at 35.88 cm from the core centerline. Figure 2 shows the radial thermal neutron flux profile as calculated by MCNP and PDQ. Both radial profiles shown contain the peak thermal neutron flux as calculated by the respective codes. The MCNP profile presented was calculated between 14.35 cm and 20.275 cm below the core midplane. The PDQ profile occurs at 15.1 cm below the core midplane.

The MCNP run used for these figures was ANS50 and the corresponding PDQ run was DD478. MCNP and PDQ calculate the same general flux profile indicating that the PDQ flux profile in the reflector is fairly accurate. However, MCNP predicts a flux peak of 7.5% higher than PDQ (7.9061E + 19 versus 7.3527E + 19 n/m²s thermal flux). In reality, this difference is more pronounced since the MCNP fluxes are evaluated from tallies averaged over regions while the PDQ fluxes are evaluated pointwise.

The volume-averaged peak thermal neutron flux calculated by MCNP between 0.0 and 0.625 eV is 7.8945 ± 0.1429 E+19 n/m² s.

PDQ cannot accurately predict the fluxes within the fuel regions. Two comparisons are presented. The first compares PDQ and MCNP flux calculations in the fuel when control rods are parked at core midplane. The second case compares PDQ and MCNP flux calculations in the fuel for the graded fuel core models without boron in the end caps. The total flux is compared as well as the fraction of total flux in each group averaged over each fuel element. Table 2 shows this comparison for the first case: control rods parked at midplane.

TABLE 2. MCNP AND PDQ FLUX COMPARISONS WHEN CONTROL RODS ARE PARKED AT CORE MIDPLANE

	Upper Fuel Element	
	PDQ (DD478)	MCNP (ANS50)
Total Flux (n/(m ² S))	8.7383E+019	8.8319E+019
Fraction of Total Flux		
Group 1	0.1807	0.2196
Group 2	0.3926	0.4033
Group 3	0.3480	0.2951
Group 4	0.0787	0.0820

	Lower Fuel Element	
	PDQ (DD478)	MCNP (ANS50)
Total Flux (n/(m ² S))	1.2024E+020	1.3660E+020
Fraction of Total Flux		
Group 1	0.1720	0.2177
Group 2	0.3901	0.4076
Group 3	0.3782	0.3046
Group 4	0.0597	0.0701

Table 3 shows the comparison for the second case: graded fuel model without boron in the end caps.

TABLE 3. MCNP AND PDQ FLUX COMPARISONS FOR THE GRADED FUEL CORE WITHOUT BORON IN THE END CAPS

	Upper Fuel Element	
	PDQ (DD470)	MCNP (ANS34)
Total Flux (n/(m ² S))	8.6214E+19	8.9523+19
Fraction of Total Flux		
Group 1	0.1739	0.2105
Group 2	0.3713	0.3921
Group 3	0.3564	0.2870
Group 4	0.0984	0.1104

	Lower Fuel Element	
	PDQ (DD470)	MCNP (ANS34)
Total Flux (n/(m ² S))	7.2701E+19	8.1997E+19
Fraction of Total Flux		
Group 1	0.1613	0.2096
Group 2	0.3699	0.3898
Group 3	0.3909	0.3040
Group 4	0.0779	0.0966

As these tables demonstrate, considerable differences exist in the flux representation predicted by PDQ and MCNP. The largest differences consistently occurs in Group 3, where MCNP predicts a lower flux. MCNP also predicts a higher thermal and fast neutron flux. Group 2 fluxes seem to be consistent between PDQ and MCNP. These differences may be large enough to warrant concern for some reactor parameters.

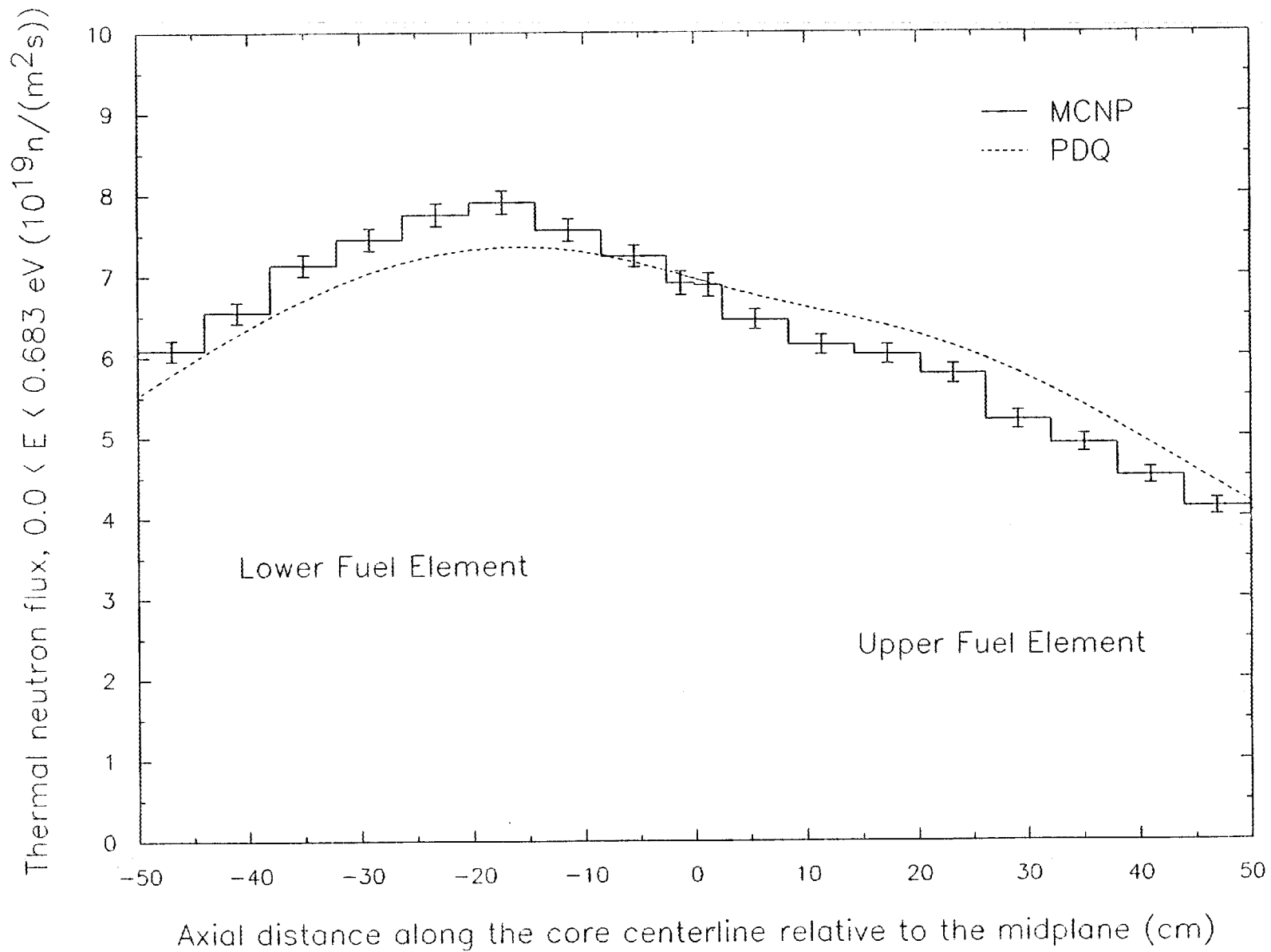


Figure 1. Axial thermal neutron flux profile in the reflector as calculated by MCNP and PDQ.

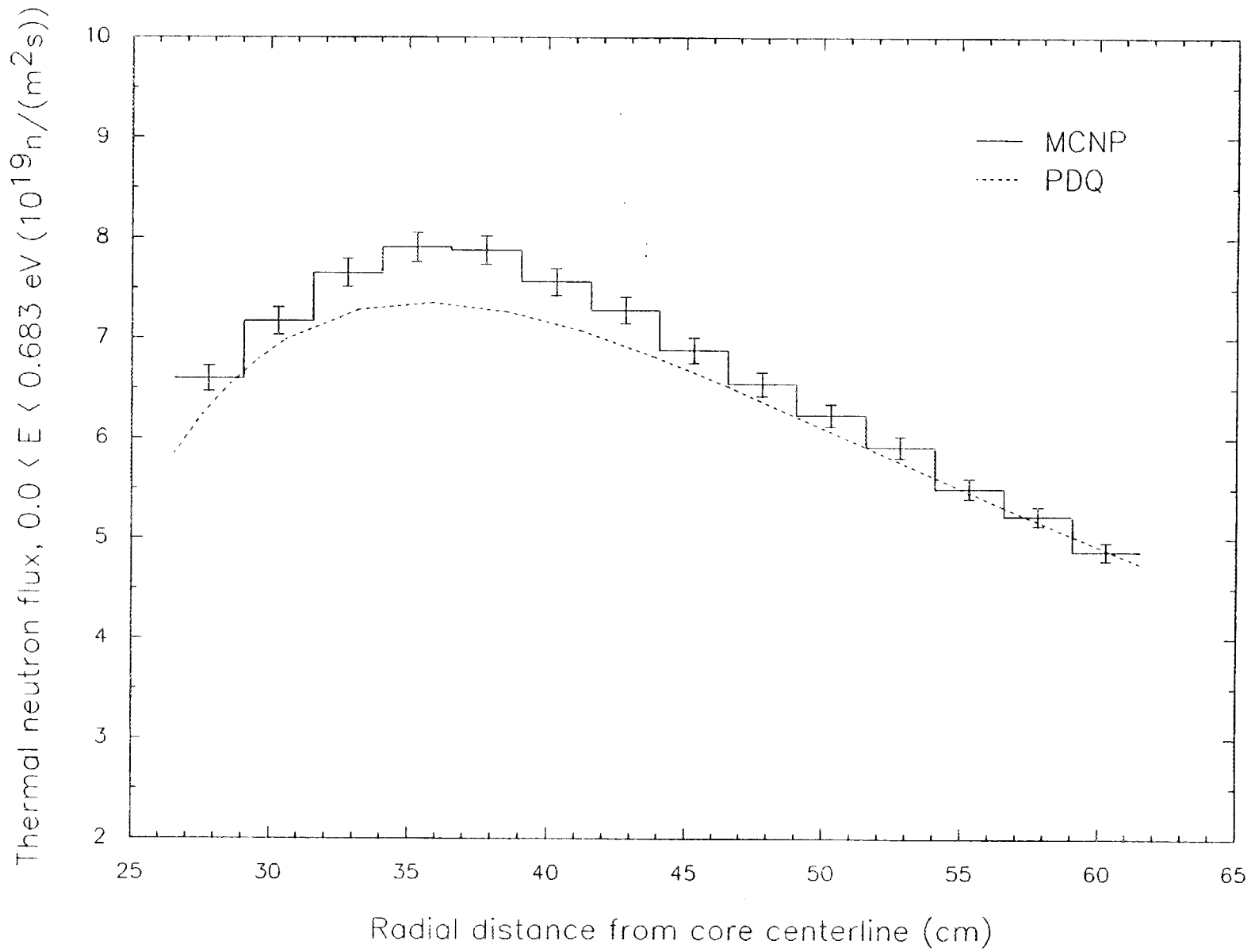


Figure 2. Radial thermal neutron flux profile in the reflector as calculated by MCNP and PDQ.

D₂O S(α, β) Thermal Library Effects

In September comparisons were made between cases utilizing the 300 K, 400 K D₂O S(α, β) library and no S(α, β) library. It was discovered later that the temperature specifications for the free gas treatment were incorrect for the no S(α, β) case. Therefore, that particular run was performed again with the correct temperatures. 300 K was used for all D₂O except in the fuel and coolant outlet channels where it was set at 350 K. A correct comparison for the D₂O S(α, β) library effect is presented in Table 4.

TABLE 4. THERMAL D₂O LIBRARY EFFECTS

<u>Thermal Library</u>	<u>Run Number</u>	<u>Core Multiplication Factor</u>
300 K S(α, β)	ANS39	1.1205 \pm 0.0045
400 K S(α, β)	ANS38	1.1368 \pm 0.0040
No S(α, β)	ANS53	1.1232 \pm 0.0033

The effect on the core multiplication factor is negligible between the 300 K S(α, β) case and no S(α, β) when the temperature representation for the free gas treatment is approximately 300 K.

The flux calculations, however, are severely altered when the S(α, β) is not used. Table 5 shows the thermal neutron flux in reflector regions C and G for the three cases listed in Table 4. The locations of the reflector regions can be found in Figure 1 of the September monthly.

TABLE 5. D₂O S(α, β) THERMAL LIBRARY EFFECTS ON THERMAL NEUTRON FLUX

The energy range for these thermal flux values is 0.0 - 0.625 eV.

<u>Thermal Library</u>	<u>Thermal Neutron Flux</u> 10 ¹⁹ n/(m ² sec)
D ₂ O Reflector Region C	
400 K S(α, β)	5.2864 \pm 0.0492
300 K S(α, β)	5.3062 \pm 0.0493
No S(α, β)	4.6813 \pm 0.0421
D ₂ O Reflector Region G	
400 K S(α, β)	5.1938 \pm 0.0556
300 K S(α, β)	5.1597 \pm 0.0557
No S(α, β)	4.3297 \pm 0.0468

Table 5 shows little difference in the flux when either the 300 or 400 K $S(\alpha,\beta)$ library is used. However, a 12 to 16% difference is seen when the $S(\alpha,\beta)$ library is removed.

As stated in the September monthly, removal of the $S(\alpha,\beta)$ library results in approximately a 15% reduction in run time. The above results indicate that for a core multiplication factor calculation, removing the $S(\alpha,\beta)$ library would be acceptable and would reduce run time. However, for a thermal neutron flux calculation, removal of the $S(\alpha,\beta)$ library would be unacceptable.

1.1.01.04.02 Effects of D₂O Voiding on the Core Reactivity

MCNP and PDQ were used to determine the effects of voiding heavy water regions on the core multiplication factor. Table 6 lists the results of these calculations. Diffusion theory does not give accurate answers when the volume of the voided region is large. However, it can identify the general magnitude and the sign of the reactivity changes, as shown when comparing the first two rows of numbers.

For example, voiding all coolant channels significantly shifts the flux spectrum in the fuel, making it harder. This changes the U-235 cross sections that are used in the MCNP model. However, the PDQ runs used the same U-235 cross sections as the base case with heavy water. If we recomputed the PDQ cross sections, we may get better answers. However, this requires a lot of work. MCNP can automatically account for cross section changes and also treat neutron streaming through voids properly.

The core reactivity drops with voiding except in the coolant bypass annulus. There is a small positive reactivity insertion when voiding the bypass annulus. MCNP could be used to check this value. However, the statistical fluctuation may be larger than the difference between the computed core multiplication factors. ORNL has performed some one-dimensional transport theory calculations that confirm there is a positive reactivity insertion with voiding in the bypass annulus. Voiding the annulus removes the moderator just outside the fuel. This produces a harder flux spectrum passing out through the core pressure boundary tube (CPBT). Thus fewer neutrons are captured in the CPBT and more leak into the reflector where they slow down. The core reactivity increases slightly.

If the coolant bypass annulus was wider, the effect could be worse. However, eventually when it is wide enough, the reactivity would drop with voiding because the CPBT would be worth less. This was confirmed by voiding the wide plenum region below the upper fuel element. When selecting the bypass width, designers must be careful not to make the width too small just because of the voiding problem. With a very small width, there may not be enough heavy water to cool the outer fuel element side plate and CPBT during an accident. This would increase the likelihood of voiding in the bypass annulus, even though the reactivity consequences would be very small. A larger bypass annulus may prevent significant voiding from ever occurring.

Voiding in the central hole is negative, even with control rods inserted to core midplane. Thus, the flux spectrum does not shift enough to significantly reduce the worth of the control rods. This may be partially because the hafnium nuclides in the rods have high epithermal cross sections as well as high thermal cross sections. The rods are very black over a wide neutron energy range.

The values listed in Table 6 lead to void coefficients that are different from those used in the RELAP5 model. New void coefficients will be computed for use in RELAP5. In addition, the MCNP values of control rod worth can be used to modify the current RELAP5 values.

TABLE 6. EFFECTS OF D₂O VOIDING ON THE CORE REACTIVITY

<u>Voided Region</u>	<u>Change in Core Multiplication Factor (Δk)</u>	
	<u>MCNP</u>	<u>PDO</u>
Coolant channels	-0.054	-0.032
Plenum above lower fuel element	-0.024	-0.034
Plenum below upper fuel element		-0.006
50 mm of void above upper fuel element		-0.003
Central hole with control rods at midplane	-0.058	
Central hole without control rods		-0.038
Central hole below midplane with control rods at midplane		-0.037
Coolant bypass annulus		+0.003
10% void in entire reflector tank		-0.021

^aThe statistical uncertainties of the MCNP calculations are typically ± 0.004 for one standard deviation.

1.1.05.01.01 Characterize Central Control Rods

Further studies on the central control rods were performed. The studies contained the four proposed control rods. The first study has no control rods modeled, the second study has the four control rods modeled at the fully removed position, the third study modeled the control rods at the fully inserted position and the fourth study modeled the control rods parked at the core midplane. All of these studies were performed with graded fuel core models containing boron in the end caps. Table 7 presents these results.

TABLE 7. CENTRAL CONTROL ROD CHARACTERIZATION RESULTS

<u>Description</u>	<u>Run Number</u>	<u>Core Multiplication Factor</u>
Base Case - No control rods	ANS39	1.1205 ± 0.0045
Control rods fully removed (100 mm above top element)	ANS45	1.1162 ± 0.0040
Control rods fully inserted	ANS36	0.9014 ± 0.0032
Control rods inserted to core midplane	ANS50	1.0036 ± 0.0040

These results indicate that the current configuration of four control rods in the central hole is adequate to shutdown the reactor. The control rods also have negligible reactivity effect when in the fully removed position. These results also indicate that four control rods inserted to core midplane are sufficient to reach criticality.

A comparison of the change in the core multiplication factor as calculated by PDQ and MCNP for control rods inserted to core midplane indicates that PDQ does a good job of estimating the control rod bank worths even though PDQ cross sections are homogenized over the central hole. Table 8 presents the change in the core multiplication factor as calculated by MCNP and PDQ. The values presented represent the effect of placing control rods inserted to core midplane in a model that did not previously contain control rods.

TABLE 8. THE CHANGE IN CORE MULTIPLICATION FACTOR FOR CONTROL RODS INSERTED TO CORE MIDPLANE

	<u>Change in Core Multiplication Factor</u>
PDQ	-0.1307
MCNP	-0.1169

1.1.05.01.02 Characterize Reflector Shutdown Rods

A study was performed with the eight proposed reflector shutdown rods at the fully inserted position. Table 9 presents the results of this study as compared to a case with no reflector rods present. No control rods were present in either calculation. The graded fuel core model containing boron in the end caps was used for these studies.

TABLE 9. REFLECTOR SHUTDOWN RODS CHARACTERIZATION RESULTS

<u>Description</u>	<u>Run Number</u>	<u>Core Multiplication Factor</u>
No shutdown rods	ANS39	1.1205 ± 0.0045
8 reflector shutdown rods fully inserted	ANS46	0.8568 ± 0.0030

These results demonstrate the reflector shutdown rods capability of safely bringing the ANS to a subcritical state when needed.

1.1.11.02.01 Evaluate Reactivity Worth of Beam Tubes

The September monthly showed a view of the ANS with four beam tubes modeled. During October this case was run to see the beam tubes effect on reactivity. Table 10 compares two studies, one with and one without the beam tubes.

TABLE 10. THE EFFECT ON REACTIVITY DUE TO INSERTING FOUR BEAM TUBES

<u>Description</u>	<u>Run Number</u>	<u>Core Multiplication Factor</u>
No beam tubes	ANS43	1.1343 ± 0.0044
4 beam tubes	ANS48	1.1302 ± 0.0033

These values indicate that the presence of beam tubes does not have a large effect on reactivity. The effect is expected to become more pronounced when all proposed beam tubes are modeled. The total effect, however, is not expected to be much more than one percent on the core multiplication factor.

It should be noted that it is possible to easily model elliptical cylinders in MCNP. If the beam tubes are going to be more elliptical than circular, it may be worth while to correctly model them. Currently the beam tubes are modeled as circular cylinders.

ATTACHMENT 2

Reactor Physics Studies R. T. Primm, III

Multithermal group calculations

Several internal and external reviews of past ANS reactor physics calculations have concluded that there was a need to perform computer studies with cross-section libraries having more than one energy group in the thermal range. To keep the cost as low as possible, the number of thermal groups should be minimized. A study has been performed to determine the minimal number of energy groups which will give acceptable accuracy. A new few group library was then generated. Finally, calculations for the Intermediate Reference Core (IRC) - Ver. 2 (documented in ANS Monthly Report for June, 1989) were performed with the new few group library and the results were compared to the four group calculations reported in the June monthly.

Using the fuel distribution for the IRC, one dimensional discrete ordinates models were prepared for the axial centerlines of both the upper and lower elements. These models were then executed with 39 group cross-sections prepared from the ANSL libraries. Normalized fission rates (power densities) at three locations in the outer element are shown in Fig. 1. Normalized fission rates for the inner element are shown in Fig. 2.

Because of the fine resolution in the thermal range - 20 groups below 0.625 eV - the data from these calculations were defined to be the correct power distributions. The goal was then to find a library with fewer energy groups which produced radial power distributions comparable to those shown in Figs. 1 and 2.

Fig. 1 Fission rate for outer element of Intermediate Reference Core (Case E3)

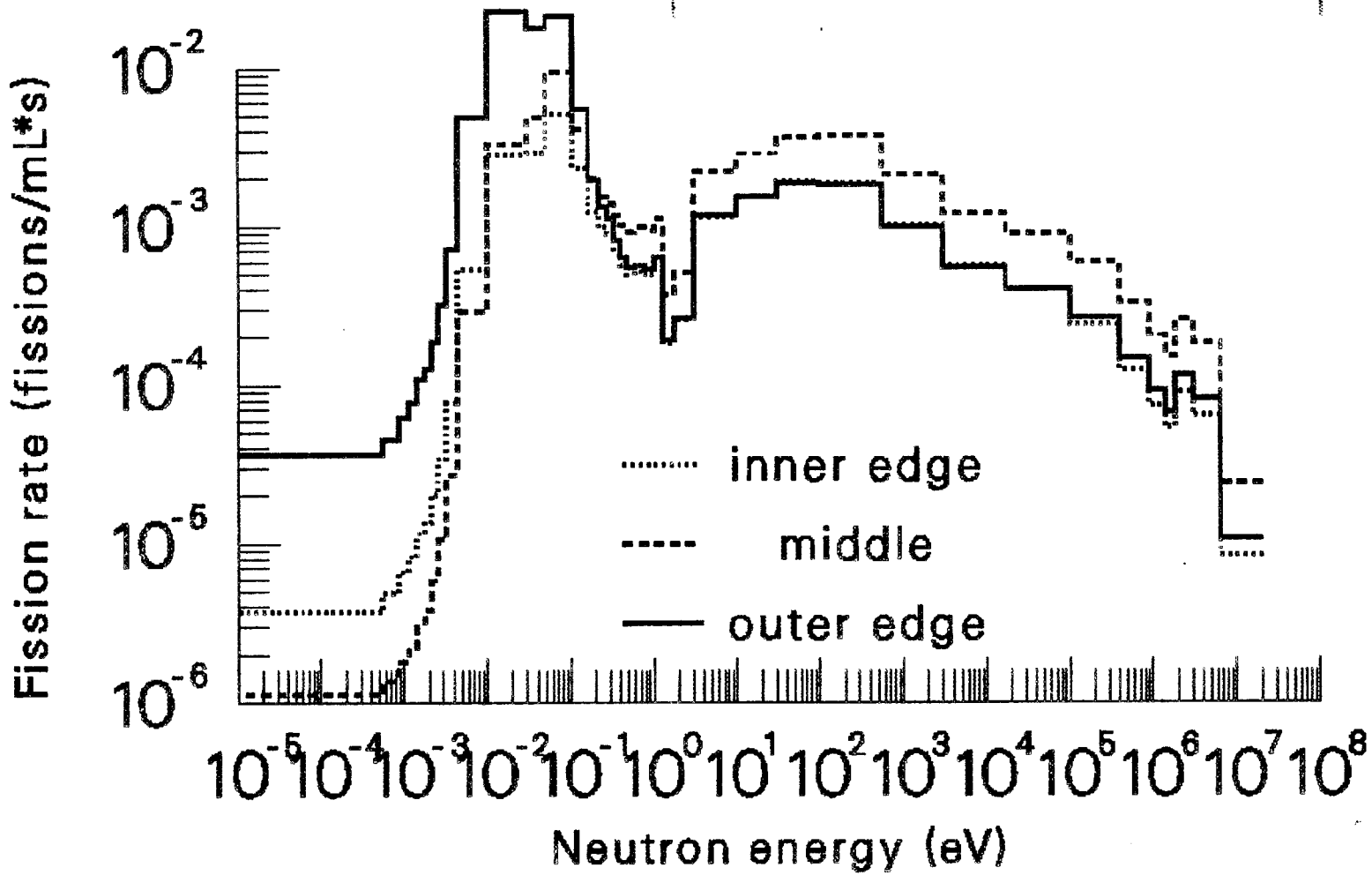
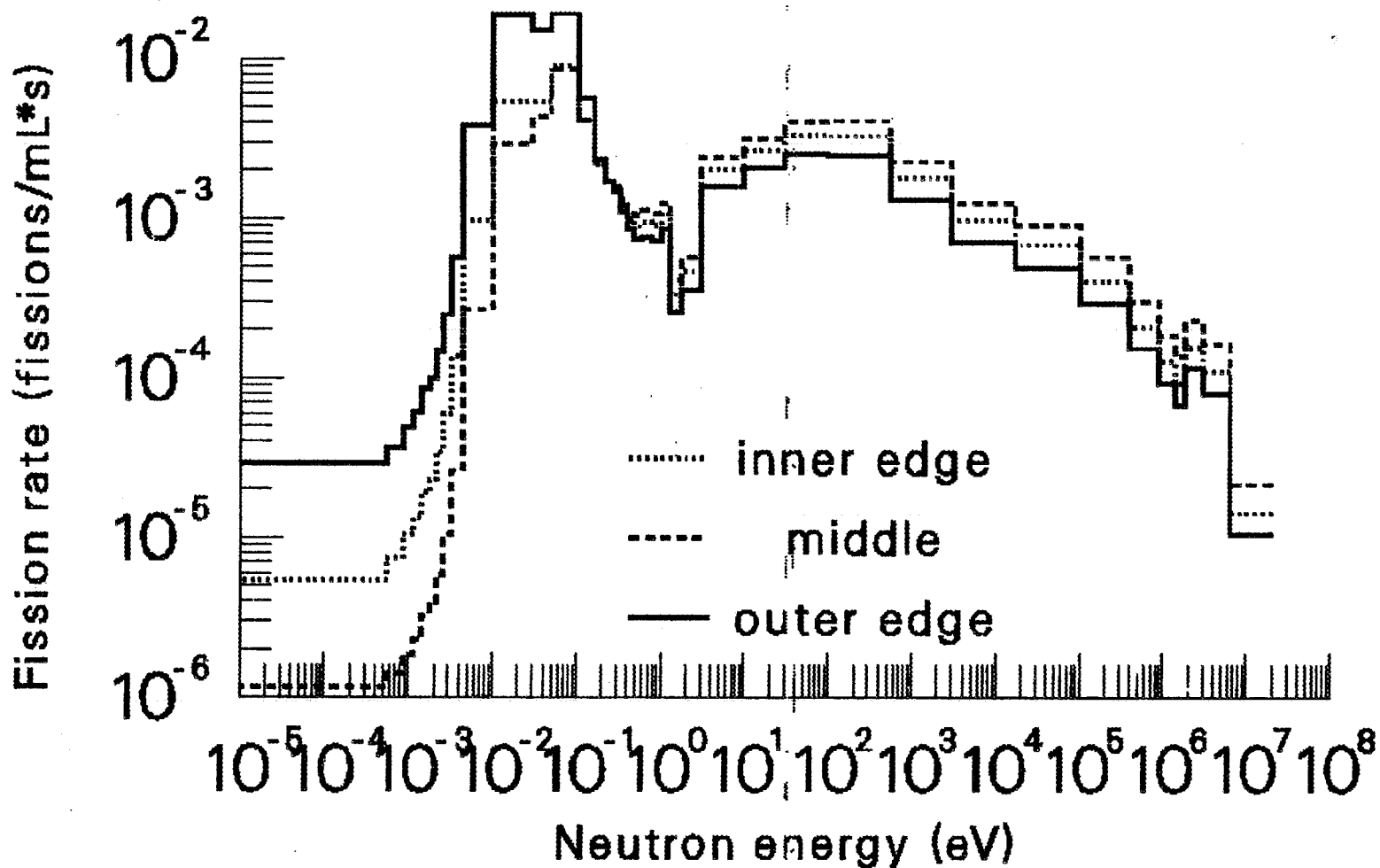


Fig. 2 Fission rate for inner element of Intermediate Reference Core (Case E3)



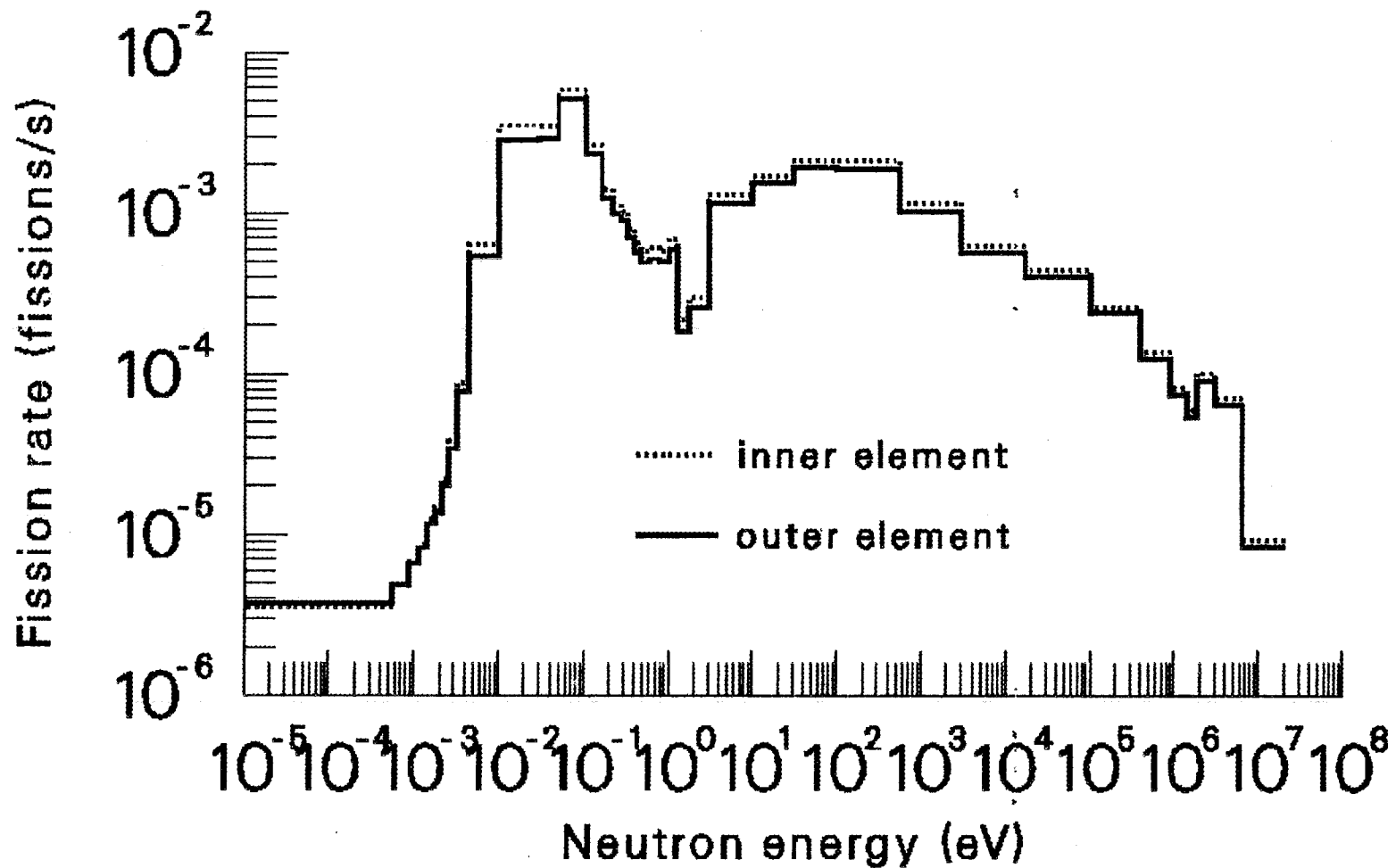
In this study, the power distribution from the few group calculation was required to be within 5% of the value from the 39 group calculation for all spatial zones.

Both Figs. 1 and 2 show that there are two peaks in the power density distribution over the range of neutron energies calculated. The largest peak occurs around 0.06 eV and a broader, but lower peak exists around 100 eV. The higher degree of neutron thermalization at the core boundary relative to the middle of the element is apparent in both Figs. 1 and 2. It is this shift in spectra as one traverses the element which necessitates the use of either a multithermal group library or a single thermal group library with multiple spatially-dependent cross-section sets for the principal nuclides.

A somewhat unexpected result is shown in Fig. 3. The upper element of the IRC has control rods along its inner edge. The lower element does not. However, when one corrects for differences in the volumes of the two elements, both the magnitude and spectral distribution of the power densities along the inner edges of the two elements are the same. Apparently, the reduction in moderation in the lower element due to the smaller central hole (relative to the upper element) exactly mimics the spectral effect due to absorption by the control rod of those neutrons thermalized in the central hole of the upper element.

Since there is little, if any, spectral shift among the fast energy groups, there is no motivation for increasing the number of groups beyond those specified as needed by project management.

Fig. 3 Fission rate for inner edges of Intermediate Reference Core (Case E3) elements



Consequently, the search for a multithermal group library was initiated by generating a four group library with a single set of cross-sections for each nuclide. This library was used with the one-dimensional outer element model, mentioned previously, to calculate spatially dependent fission rates. These data were then compared to the results from the 39 group calculation and the percentage differences are shown in Fig. 4.

The four group calculation overpredicts the power density in the center of the element and underpredicts it at the element outer edge. Fig. 4 is an apt justification for generating multiple spatial sets if one intends to use a four group cross-section library.

The number of thermal groups in the few group library was increased until the few group and 39 group calculations were in agreement (see Fig. 5). For the outer element, agreement was obtained with six groups (three thermal). However, the six group library did not quite meet the 5% agreement criterion for the inner element. Seven groups were needed to insure agreement for both elements. The locations of the group boundaries are shown in Fig. 6.

The final step in this study was to recalculate the IRC with the newly prepared seven group library. Due to the significantly higher cost of performing seven group calculations, only a beginning-of-life calculation was performed. The results of the two calculations are shown in Table 1.

The higher value of k-effective likely reflects the use of updated cross-section preparation models. The flux magnitudes, locations of peaks, and efficiencies are in excellent agreement. The shape of the 80%-of-peak region in the reflector is slightly different - the upper axial (at peak) 80% max locations are different - but the flux volume is essentially the same.

Fig.4 Comparison of power densities from 4 - group calculation to 39 - group power densities $(4 \text{ gp} - 39 \text{ gp})/39 \text{ gp}$

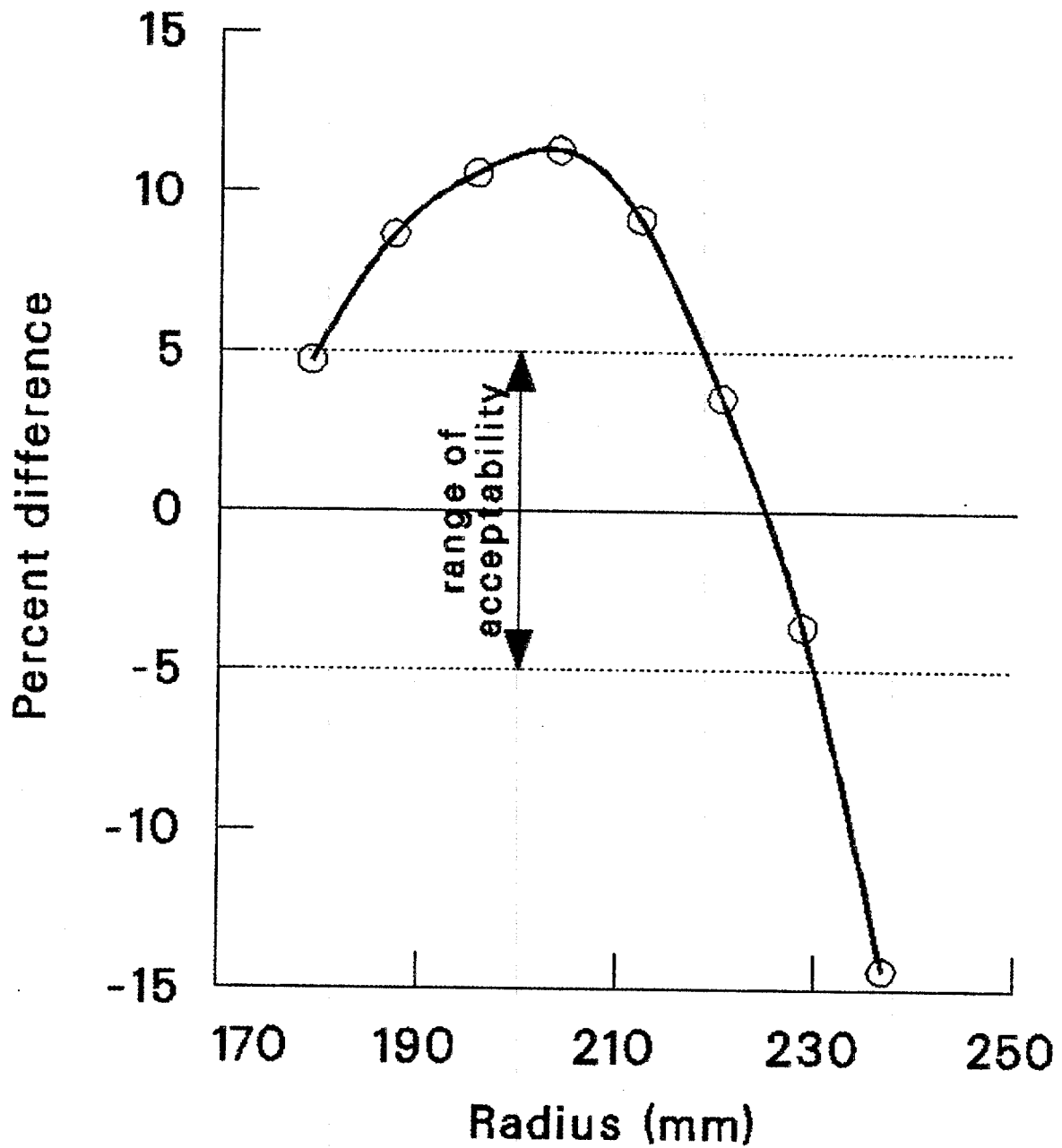


Fig.5 Comparison of power densities from few - group calculations to 39 - group power densities (few gp - 39 gp)/39 gp

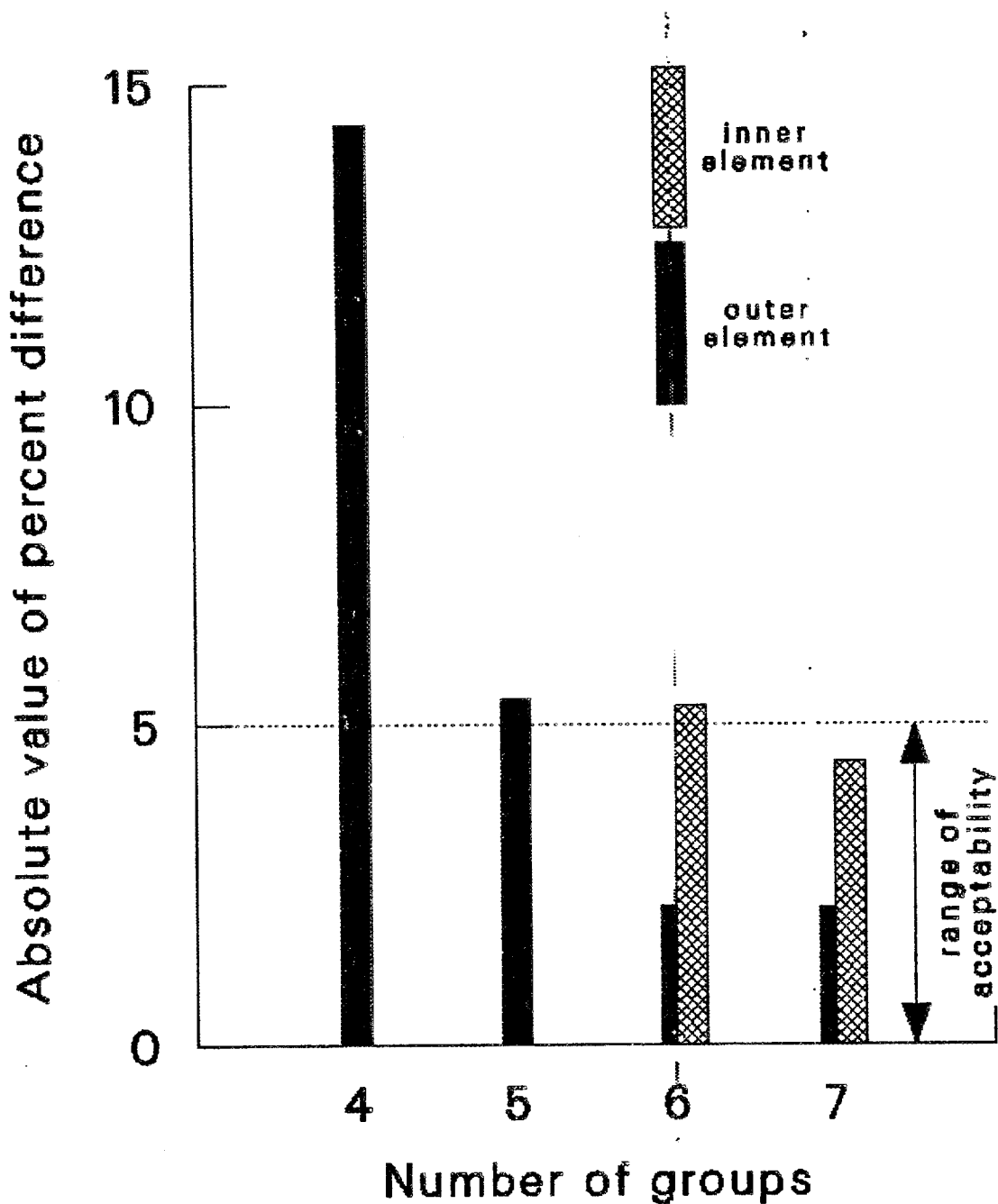


Fig.6 Fission rate for middle (dashed) and outer edge (solid) of outer element of Intermediate Reference Core (Case E3) showing 7 - group energy boundaries

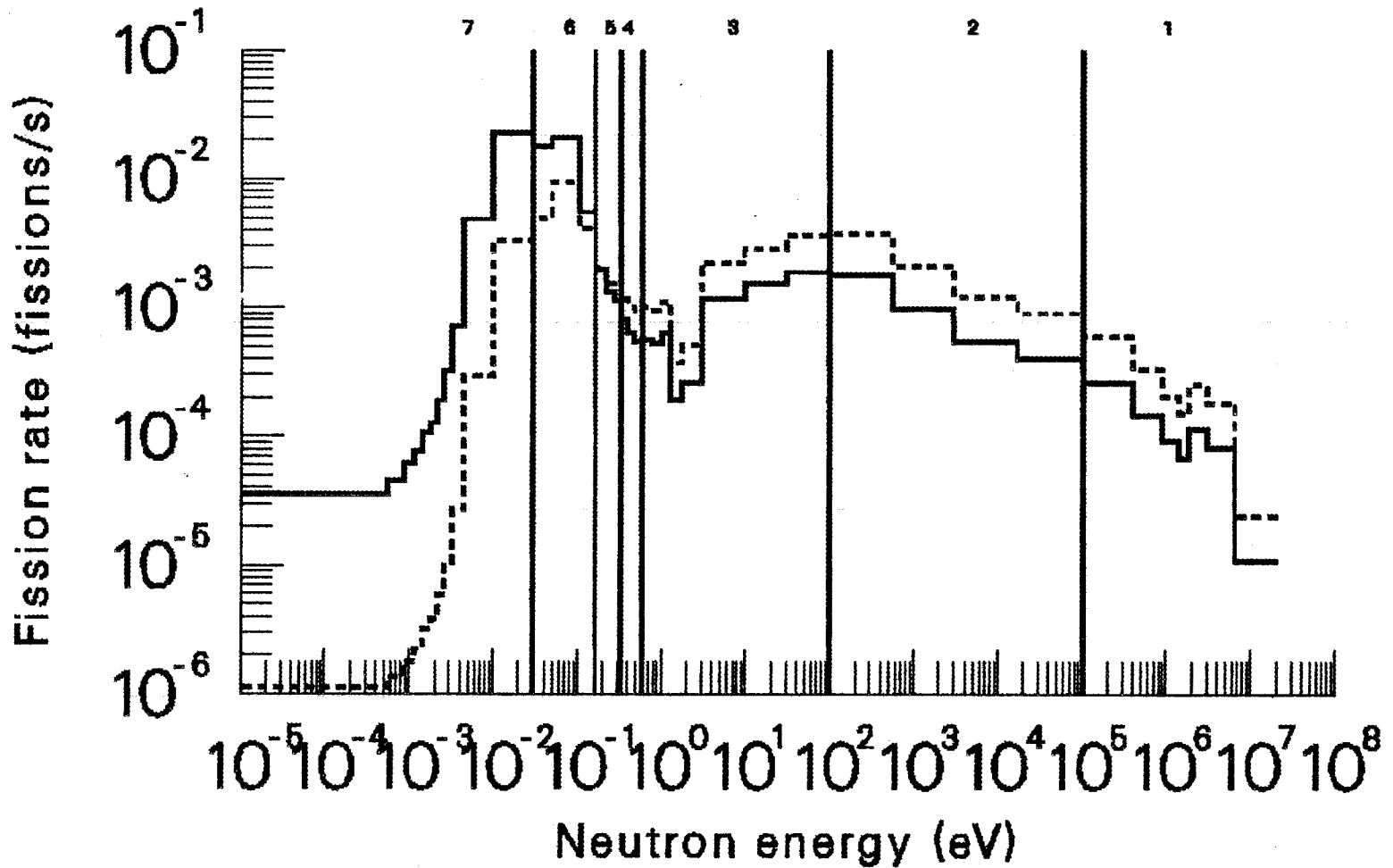


TABLE 1
 INTERMEDIATE REFERENCE CORE VER. 2
 THERMAL FLUX PARAMETERS
 (BEGINNING-OF-LIFE)

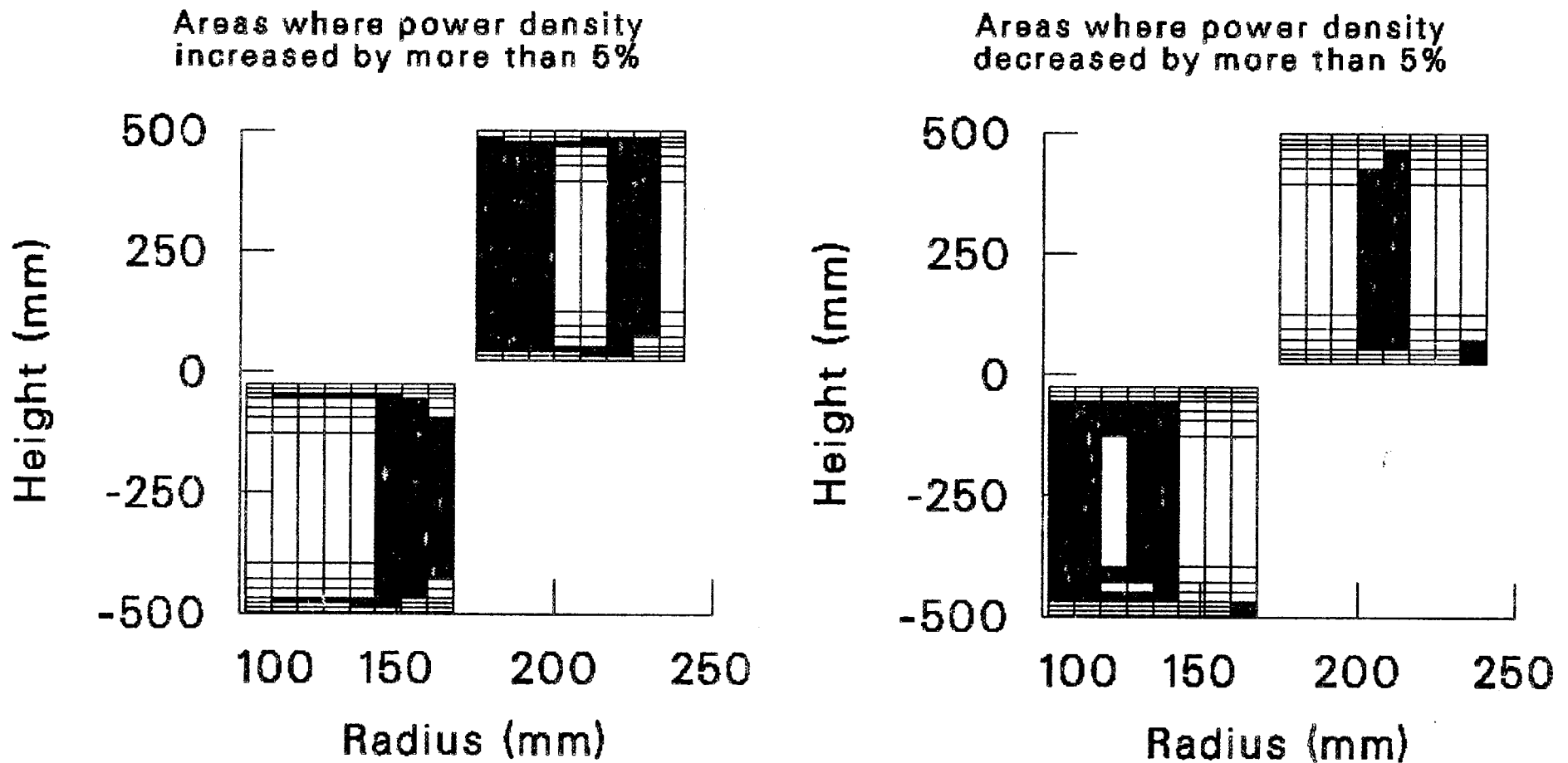
	7 GROUP	4 GROUP
K-EFFECTIVE	1.004	0.973
POWER (MW FISSION)	355.0	355.0
PEAK THERMAL FLUX IN REFLECTOR (N/M**2 S)	7.68E+19	7.67E+19
EFFICIENCY (M**-2)	2.891	2.889
RADIAL LOCATION OF PEAK (MM)	349.3	349.3
AXIAL LOCATION OF PEAK (MM)	-172.0	-172.0
INNER RADIAL 80% MAX LOCATION (MM)	239.7	235.2
OUTER RADIAL 80% MAX LOCATION (MM)	510.6	507.3
AXIAL (AT PEAK) 80% MAX LOCATION (MM)	-458.1	-455.4
VOLUME WITH THERMAL FLUX > 80% OF PEAK VALUE (L)	157.1	195.5
	276.8	266.5

For the past few years, all ANS calculations have been performed with four group cross-section libraries having multiple spatial sets. The proper assignment of a cross-section set to a particular location has been based largely on intuition. Furthermore, these libraries were developed during the Feb. 1988 time frame for a reactor design which had a much higher volumetric U-235 loading than exist in the IRC. Consequently, one might expect to find significant differences in local power densities when comparing the new, seven group results to the IRC results presented in June. Fig. 7 shows that this is indeed the case. Those regions where the power density varied by more than 5% are shown in Fig. 7. Large volumes of each of the two elements are affected.

Interestingly, the values of the peak power densities were not significantly different. For the seven group calculation, the peak point power density was 10.78 Mw/L. The four group value was 10.86. The location of the peak value was the same in each calculation. The values and locations of the hot streak factors were also the same in each calculation.

The seven group cross-section library is available for use on the ORNL IBM-3033 and the LLL CRAY f machine. Next month it will be installed on the ORNL UNICOS CRAY.

**Fig.7 Comparison of zone averaged power densities
for Intermediate Reference Core (Case E3)
using new 7 - group and old 4 - group cross-sections
(7 group - 4 group)/4 group**



Internal Correspondence

MARTIN MARIETTA ENERGY SYSTEMS, INC.

November 1, 1989

D. L. Selby

October 1989 Monthly Progress Report for the ANS Project (Heat Removal)

In addition to the matters described in the attached report, I participated in nine meetings concerning ANS R&D, decay heat removal, flow instability criteria, core operating limits, T/H loop design, and research reactor design methods. Additional heat transfer and pressure drop correlations were provided to J. R. Dixon, and dimensions of the conceptual spent-core transfer vessel were obtained from C. C. Queen for use in thermal calculations during November. Finally, it was noted that water-cooled aluminum has been operated during short-term tests at heat fluxes up to 46.0 MW/m^2 (CHF tests by the writer, 1960).



W. R. Gambill

WRG:mrm

Attachment

cc: R. G. Alsmiller
J. M. Begovich
R. T. Primm, III
G. L. Yoder
WRG File

Heat Removal Monthly Progress Report for October 1989

Advanced Neutron Source Project

W. R. Gambill

1. My letter report of October 19th documenting three proposed single-phase friction factor correlations for the ANSR core is included as Attachment A. Two additional points are noted here:
 - (a) For laminar flow in a flat duct ($AR = \infty$), the hydrodynamic entrance length $L_{hy}^+ = L_{hy}/D_c Re$ is 0.011. For the ANSR core (average $AR = 68.11$), my estimate of L_{hy}^+ is 0.016.
 - (b) If line segment d of Fig. 1 of the subject letter is adopted to represent transitional flow, rather than segment g, the former can be closely approximated by Eq. 14 of the letter--i.e., simply by extending its lower limit from $Re = 4240$ to $Re = 1500$.
2. Additional critically-evaluated T/H correlations for project-wide use will have to be selected and/or developed in several areas, which include:
 - (a) Single Phase:
 - f for rod bundle flow (control rods in central hole).
 - f for concentric annulus flow (gaps between outer side plates and the CPBT).
 - Inlet loss coefficients (laminar and turbulent) for the core.
 - Heat transfer coefficients (laminar, transition, and turbulent) for three geometries: rectangular channels, annuli, and rod bundles.
 - Flow instability criterion.
 - Incipient boiling heat flux (the upper limit of the single-phase regime)--for forced convection and for natural circulation.
 - (b) Two Phase:
 - Heat transfer coefficients (local boiling).
 - Friction coefficients (local boiling).
 - CHF for forced convection, natural circulation, and blocked-base cases.
 - Void fraction.
 - Singularity ΔP (expansions, contractions, bends, e.g.).
 - Bulk boiling (net vapor generation).
 - Film boiling (post-CHF region).

- Critical flow rate with flashing flow.
- Post-accident heat removal (debris beds, e.g.).

(c) Related:

- Oxide growth rate correlation.
- D₂O properties (uniform set).

As already stated in the Task Initiating Document for development of preliminary T/H correlations, documentation will include, in each case, the correlation, reasons for which chosen, variable ranges, validity limits, uncertainty estimates, and references. This task in its entirety is clearly a large and important one.

3. For the current scoping analyses of decay heat removal, preliminary single-phase heat transfer correlations were suggested; see Attachment B. These do not include buoyancy effects, which are being evaluated separately. For the ANSR core, it appears that buoyancy will be unimportant at velocities exceeding about 1 m/s.

Internal Correspondence

MARTIN MARIETTA ENERGY SYSTEMS, INC.

October 19, 1989

D. L. Selby

Proposed Single-Phase Friction Factor Relationships for the ANSR Core

This letter report proposes "semi-final" single-phase friction factor relationships for the specific geometry of the ANS reactor core. Fanning friction factors are used throughout, and the fuel plates are taken to be hydrodynamically smooth (regarding which, see my letter of August 14, 1989).

1. Laminar Isothermal Flow: For flat ducts (infinitely wide parallel plates), $f Re = 24$. For the current reference core, the fuel plate spans are 92 and 81 mm = 86.5 mm average. The aspect ratio AR, defined as the ratio of coolant-channel span to gap, is $86.5/1.27 = 68.11$, and the inverse aspect ratio $\alpha^* = 1/AR = 0.0147$. Values of $f Re$ vs. α^* have been computed for fully developed laminar flow in rectangular channels to seven-digit accuracy, and these values have been represented within 0.05% by Shah and London (1978):¹

$$f Re = 24 [1 - 1.3553 \alpha^* + 1.9467 (\alpha^*)^2 \pm \dots] , \quad (1)$$

in which $\pm \dots$ denotes three additional higher-order terms of no consequence in this context. Evaluating Eq. (1) for $\alpha^* = 0.0147$,

$$f = \frac{23.532}{Re} , \quad (2)$$

in which f is for laminar, isothermal, fully developed flow. An exact treatment would have to account for the additional pressure drop in the hydrodynamic entrance region caused by the momentum change (from the change in the shape of the velocity profile) and by the accumulated increment in wall shear for the developing flow as compared with developed flow. This can be done in terms of either the apparent friction factor f_{app} , which is based on the total ΔP from $x = 0$ to x , or of the incremental ΔP number $[K(x)]$, which accounts only for the difference between the total ΔP and the fully developed ΔP . This accounting has not been done here for two reasons: (a) laminar flow is not experienced until long times after shutdown when heat fluxes are relatively small and therefore the most exact calculations are not needed, and (b) in several laminar-flow cases examined in the recent past, the flow in approximately the downstream 90% of the core length was fully developed.

2. Laminar Heated Flow: When a flowing liquid is heated, f is decreased, but for laminar flow, this decrement has never been comprehensively correlated. Nevertheless, work in this area over the past twenty years seems to have diminished to zero. The dependence can be expressed by:

$$\left(\frac{f_h}{f}\right)_{\text{lam}} = C \left(\frac{\mu_b}{\mu_w}\right)^m, \quad (3)$$

in which f_h is the friction factor for the diabatic (heated) flow. The following tabulation summarizes the values of C and m which have been proposed for heated laminar liquid flows.

Proponent(s)	Comments	C	m
Sieder and Tate (1936) ²	Tube flow	10/11	-0.25
Deissler (1951) ³	Tube flow, constant ϕ , μ vs. t relation used corresponds approximately to liquid metals	1	-0.58
Bonilla (1958) ⁴	Empirically satisfactory	1	-0.32
Test (1968) ⁵	Oils, $Re > 30$, sign of m in paper corrected here	9/8	-0.20
Perry (1973) ⁶	Oils, chosen by Boucher and Alves, based on Sieder and Tate	1	-0.38

Of these, I recommend, on the basis of favorable past experience, Bonilla's form - i.e.,

$$\left(\frac{f_h}{f}\right)_{\text{lam}} = \left(\frac{\mu_b}{\mu_w}\right)^{-0.32} \quad (4)$$

Combining Eqs. (2) and (4),

$$(f_h)_{\text{lam}} = \frac{23.532}{Re} \left(\frac{\mu_b}{\mu_w}\right)^{-0.32} \quad (5)$$

3. The Critical Re and Transitional Flow: Hanks (1966)⁷ showed that the Re_c for rectangular ducts with $AR \geq 10$ (i.e., $\alpha^* \leq 0.1$) is 2800. For a completely disturbed (fully chaotic) inlet flow state, Hanks (1963)⁸ theoretically derived a Re_c value of 2288 for a flat duct. Hanks' 1966 result is in reasonable agreement with those of Davies and White (1928),⁹ who found $Re_c = 2920$ for $\alpha^* = 0.01$, and of Beavers, et al. (1970),¹⁰ who determined that $Re_c = 3400$ for a rectangular

channel ($\alpha^* = 0.0145$) with a symmetric rounded entrance. The nominal isothermal critical Re is taken here to be:

$$Re_c = 2800 . \quad (6)$$

Discussion of the $f - Re$ relation for transitional flows will be deferred, to follow treatment of the important turbulent flow regime. At this point, it is merely noted that for high AR (small α^*) channels, the transition, laminar \leftrightarrow turbulent, is smoother (more regular) than that associated with tube flow [Bonilla (1958),¹¹ e.g.].

4. Turbulent Isothermal Flow: Until the mid-1970s, the approach universally taken to turbulent flow in rectangular channels was to use the round tube $f - Re$ curve, basing Re and f on the standard wetted equivalent diameter D_e . This method correlated many rectangular channel data to within $\sim \pm 5\%$ for $6 \times 10^3 \leq Re \leq 500 \times 10^3$. This approach, which is often a good-to-excellent approximation, was treated at some length in a paper by Hartnett et al. (1962).¹²

Jones (1976),¹³ however, using all the available f data ($\alpha^* = 0.025$ to 1.0), showed that for rectangular channels f can indeed be obtained accurately from the tube curve for f vs. Re, but only if Re is based on the "laminar equivalent diameter" D_l . The diameter D_l is approximated within 2.0% by:

$$\frac{D_l}{D_e} = \frac{2}{3} + \frac{11}{24} \alpha^* (2 - \alpha^*) , \quad (7)$$

which gives, for the ANSR core, $D_l/D_e = 0.6801$. After evaluating f from Re based on D_l , the standard D_e is used to compute ΔP . This procedure reduced the scatter in the experimental f data from $+20\%/-5\%$ to $\pm 5\%$. Using Eq. (7), the maximum deviation is $\sim \pm 7\%$. As noted by Kakac (1987),¹⁴ Jones' correlation gives f factors that are lower by 3% for a square duct and are higher by 11% for infinite parallel plates than for a circular tube at the same Re.

Equivalent to the preceding in accuracy ($\pm 7\%$), but more direct, is the correlation of Bhatti and Shah (1987),¹⁵ which applies to rectangular ducts with $0 \leq \alpha^* \leq 1$ and for $5 \times 10^3 \leq Re \leq 10^7$:

$$f = (1.0875 - 0.1125 \alpha^*) f_T , \quad (8)$$

in which f_T represents the turbulent tube-flow correlation of Techo (1965):¹⁶

$$\frac{1}{(f_T)^{1/2}} = 1.7372 \ln \frac{Re}{1.964 \ln Re - 3.8215} . \quad (9)$$

Equation (9) agrees with the von Kàrmàn-Nikuradse equation (with which the most accurate tube data agree within $\pm 2\%$) within $\pm 0.1\%$. From Eq. (8), the ANSR turbulent f is given by:

$$f = 1.0858 f_T . \quad (10)$$

Some values from Eqs. (9) and (10) are:

Re	f_T	f
5×10^3	0.009330	0.010131
10^4	0.007718	0.008380
5×10^4	0.005227	0.005675
10^5	0.004502	0.004888
3×10^5	0.003618	0.003928
10^6	0.002912	0.003162

Three other f correlations have been compared with the preceding tabulation of Re vs. ANSR f . For $Re = 10^4 - 10^6$, the simple Colburn-McAdams relation $f = 0.046/Re^{0.2}$ fits the values within $+2.3\%$ and -5.5% when the numerator is increased to 0.05 - i.e.:

$$f = \frac{0.0500}{Re^{0.2}} . \quad (11)$$

For the same Re range, the INEL correlation:¹⁷

$$f = 0.0024 + \frac{0.358}{Re^{0.437}} \quad (12)$$

fits the values within $+3.2\%$ and -4.7% ; and the Filonenko correlation:¹⁸

$$f = \frac{0.2500}{(1.82 \log Re - 1.64)^2} , \quad (13)$$

fits within $+1.6\%$ and -0.6% when rewritten as:

$$f = \frac{0.2709}{(1.82 \log Re - 1.64)^2} . \quad (14)$$

Equation (14) is recommended for the isothermal f_{turb} . It gives f values 8.36% higher than Filonenko's original relation [Eq. (13)] for tube flow. In Petukhov's Nusselt modulus correlation, f appears three times, but that f is the Darcy friction factor (4 times Fanning). Therefore, the f relation to use in the Petukhov correlation is:

$$f_{\text{Darcy}} = \frac{1.0836}{(1.82 \log Re - 1.64)^2} . \quad (15)$$

Note that the increase in f , which is related solely to the geometry, will increase the single-phase heat-transfer coefficient from the Petukhov equation by a similar, but unidentical, amount.

5. Turbulent Heated Flow: The relation proposed by Petukhov (1970)¹⁹ for heating liquids:

$$\left(\frac{f_h}{f}\right)_{\text{turb}} = \frac{1}{6} \left(7 - \frac{\mu_b}{\mu_w}\right), \quad (16)$$

was based on turbulent-flow H₂O data and is recommended. The data base spanned the following ranges: Pr = 1.3 - 10, Re = 10⁴ - 2.3 × 10⁵, and $\mu_b/\mu_w = 1 - 2.9$. Incidentally, for $\mu_b/\mu_w = 1.0$ to 2.5, Eq. (16) agrees with Eq. (4) within an average deviation of -2.2%. Note that for $\mu_b/\mu_w = 2.0$, which is probably a representative core-average value for the ANSR, Eq. (16) gives a decrease in f for turbulent flow of -17%, while Eq. (4) projects a decrease in f for laminar flow of -20%. Combining Eqs. (14) and (16),

$$(f_h)_{\text{turb}} = \frac{0.2709}{(1.82 \log Re - 1.64)^2} \left[\frac{7 - (\mu_b/\mu_w)}{6} \right]. \quad (17)$$

6. Transitional Isothermal Flow: There appear to be no reliable, critically evaluated correlations for friction (or heat transfer) coefficients applicable to transition flow in rectangular channels of various aspect ratios. In Fig. 1, the isothermal f correlations for laminar and turbulent flows [Eqs. (2) and (14)] are shown as line segments a and e, respectively. The transition region is represented by a minimum boundary (b-c), a suggested maximum boundary (d), and by an approximately constant f value (g). The transition-region vertical scatter of f data typical of rectangular ducts is shown by curve (c) of Fig. 2 for a small AR channel ($\alpha^* = 2/7$); the points are the classical data of Nikuradse (1930).²⁰ There is some indication in the literature that in Fig. 1, the curve a-b-c-e is followed as the flow rate increases, whereas with a decreasing flow rate, e-d-a or e-g-a is the preferential path.

Although path d gives maximum f values, its terminal points are uncertain, and I now favor curve g, i.e.,

$$f = 0.0110, \quad (18)$$

for the range of Re = 2140 to 4240.

7. Transitional Heated Flow: Lacking any specific rectangular-channel data, I propose:

$$\left(\frac{f_h}{f}\right)_{\text{trans}} = \left(\frac{\mu_b}{\mu_w}\right)^{-0.32}, \quad (19)$$

i.e., the same dependence as for laminar flow [Eq. (4)]. As noted following Eq. (16), this relation is also acceptable for turbulent flow for the limited range of $\mu_b/\mu_w = 1.0 - 2.5$. Combining Eqs. (18) and (19):

$$(f_h)_{\text{trans}} = 0.0110 \left(\frac{\mu_b}{\mu_w} \right)^{-0.32} \quad (20)$$

8. Circular Tube Comparison: In Fig. 1, the $f - Re$ relation is also shown for smooth round ducts. For this case, $f_{\text{lam}} = 16/Re$, f_{turb} is from Techo's correlation [Eq. (9)], and f_{trans} was computed with the correlation of Churchill (1977),²¹ which encompasses all three flow regimes for tube flow. The proposed ANSR core $f - Re$ curve (a-g-e) falls above that for tubes at all values of Re .

9. Concluding Remarks: The f correlations proposed for laminar, turbulent, and transition flows in the current core are Eqs. (5), (17), and (20), respectively. Equation (15) should be used in the Petukhov heat transfer equation; no heating correction is applied to f in that instance, since the Petukhov correlation includes its own correction factor - i.e., $(\mu_b/\mu_w)^{0.11}$. The correlations are summarized in Table 1, and the approximate core flow regimes are identified by per cent flow rate in Table 2. Changes in the aspect ratio α^* will alter each correlation to some extent; all relations needed to calculate such changes are included in this letter. In computing the total ΔP , components other than frictional ΔP must also be calculated; these include the acceleration (momentum change) ΔP , inlet contraction ΔP , outlet expansion ΔP , and hydrostatic ΔP . In addition, the $f-Re$ relationships for flow paths parallel to the core will each be somewhat different. Examples include flow parallel to the group of control rods in the central hole and flow through the concentric annuli between the outer side plates of the fuel elements and the CPBT. \

As always, comments, questions, and suggestions are welcome.

W. R. Gambill

W. R. Gambill

WRG:wpc

cc:	J. M. Begovich	B. S. Maxon	W. E. Thomas
	N.C.J. Chen	R. Miller	C. D. West
	J. R. Dixon	F. J. Peretz	G. L. Yoder
	R. M. Harrington	H. Reutler	WRG File (2)
	J. A. March-Leuba	A. E. Ruggles	

Table 1
 Summary of Single-Phase Friction
 Factor Correlations

Flow regime	Equation No.	Re range
Laminar	5	$Re \leq 2140$
Transitional	20	$2140 < Re < 4240$
Turbulent	17	$10^4 \leq Re \leq 10^6$ ^a

^aWith a slightly increased deviation, Eq. (17) also applies to $4.24 \times 10^3 \leq Re < 10^4$.

Table 2
 Core Single-Phase Flow Regimes^a

Full flow (%)	\overline{Re}_{core}	Regime
100	1.54×10^5	Fully turbulent Early turbulent Transitional
6.5	1×10^4	
2.8	4.24×10^3	
1.4	2.14×10^3	
<1.4	$<2.14 \times 10^3$	Laminar

^aFor a constant power-to-flow ratio equal to that at full power.

Notation

AR	channel aspect ratio (span/gap)
a_x	cross-sectional flow area
C	coefficient in Eq. (3)
D_e	wetted equivalent diameter ($4a_x/p_w$)
D_l	laminar equivalent diameter [Eq. (7)]
f	isothermal Fanning friction factor
f_{app}	apparent Fanning friction factor
f_{Darcy}	isothermal Darcy friction factor ($4 f$)
f_h	Fanning friction factor for a diabatic (heated) flow
f_T	f for turbulent tube flow from Techo's correlation
$K(x)$	incremental pressure-drop number
m	exponent in Eq. (3)
p_w	wetted perimeter of flow channel
ΔP	streamwise static pressure difference
Re	Reynolds number
Re_c	critical Reynolds number
t	liquid temperature
x	streamwise distance from beginning of channel
α^*	inverse aspect ratio ($1/AR$)
μ	liquid viscosity
μ_b	viscosity at bulk temperature t_b
μ_w	viscosity at wall temperature t_w
ϕ	wall heat flux

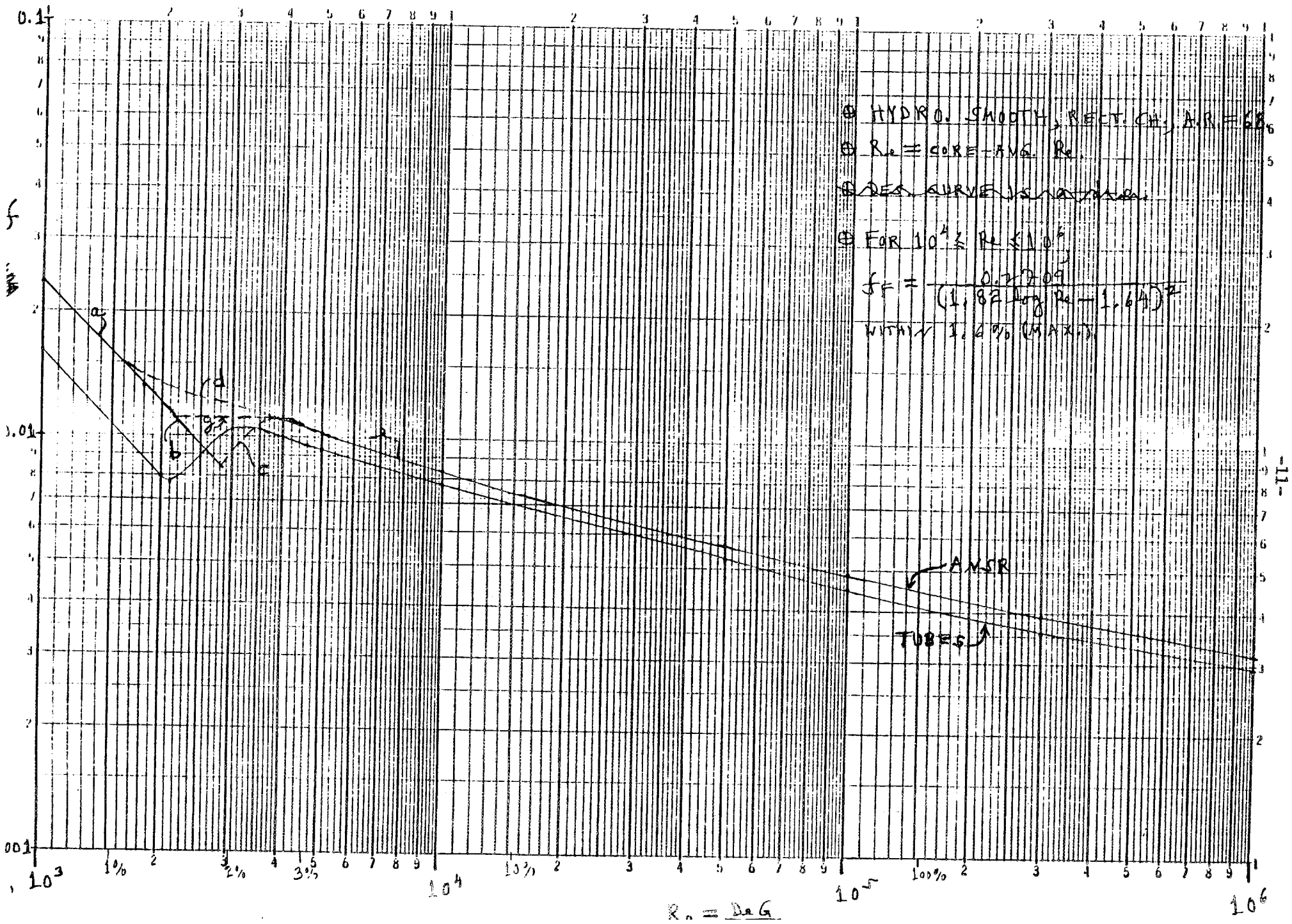
REFERENCES

1. R. K. Shah and A. L. London, "Laminar Flow Forced Convection in Ducts," *Advances in Heat Transfer, Supplement 1, Chapter VII, Rectangular Ducts*, pp. 199-201, Academic Press, 1978.
2. E. N. Sieder and G. E. Tate, "Heat Transfer and Pressure Drop of Liquids in Tubes," *Ind. Eng. Chem.*, 28, pp. 1429-1436, 1936.
3. R. G. Deissler, *Analytical Investigation of Fully Developed Laminar Flow in Tubes with Heat Transfer with Fluid Properties Variable Along the Radius*, NACA TN 2410, 1951.
4. C. F. Bonilla, "Fluid Flow in Reactor Systems," p. 9-31 of *Nuclear Engineering Handbook*, H. Etherington (Ed.), 1st Ed., McGraw-Hill, 1958.
5. F. L. Test, "Laminar Flow Heat Transfer and Fluid Flow for Liquids with Temperature-Dependent Viscosity," *J. Heat Transfer*, 90, pp. 385-393, 1968.
6. R. H. Perry (Ed.), *Chemical Engineers' Handbook*, 5th Ed., Sect. 5, p. 5-23, McGraw-Hill, 1973.
7. R. W. Hanks and H. C. Ruo, "Laminar-Turbulent Transition in Ducts of Rectangular Cross Section," *I&EC Fundamentals*, pp. 558-561, November 1966.
8. R. W. Hanks, "The Laminar-Turbulent Transition for Flow in Pipes, Concentric Annuli, and Parallel Plates," *AIChE J.*, 9, pp. 45-48, 1963.
9. S. J. Davies and C. M. White, "An Experimental Study of the Flow of Water in Pipes of Rectangular Section," *Proc. Roy. Soc.*, A119, pp. 92-107, 1928.
10. G. S. Beavers, et al., "Experiments on the Breakdown of Laminar Flow in a Parallel-Plate Channel," *Intl. J. Heat & Mass Transfer*, 13, pp. 809-815, 1970.
11. C. F. Bonilla, "Fluid Flow in Reactor Systems," p. 9-35 of *Nuclear Engineering Handbook*, H. Etherington (Ed.), 1st Ed., McGraw-Hill, 1958.
12. J. P. Hartnett, et al., "A Comparison of Predicted and Measured Friction Factors for Turbulent Flow Through Rectangular Ducts," *J. Heat Transfer*, 84, pp. 82-88, 1962.
13. O. C. Jones, Jr., "An Improvement in the Calculation of Turbulent Friction in Rectangular Ducts," *J. Fluids Eng.*, 98, pp. 173-181, 1976.

14. S. Kakac, "The Effect of Temperature-Dependent Fluid Properties on Convective Heat Transfer," Chapter 18 (p. 18.20) of *Handbook of Single-Phase Convective Heat Transfer*, Wiley, 1987.
15. M. S. Bhatti and R. K. Shah, "Turbulent and Transition Flow Convective Heat Transfer in Ducts," Chapter 4 (pp. 4.76-4.77) of *Handbook of Single-Phase Convective Heat Transfer*, Wiley, 1987.
16. R. Techo, et al., "An Accurate Equation for the Computation of the Friction Factor for Smooth Pipes from the Reynolds Number," *J. Appl. Mechs.*, 32, p. 443, 1965.
17. R. P. Wadkins (INEL), personal communication to W. R. Gambill (ORNL), October 23, 1986.
18. G. K. Filonenko, "Hydraulic Resistance in Pipes," *Teploenergetika*, 1, No. 4, pp. 40-44, 1954.
19. B. S. Petukhov, "Heat Transfer and Friction in Turbulent Pipe Flow with Variable Physical Properties," in *Advances in Heat Transfer*, Vol. 6, pp. 504-564, Academic Press, 1970.
20. J. Nikuradse, *Ing.-Arch.*, No. 1, pp. 306-332, 1930.
21. S. W. Churchill, "Comprehensive Correlating Equations for Heat, Mass, and Momentum Transfer in Fully Developed Flow in Smooth Tubes," *I&EC Fundamentals*, 16, No. 1, pp. 109-116, 1977.

Fig. 1. ANSR core, f vs Re (with $\phi = 0$).

WRG
9/29/89



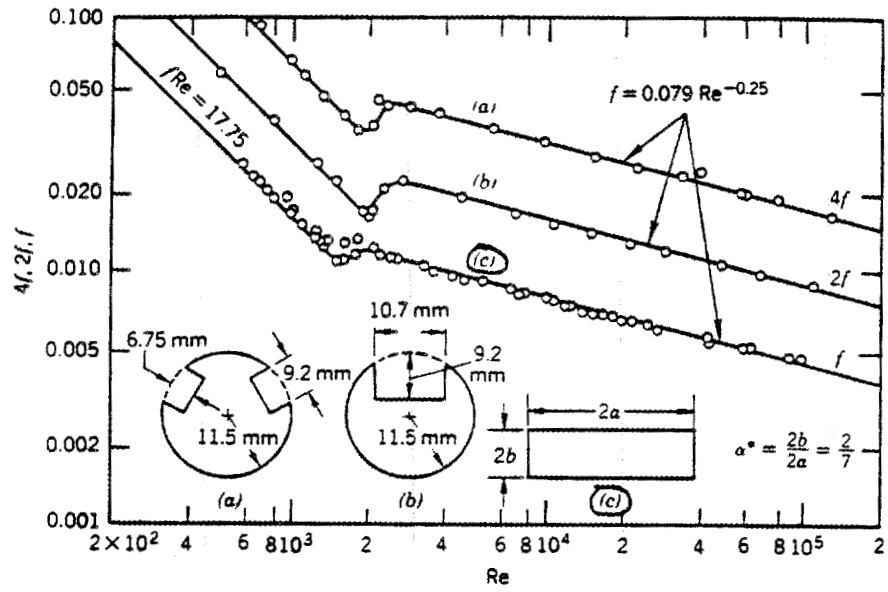


Fig. 2. Friction factors for fully developed turbulent flow in smooth circular ducts with rectangular indentations and in a rectangular duct.

ATTACHMENT B

Preliminary Single-Phase Heat Transfer
Correlations for Decay Heat Removal Analysis

I. Laminar Flow: [$Re_b < 2300$].

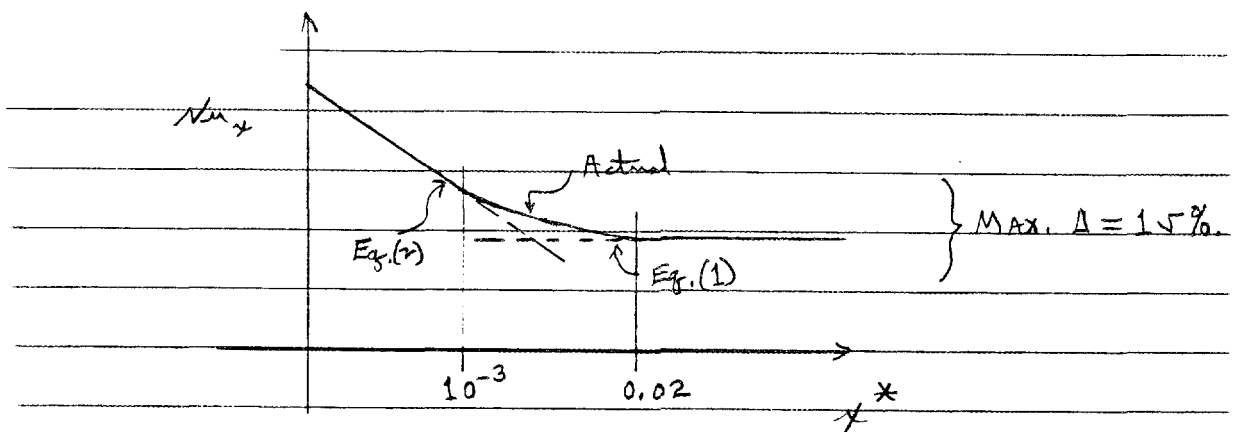
BASIS → Rect. Channel, AR=68.11 (ANSR), LOCAL Nu for Developed V and
Developing T, B.C. = $\frac{UHF + UWT}{2}$.

For $x^* \equiv \frac{x}{D_o Re Pr} > 0.0058$, use $Nu_x = 7.627$. (1)

For $x^* \leq 0.0058$, use $Nu_x = \frac{1.3526}{(x^*)^{1/3}}$. (2)

To account for variable props., multiply Eqs (1) and (2) by $(\mu_b / \mu_w)^{0.11}$. Yang → flow (3)

IN CONTEXT:



NOTE: Mixed-convection buoyancy effects (important at low V) must be treated separately to avoid entanglement of the variables.

II. TURB. AND TRANSITION FLOW:

For $Re_b \geq 2300$, use Gnielinski's (1976) correlation:

$$Nu_{b,t} = \frac{(f/r)(Re_b - 1000) Pr_b}{1 + 12.7 (f/r)^{1/2} (Pr_b^{2/3} - 1)} * \left(\frac{\mu_b}{\mu_w}\right)^{0.11} * \left[1 + \frac{1}{3} \left(\frac{D}{L}\right)^{2/3}\right] \quad (4)$$

$$\text{WITH } (f_{\text{Fanning}})_{\text{Mod. Eckhart}} = \frac{1.0836}{[1.58 \ln Re_b - 3.28]^2} \quad (5)$$

Eqs (4) and (5) together are valid for $Re_b = 2300 - 5 \times 10^6$.

and $Pr_b = 0.5 - 2 \times 10^3$.

CONTEXT:

1. The Petukhov correlation we have been using [Petukhov and Popov, 1963 and 1970] is the best for $Re \geq 10^4$ and $Pr \geq 0.5$.
2. To include the transition-flow regime, Gnielinski modified the simpler Petukhov-Kirillov correlation (1958), using Hausen's technique [1974, e.g.].
3. Eq. (4) agrees with Petukhov-Kirillov within $\pm 5\%$ at $Re \geq 10^4$.
4. The last two factors in Eq. (4) are Petukhov's variable-property correction and Hausen's (L/D) term.
5. In Eq. (5), the 8.36% increase in the numerator is my correction for our geometry (letter of October 19, 1989).

Internal Correspondence

MARTIN MARIETTA ENERGY SYSTEMS, INC.

November 13, 1989

J. A. Johnson
D. L. Selby**ANS Reactor Core Analysis Task Monthly Progress Report for October 1989**Steady State Thermal Hydraulics Code Analysis (N. C. J. Chen, W. R. Nelson, G. L. Yoder)

A comparison between the thermal hydraulic performance of the E3 and E8 core neutronics has been performed. Figure 1 shows a comparison of the maximum permissible core power during the core life for each core. These comparisons have used the same uncertainty assumptions as were used in the PS-2 design exercise. In this figure, if the curves lie above the desired 333 Mw thermal line, the core can operate at that level without exceeding the incipient boiling limit (uncertainties included). If the curves lie below the line, the core would operate in the nucleate boiling region. The figure indicates that the E8 design is an improvement over the E3 design at the end of core life; however, the E8 design still lies below the incipient boiling limit at the beginning of core life. Figure 2 shows a similar plot for just the E8 core; however, the second curve on the figure shows the predicted core performance with the uncertainties suppressed. An increase of approximately 40 percent in the maximum power is indicated with no uncertainties included.

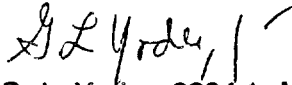
Figure 3 shows the maximum centerline temperatures (solid lines) and corresponding oxide thickness (dashed lines) for each of the E8 cores over the fuel cycle. In this calculation, the standard Griess correlation has been used to calculate the oxide growth rate. Centerline temperatures and oxide growth have been calculated without using the uncertainty associated with fuel segregation to predict oxide growth rate, but rather using the uncertainty associated with the hot streak. This method has been used because the oxide tends to decrease the local peaking factor as was implied by the August monthly report. This technique should be viewed as interim until a better method is devised based on the hot spot uncertainty/oxide results presented in August. As is obvious from the figure, the lower core is limiting with respect to centerline temperatures and exceeds the 400°C limit over about one half of the cycle. The limiting location within the core for both incipient boiling and maximum centerline temperature is always near the core exit, indicating that additional fuel may be moved nearer the core inlet to improve thermal performance. A similar calculation was performed without the uncertainties included and is shown in Figure 4. In this case, the maximum centerline temperatures are always below the 400°C temperature limit and oxide thicknesses are limited to approximately 25 microns. In order to examine the sensitivity of maximum centerline temperatures to the assumed oxide growth rate, the Griess correlation was divided by a factor of two and the calculation (including uncertainties) was repeated. The results are shown in Figure 5. In this case, centerline temperatures remain just below the 400°C limit.

Thermal Hydraulic Correlation Selection (A. E. Ruggles)

Graphical and tabular representations of the incipience of boiling limit and the departure from nucleate boiling limit (CHF) were distributed to various engineering and development personnel.

J. A. Johnson
D. L. Selby
Page 2
November 13, 1989

The selection of an appropriate model for the onset of excursive instability (also termed flow excursion of flow redistribution and occasionally referred to as secondary burn-out) is being documented for internal review. A database to support the selected model is also being developed.



G. L. Yoder, 9204-1, MS-8045 (4-5282)

GLY:beh

cc: N. C. J. Chen
W. G. Craddick
W. R. Gambill
J. R. Kirkpatrick
D. G. Morris
W. R. Nelson
A. E. Ruggles
C. D. West

Figure 1

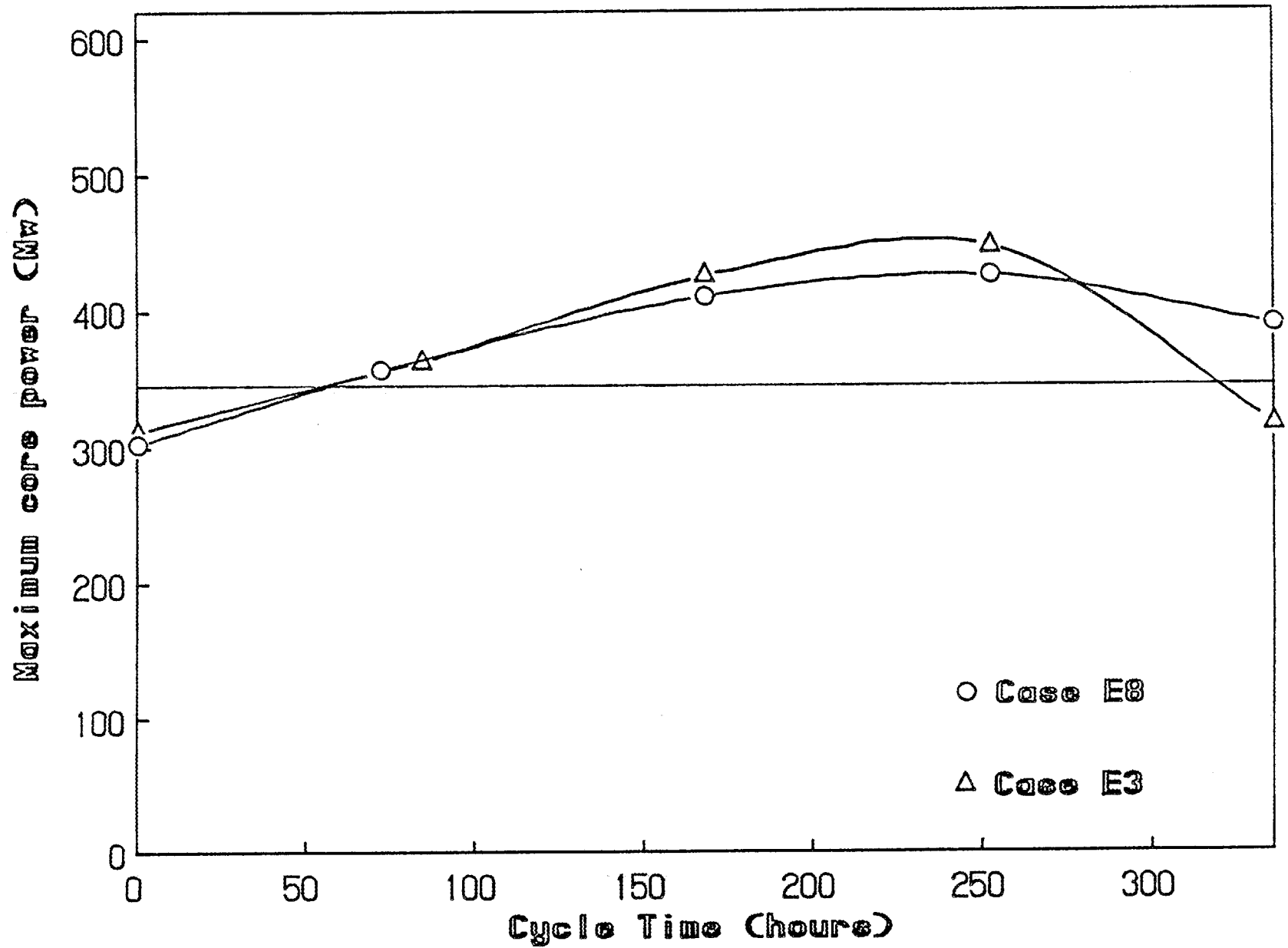


Figure 2

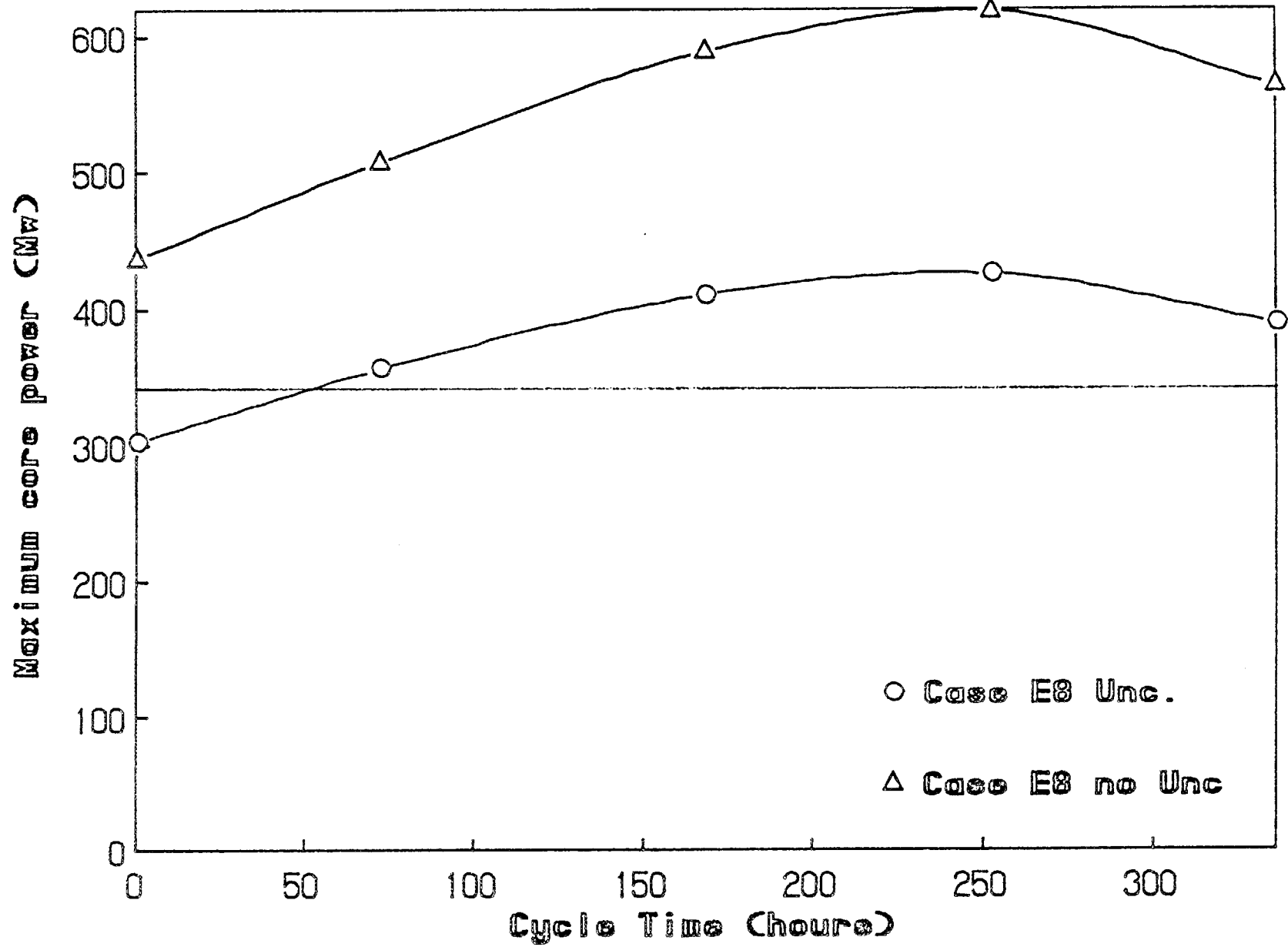


Figure 3

Case E8

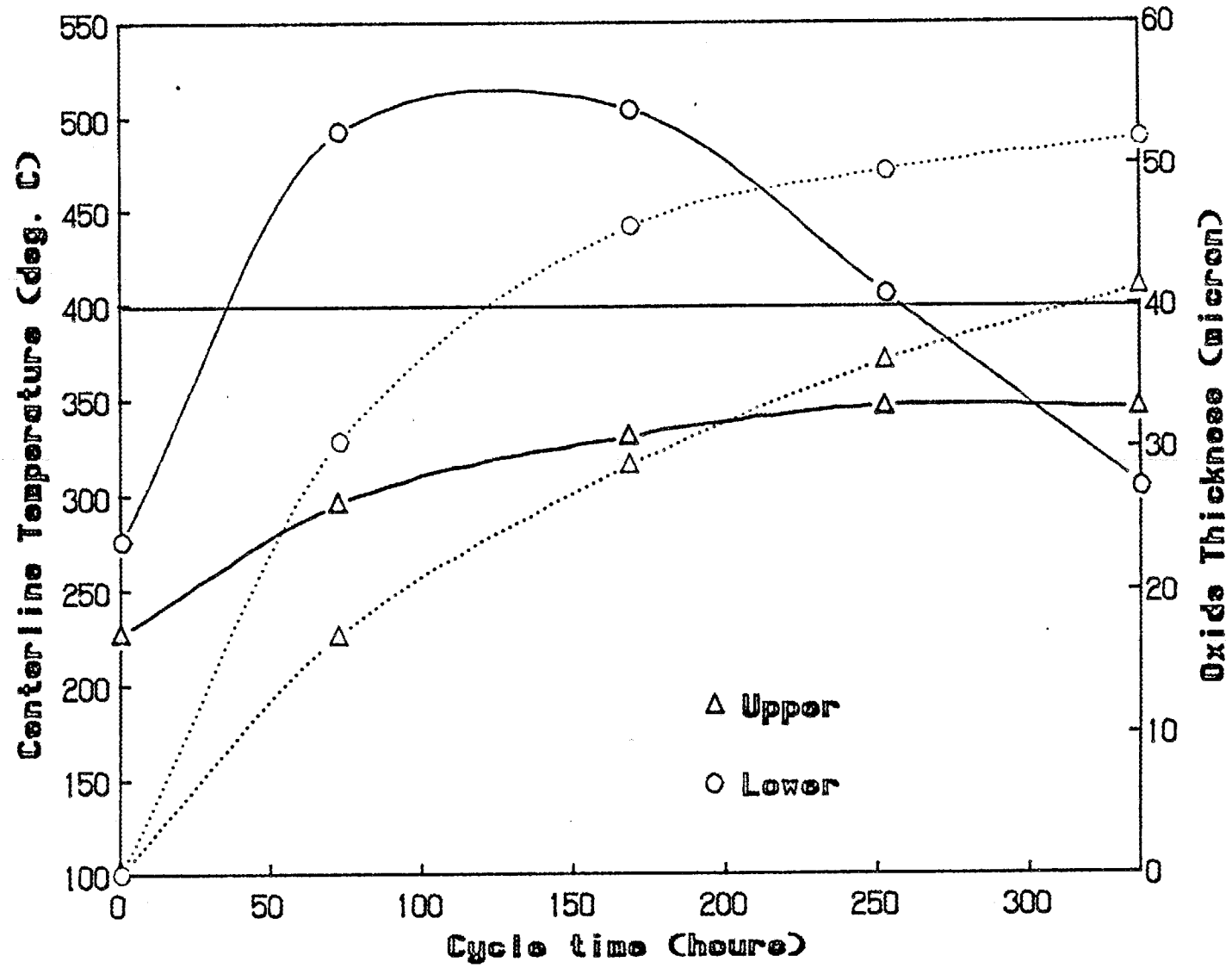


Figure 4

Case E8 no Uncertainties

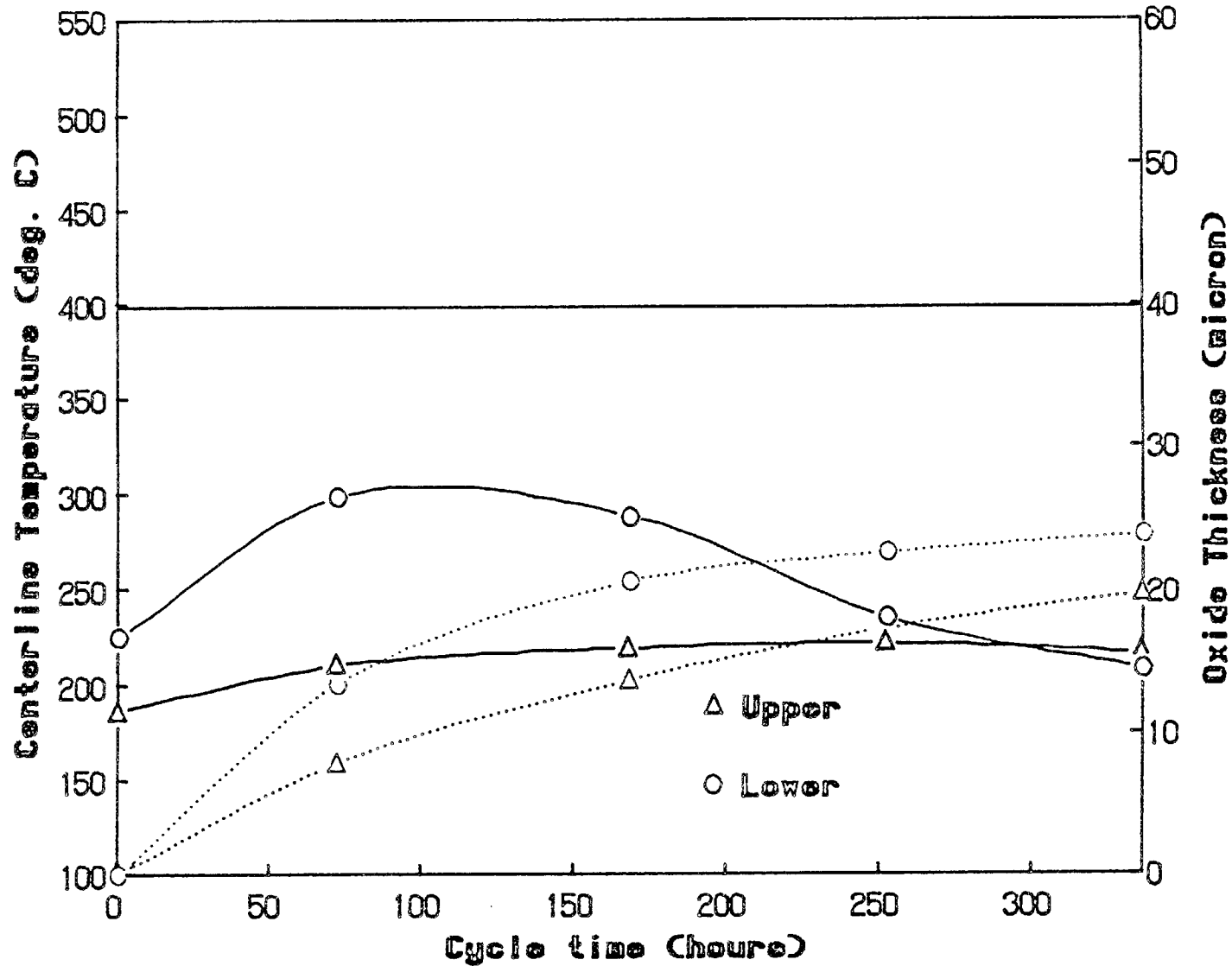
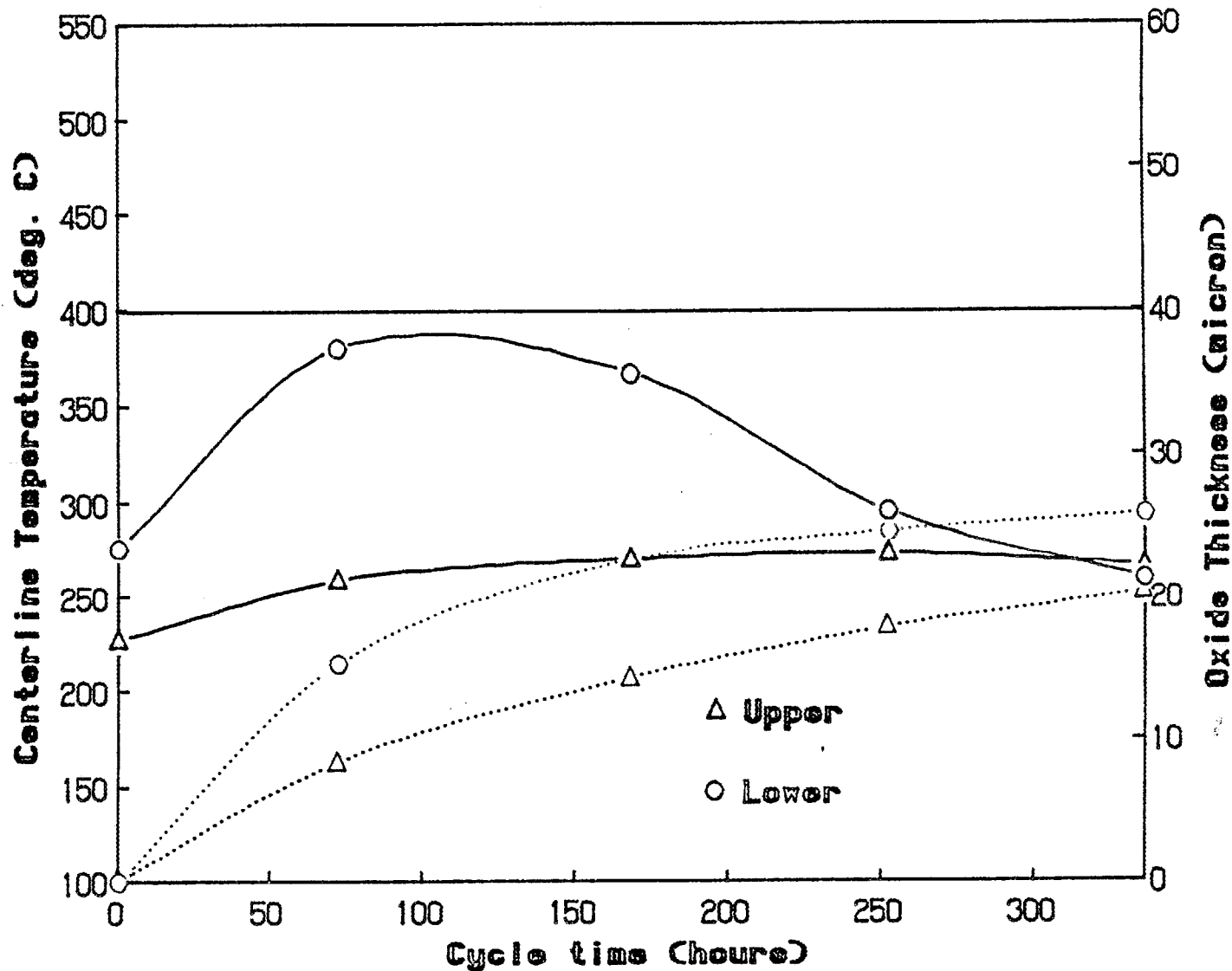


Figure 5

Case E8 Griess/2



ANS PROGRESS REPORT FOR THE MONTH OF OCTOBER 1989

Control and Core Developments
F. C. Difilippo

1. Control Calculations

The calculations were related to the effects of Xe transients on reactor parameters and the differential worth of the safety rods.

- a. Influence of Xe transients and control rods movements on the performance. The effects of the Xe transient on several parameters are shown in Table 1 for the case of the PS2 core, E8 grading (see FCD, progress report August '89).

Table 1. Effects of Xe transients on Reactor Parameters (Case E8)

Parameter	BOL + Xe at full power ^a	BOL NoXe ^b	BOL NoXe + move CR ^c
CR position ^d (mm)	152.	152.	-25.
k	0.974	1.019	0.979
PF ^e	2.14	2.11	2.20
$\epsilon(1/m^2)$ ^f	2.90	2.92	2.91
Power peak position ^g			
r (mm)	167.	167.	167.
z (mm)	-222.	-222.	-252.
Flux peak position			
r (mm)	328.	328.	328.
z (mm)	-192.	-192.	-222.

^a Beginning of life (BOL) conditions with Xe at full power.

^b BOL, no Xe , no change in control rod position.

^c BOL, no Xe , control rod moved to compensate Xe reactivity.

^d Bottom of control rod (CR) with respect horizontal center line.

^e Peaking factor.

^f Rendement.

^g Peak positions with respect to horizontal center line.

The table shows that near BOL the Xe distribution in itself does not affect the position and magnitude of the peaks of the thermal flux and power distribution; but the movement of the control rods associated to the Xe affects the flux and power distributions.

With these new calculations, it is possible to complete the picture of the movement of the thermal flux as function of time from the very beginning of the cycle (no Xe present) to the end. The results are shown in Fig. 1.

b. Calibration of Safety Rods

Integral and differential worth of the safety rods described in FCD, September 1989 Progress Report were computed for grading E10, BOL of the PS2 core. Figure 2 shows the results under two conditions: with and without the presence of regulating rods (see Sept. '89 Progress Report for the methodology.)

The effects of the structural parts of the control rods were simulated by simply extending the rods to "infinity," the z coordinate in Fig. 2 represents the distance from the top of the rod to the upper active edge of the upper core, the rods move downward $\Delta k/k$ means $[k(z) - k(z=\infty)]/k(z=\infty)$ i.e. the relative change of k with respect to the case of total withdraw (that is, total lack of control materials in the reflector).

2. Core Calculations

The iterative process to improve the power distributions continued. Case E10 corresponds to the following optimization criteria: the lower core and the bottom corner of the upper core were optimized at 7 days, the outer edge of the upper core was optimized at 0 day and the inner part of the upper core was optimized at 14 days; this combination produced (to the present) the best results.

Table summarizes the performance of this grading.

Table 2. Performance of Grading E10

t(d)	k ^b	M U ²³⁵ (Ug)	M ¹⁰ B (g)	PF ^c	ε(1/m ²) ^d
0 ^a	0.9726	14.89	13.44	1.97	2.90
3.5	0.9734	13.31	5.29	1.79	2.99
7.	1.0232	11.74	1.35	1.65	3.05
10.5	0.9907	10.19	0.23	1.65	3.12
14.	0.9895	8.65	0.036	1.75	3.09

^aXe at equilibrium included (fission power 350 Mw).

^bk is maintained near 1 by moving the control rods.

^cPeaking factor, maximum power density divided average.

^dRendement.

Figure 3 shows the maximum temperature profile for the hottest channel at each time step. Figures 4 to 9 show the entire temperature distribution as function of space and time. Note that the maximum fuel temperature would be 228°C.

A warning about these results: 1) the power distributions were computed with a detailed model but with only one thermal group so the power distributions are not very accurate. 2) the thermal hydraulic calculations correspond to the case of a perfect core and correlations; no uncertainties are included in the model. The working conditions in the simulation are: 350 Mw fission, 95% of which heats the fuel, 27.4 m/s coolant velocity and 49°C inlet temperature.

Despite these limitations one concludes that the automatic procedure developed to tailor the power distributions works, the final accuracy will depend on the availability of accurate power distributions.

DESIGN E8, EVOLUTION OF THE PROFILE OF THE PEAK THERMAL FLUX

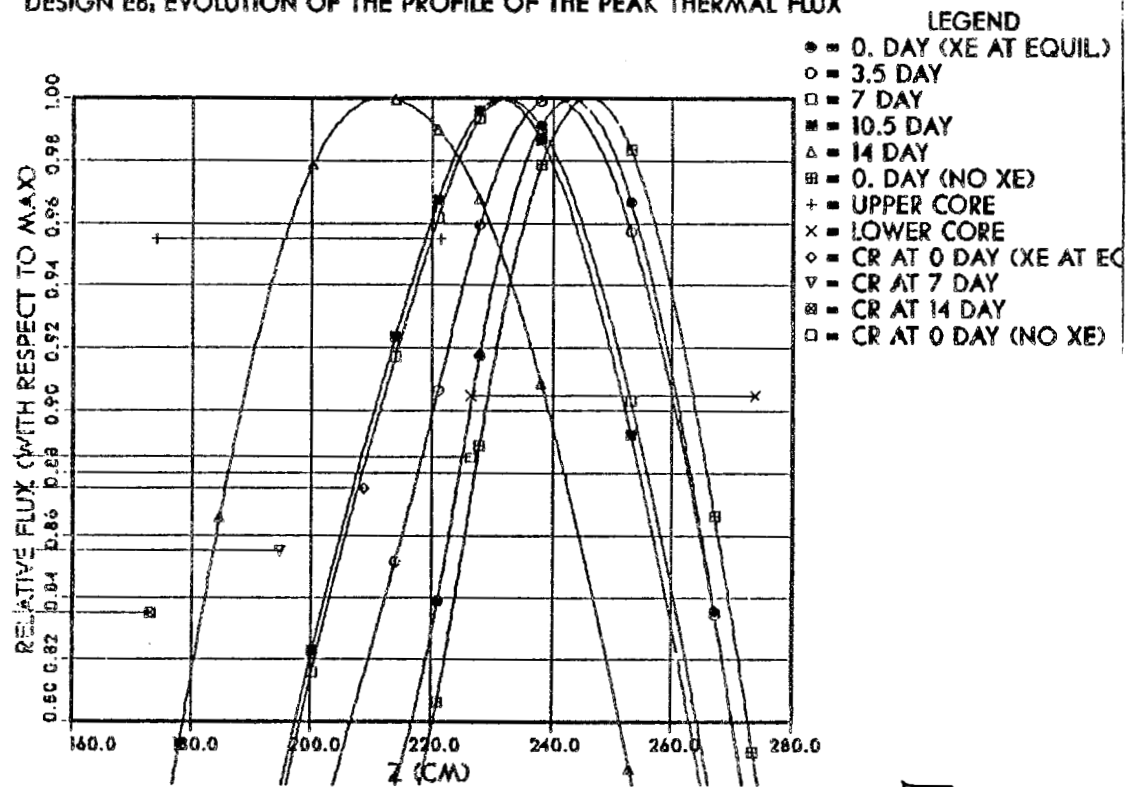


Fig. 1

CALIBRATION OF THE 8 SAFETY RODS (AT R=369MM)

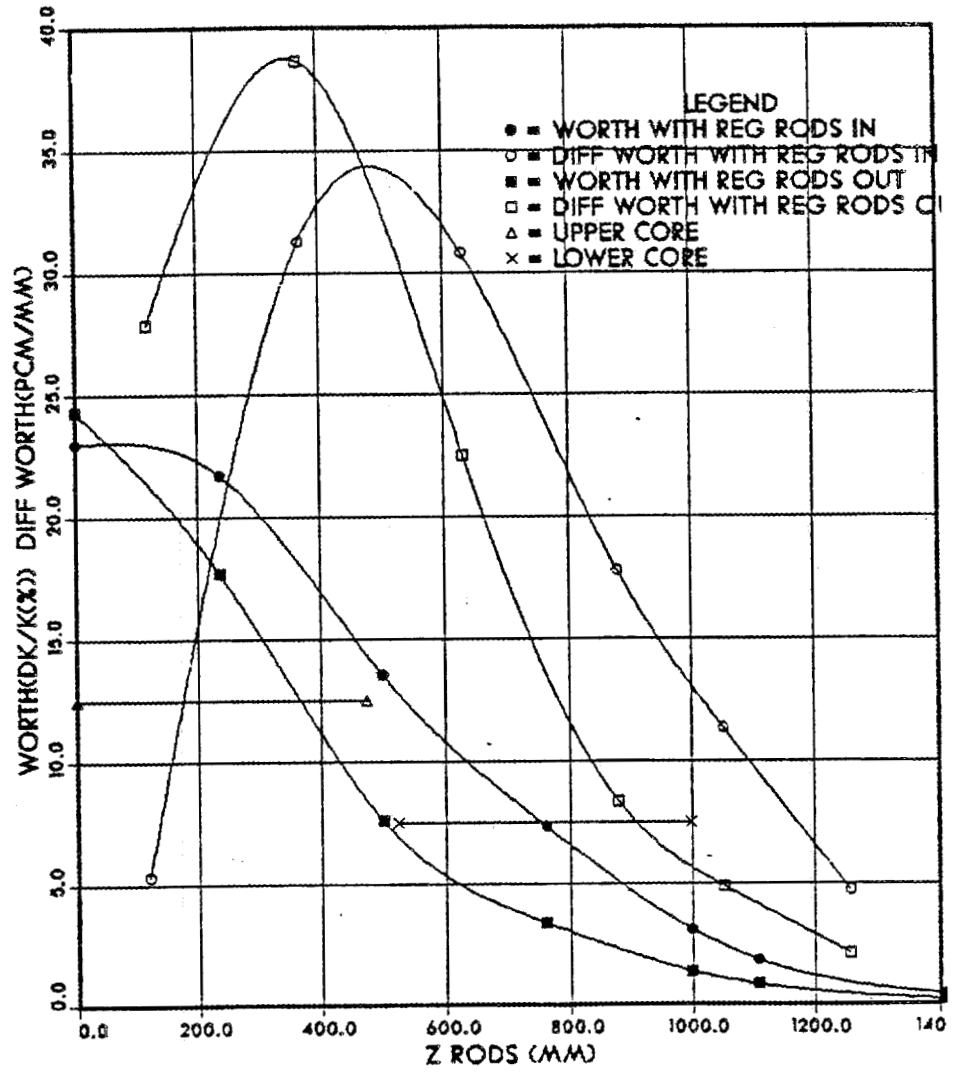
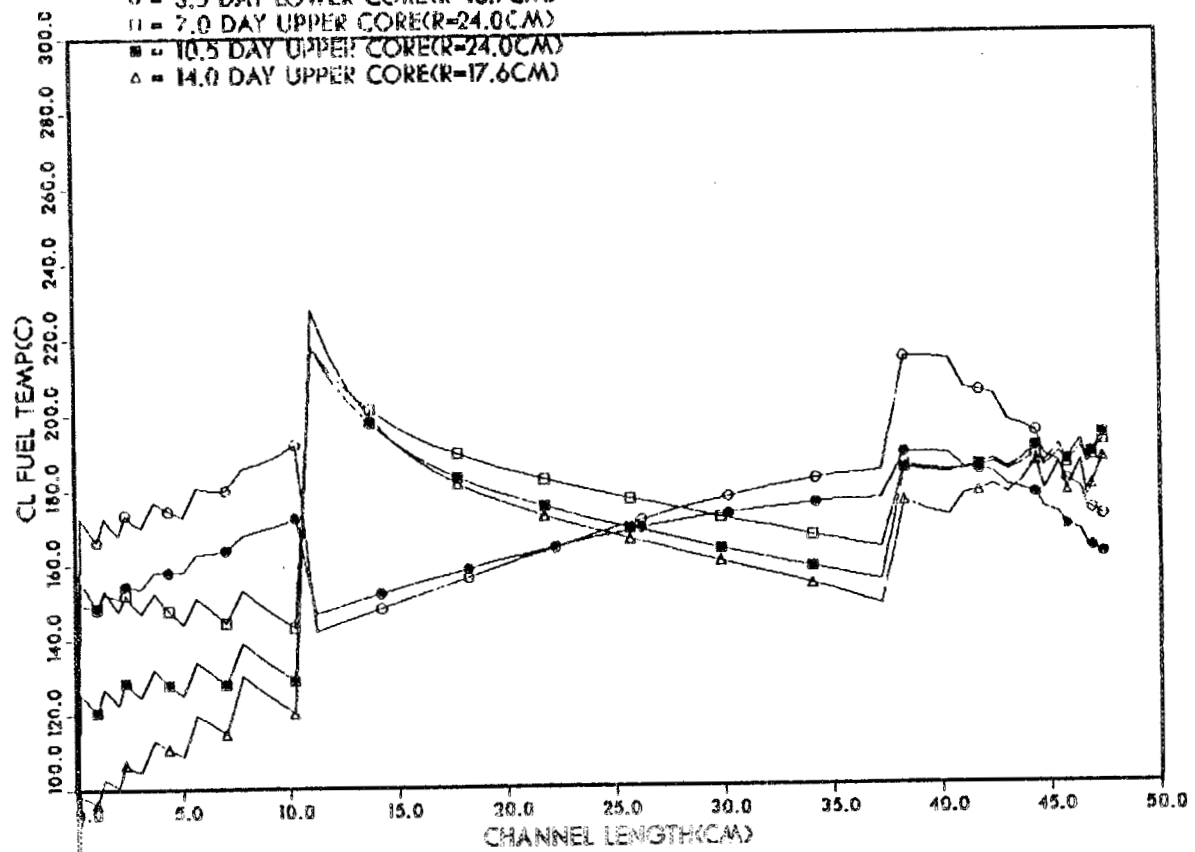


Fig 2

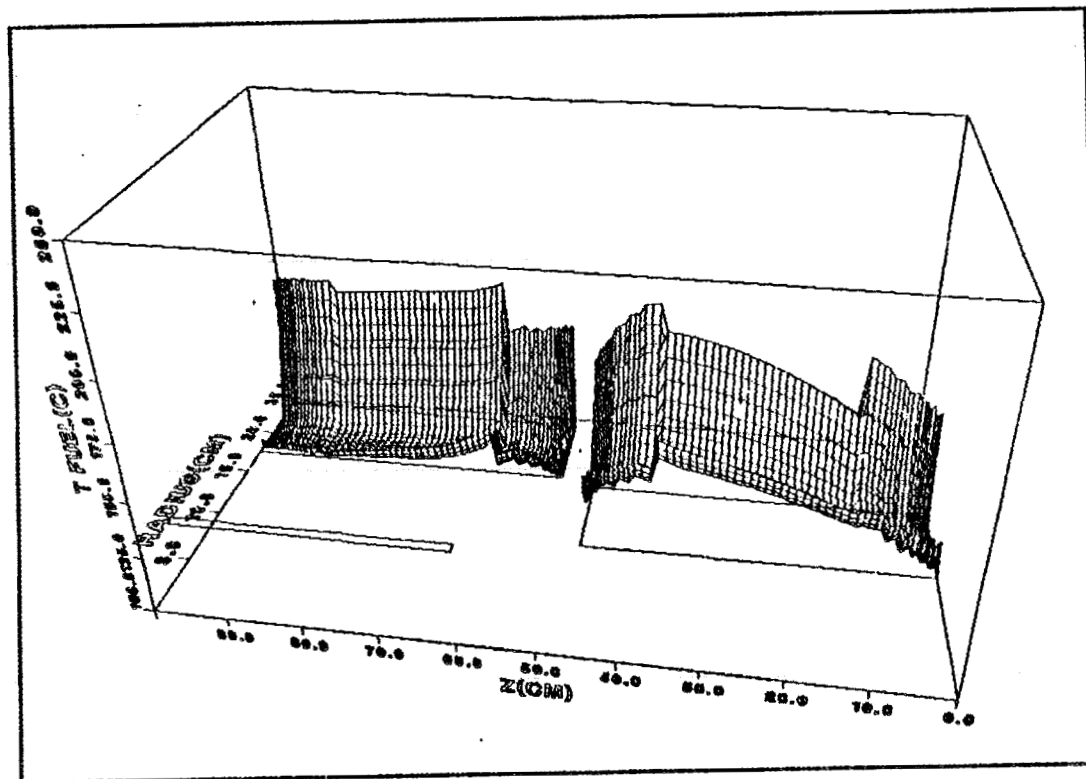
DESIGN E10: FUEL TEMP PROFILE(CHANNEL WITH MAX TFUEL)

LEGEND

- = 0 DAY LOWER CORE(R=16.7)
- = 3.5 DAY LOWER CORE(R=16.7CM)
- = 7.0 DAY UPPER CORE(R=24.0CM)
- = 10.5 DAY UPPER CORE(R=24.0CM)
- △ = 14.0 DAY UPPER CORE(R=17.6CM)



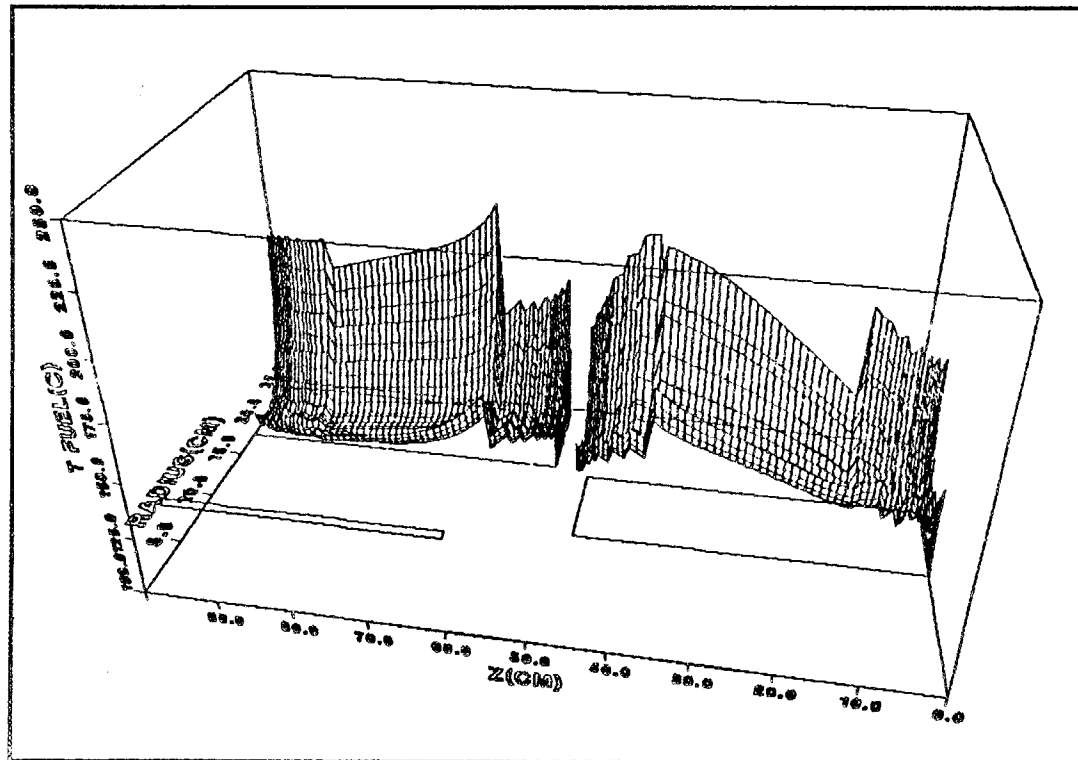
DESIGN E10 0 DAY T FUEL



14-45-48 THU 26 507 1985 JOB=FCO / 15500 DISSEPLA 10.0

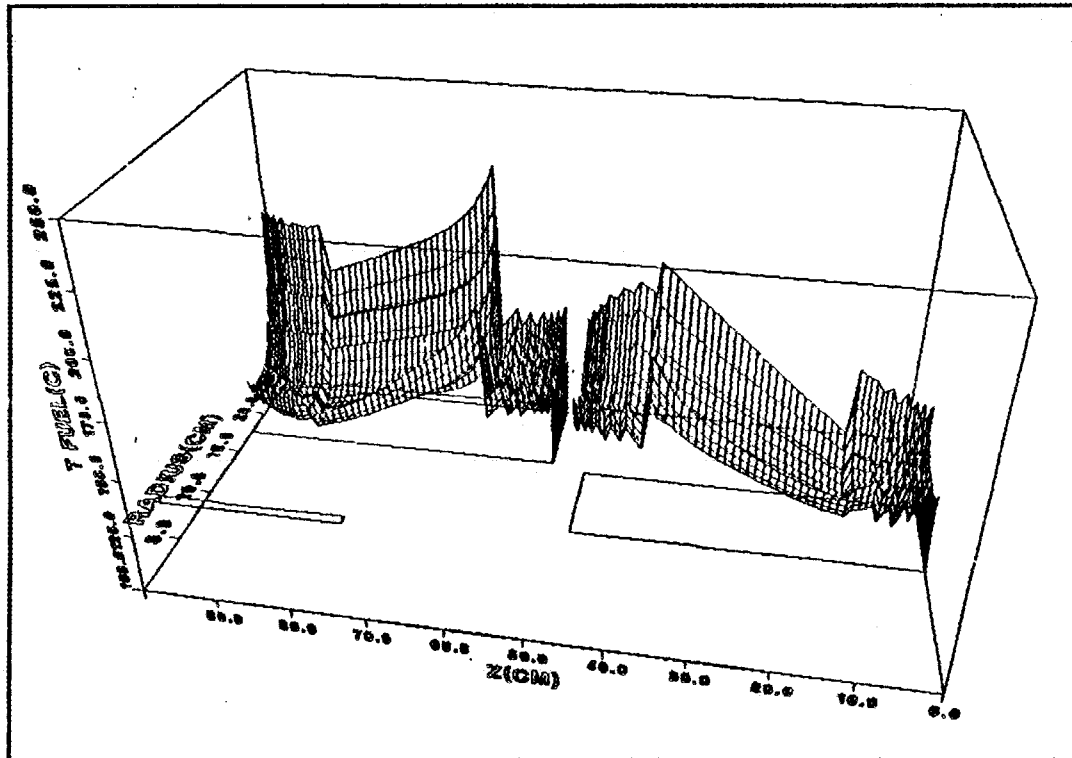
DESIGN E10 3.5 DAY TFUEL

11.15.57 MAR 20 2007 1986 J05-700 15:44 WISCONSIN 1000



F.0 5

DESIGN E10 7 DAY TFUEL



11-46-05 THU 26 SEP 1989 JOB=F10 11500 DISPLAY 10.0

F10 6

1 14-16.13 INR 20 50' 1983 JOB-750 , ISSOC DISPLAY 10.0

DESIGN E10 10.5 DAY TFUEL

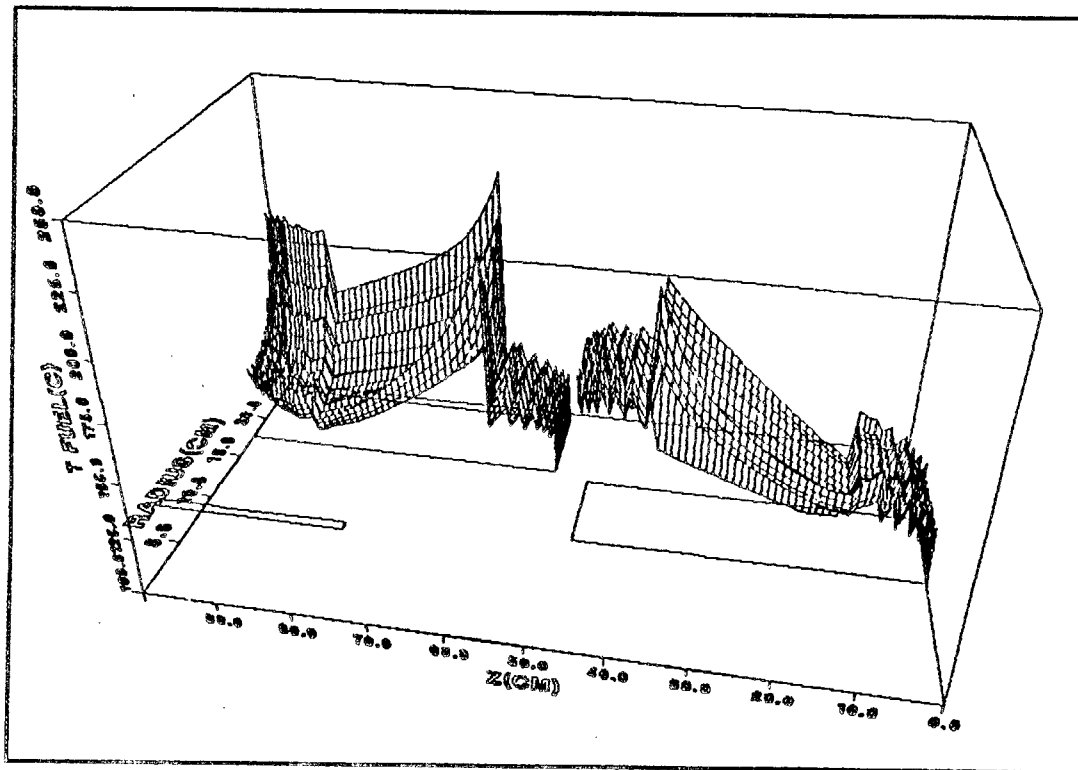
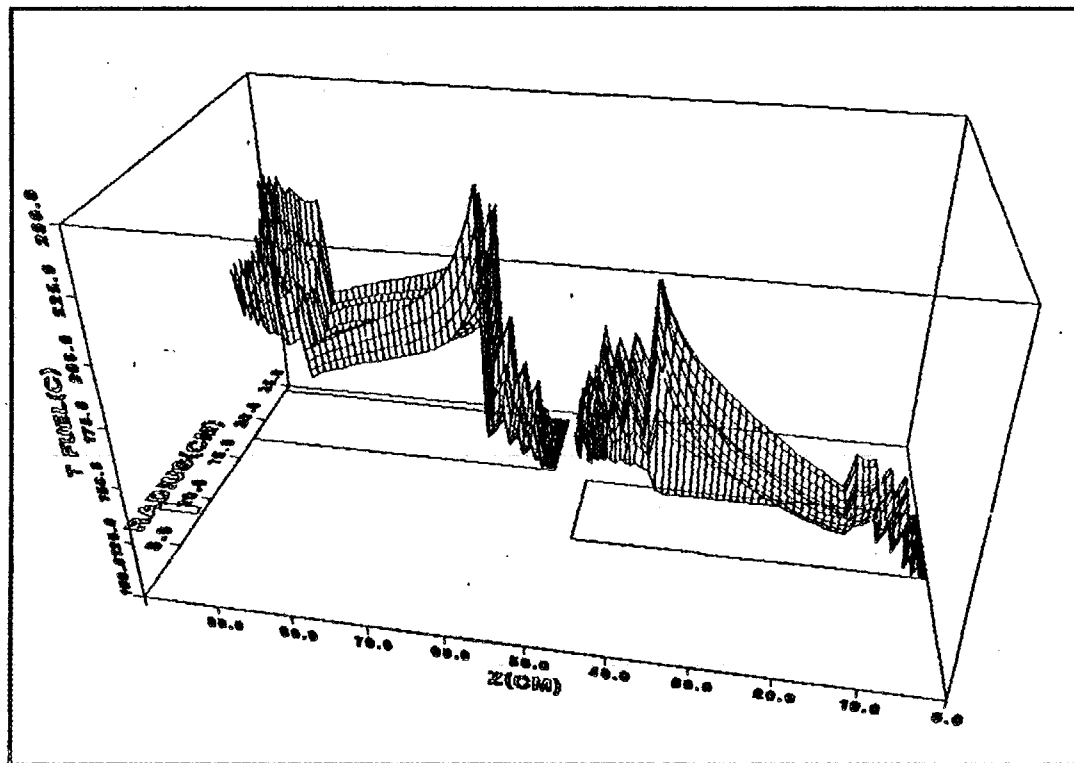


Fig 7

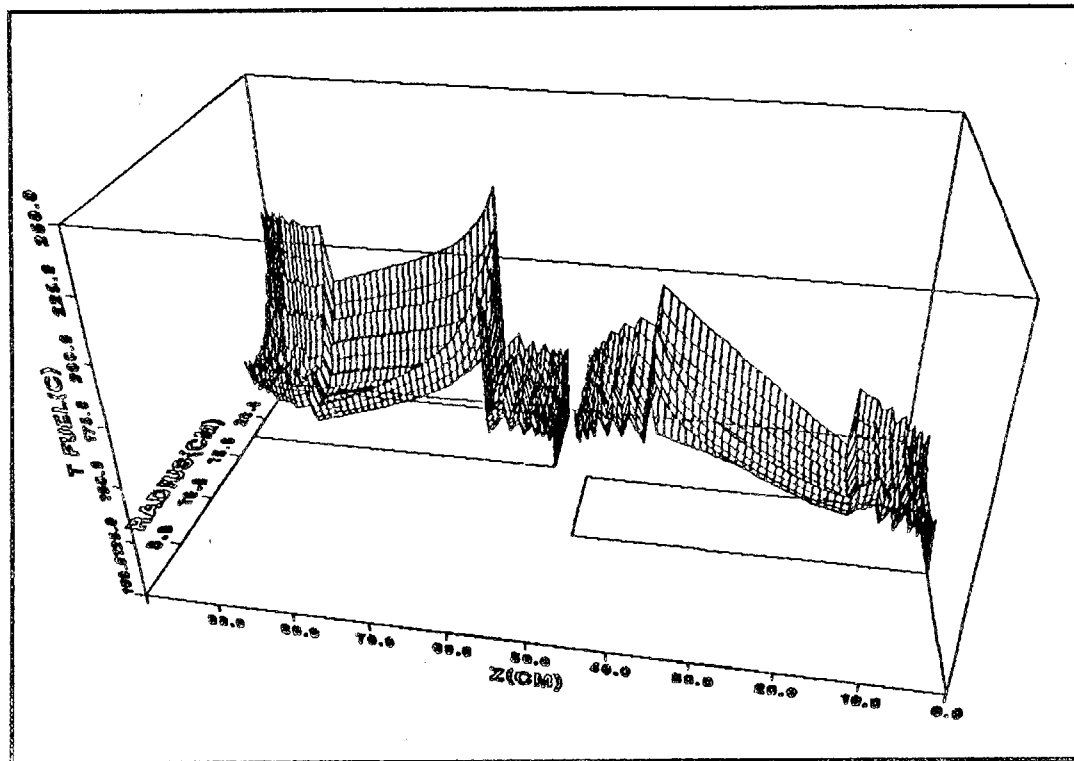
DESIGN E10 14 DAY TFUEL



14.06.44 THUR 26 SEP, 1965 JOB-T02 / 15520 U133P1A 11.00

Fig 8

DESIGN E10 TIME AVERAGE T FUEL



14.46.55 THUR 28 SEP, 1988 JOB=FOO, 15500 DISPLA 10.0

F. 0

FUEL DEVELOPMENT AND EVALUATION OCTOBER 1989

G. L. Copeland

We are continuing to gather information on the testing of U_3Si_2 by JAERI in support of its use in the JMTR. It appears that very valuable information for ANS can be gained by cooperating in these experiments.

Preparations continue at Babcock and Wilcox for the rolling of the first full sized developmental plates for ANS.

Work is continuing at Argonne National Laboratory (ANL) on fabrication development, fuel performance modeling, and the irradiation simulation. A quality assurance assessment was conducted by DOE in October on the ANS work at ANL. The written report is not yet available. The ANL contribution to the monthly report follows.

ANL Contribution to the ANS Monthly Report for October 1989

I. Management/Experiment Design (J. L. Snelgrove)

The ANL portion of the ANS fuels work was under budget by \$33k at the end of FY 1989. An additional \$75k in interim funding has been provided by ORNL during October. The \$108k available thus far for FY 1990 will allow work to continue at a normal pace at least through the end of November. With the cutoff of RERTR funds for fuel development, we have requested \$565k of ANS funds for FY 1990 to allow us to continue meaningful fabrication development along with the ongoing simulation and modeling efforts.

II. Fuel Development and Fabrication (R. F. Domagala, T. C. Wiencek, and H. R. Thresh)

As was done last month, this report has been prepared before the end of the month in order to accommodate the travel schedule of one of the authors of this section (RFD) and still have the report at ORNL in a timely fashion.

An important but time-consuming activity which took place in October was a DOE mandated and conducted Q-A "assessment" of our work on this project. The actual assessment took place on October 17-18 but prior to that considerable effort had to be expended in reviewing the organization of the documentation of all the paperwork required for the assessment. This will be followed sometime in the immediate future by a written report by DOE personnel who will require explicit action and a written response to any items they may feel are not documented to their satisfaction.

A total of 14 slices with a nominal thickness of 0.015 in. (0.38 mm) were cut from three different U-Si alloy ingots. These pieces have been delivered to R. C. Birtcher (ANL/MSD) for ion-irradiation studies. The specific depleted uranium-base alloys cut include: ingot D259A, an as-arc-cast alloy at a composition of 7.3 wt% Si, ingot D256, an as-arc-cast alloy at a composition of 7.0 wt% Si, and ingot D266D, arc-cast and heat treated at 800°C for 72 h at a composition of 4.0 wt% Si. All compositions are nominal since the cost of conducting analyses was considered prohibitive. Nevertheless, based on our practice and experience with many other U-Si arc-melted alloys, the true compositions are almost certainly very close to the nominal (intended) compositions.

Plans are being formulated for the production of tapered-compact miniplates at U loadings in the range of ~1.5 to 2.0 gU/cm³ in the 0.030 in. (0.76 mm) thick fuel zone of 0.050 in. (1.27 mm) thick plates. Early experiments will be conducted with W powder as a surrogate fuel. The objectives of these experiments will be to determine how homogeneously the fuel zone concentration of W (representing U₃Si₂) can be fabricated and how smoothly the concentration gradient will develop at the longitudinal (compact taper) ends of the plates.

Preliminary to work on the compacts and miniplates fabricated from them, we are conducting a thorough inventory of materials left from the RERTR program. Such items include W and Al powders, B₄C powder, 6061 clad and

frames, as well as dies and punches. With a restricted budget we must use existing materials and hardware to the greatest extent possible.

Since the present ANS core design incorporates burnable poison at the ends of the plates, effort has been directed to locate sources of supply not only of B_4C but also of "BORAL" a trademark product which apparently covers an Al-clad dispersed phase B_4C -Al composite in one instance but also describes a B-Al alloy used as a master alloy in the aluminum industry. Information and samples are being gathered although it is not clear that a commercially available product will satisfy the needs of the fabrication aspect of this project. Therefore, additional up-to-date information is being accumulated on B_4C powder availability, size, price, and purity.

Finally, the 22 FANS described in several previous monthly reports are ready for machining to final dimensions, at which point they become "HANS" and will be identified as such according to serial numbers assigned by ORNL. These HEU units contain either U_3Si_2 , UAl_2 , UAl_x , or U_3O_8 powders in the fuel zone.

One point concerning the FANS should be recorded. In the radiographs taken after e-beam welding and He leak testing, a number of tiny "white spots" are visible at the top of several FANS. These particles are almost certainly bits of W which sputtered from the run-off and run-on tabs which are standard components of the fixturing for weld closures. We will identify the exact location, size and number of these particles and will discuss with cognizant personnel at ANL and ORNL if these particles should be removed or may be left in place.

III. Other Tasks

Postirradiation Examinations (G. L. Hofman, and L. A. Neimark)

No report this month.

Analytical Modeling (J. Rest, G. L. Hofman, M. C. Billone, and S. A. Zawadzki)

In order to understand the recently observed rate dependence of fission gas bubble swelling in U_3Si_2 , the effects of trapping of interstitials and vacancies on the irradiation-enhanced gas atom diffusivity are being analyzed. The concept of defect trapping has frequently been invoked to explain the improved swelling resistance of metals and alloys brought about by minor solute additions. In studies on the swelling behavior of irradiated alloys¹ it has been shown that solute segregation and trapping effects must be taken into account simultaneously in order to predict the temperature, the defect-production rate, and the compositional dependence of void swelling. Binding between defects and solutes can lead to the coupling of solute fluxes to defect currents which, in turn, can cause a redistribution of solute and

¹P. R. Okamoto, N. Q. Lam, and H. Wiedersich, "The Effects of Defect Trapping and Radiation-Induced Solute Segregation on Void Swelling," Proceedings of the Workshop on Correlation of Neutron and Charged Particle Damage held at Oak Ridge National Laboratory, June 8-10, 1976.

solvent atoms in the material. Trapping of defects by solute atoms enhances defect recombination and thereby reduces the fraction of radiation-produced defects which contribute to the formation of dislocation loops and voids. Solute segregation can deplete regions away from sinks of strong trapping solute elements and, thereby, reduce the extent of defect recombination in the matrix and the swelling resistance of the alloy.

In all cases reported to date, "small size" alloying elements segregate towards defect sinks if the fractional change in lattice parameter per unit change in solute concentration is taken as a measure of solute size in an alloy. The solute size effect may be associated with the formation of mixed <100> dumbbell interstitials in which an undersized solute, but not an oversized one, can occupy one end of the dumbbell. If tightly bound mixed dumbbells can migrate as complexes with energies less than or comparable to the vacancy migration energy, the mixed dumbbell component will constitute a large fraction of the total interstitial flux to sinks. As the solute concentration builds up at sinks, back diffusion induced by the concentration gradient increases. If back diffusion occurs predominantly by the vacancy mechanism, solute segregation to sinks, and hence, solute depletion of the matrix may become especially severe under conditions which favor relatively long transient times and low vacancy mobilities, i.e., low defect production rates and low temperatures.

Appreciable void swelling is not expected in U_3Si_2 at the low temperatures characteristic of the miniplate irradiations (significant void swelling in the Al matrix and cladding is a possibility). However, as the fission spike-induced gas atom diffusion coefficient can be expressed as a function of the effective concentration of vacancies, a reduction in the vacancy population will have a direct effect on the long-range diffusion of gas atoms and, thus, on gas bubble swelling. The fission gas bubbles, on the other hand, act as sinks for vacancies and as possible sites for defect recombination and, thus can, in principle have an indirect effect on the mobility of the gas atoms. In addition, defect structures within the matrix (e.g., dislocations), act as sinks for gas atoms and as sites for preferential bubble growth.² In effect, the effects of bubble segregation to sinks (dislocations) may be analogous to solute segregation in metals. Bubble segregation can deplete regions away from sinks of bubbles and, thereby, reduce the extent of defect recombination and vacancy getting (by bubbles) in the matrix and subsequent matrix bubble growth. A theoretical model is in the process of being formulated in order to assess the viability of the above ideas.

²J. Rest, G. L. Hofman, and R. C. Birtcher, "The Effect of Crystal Structure Stability on the Mobility of Gas Bubbles in Intermetallic Uranium Compounds," to be published in the proceedings of the 14th International Symposium on Effects of Radiation on Materials, June 27-30, 1988, Andover, Massachusetts, and J. Rest, G. L. Hofman, and R. C. Birtcher, "The Effect of Crystal Structure Stability on Swelling in Intermetallic Uranium Compounds," to be published in the proceedings of the 1988 International Meeting on Reduced Enrichment for Research and Test Reactors, San Diego, CA, Sept. 19-22, 1988.

Internal Correspondence

MARTIN MARIETTA ENERGY SYSTEMS, INC.

B.H.Montgomery
D.L.Selby

November 3, 1989

J.A.Johnson

Monthly Activities, October 1989ANS Corrosion Test Loop

R.E.Pawel	G.L.Yoder
M.T.McFee	B.H.Montgomery
S.P.Baker	T.J.Henson
J.F.King	J.D.McNabb
O.B.Cavin	L.D.Chitwood
R.R.Leedy	

1. CTEST No.15 was completed on October 6, 1989 after 24 days of operation. As noted in the last Monthly Report, this test was the second in the series in which the heat flux is being varied while holding the inlet coolant temperatures and coolant velocities constant. For an average heat flux twice that of CTEST No.14, the oxidation rate was more rapid, but films of only modest thickness were measured at the conclusion of the experiment. In addition, a heavy Fe-rich layer was apparent and no spallation was found. The calculated rate curves for CTESTS No.14 and No.15 are given in Figures 1 and 2.

CTEST No.14 exhibited very little oxide build up, with no significant difference in thickness observed along the length of the specimen. While the average thickness of the film was small (4 or 5 μm), as indicated in the Figure, it also exhibited numerous irregular areas - a few were much thicker. Such features have been observed previously and are apparently common in the thinner films, or in the early stages of growth.

CTEST No.15 exhibited a higher rate of film thickening. The rate curves drawn in Figure 2 are computer-smoothed curves and do not really include an apparent change in the rate behavior after about 100 hours. The cause of this inflection is not known, but the coolant pH was observed to increase from its initial operating range (4.9 to 5.0) up to about 5.1 for about 12 hours during this time period.

2. CTEST No.16 was the third in the above series with the average heat flux set at an average heat flux of three times that of CTEST No.14, or 18.6 MW/m^2 . This was the highest power level (by almost 20 percent) that has been undertaken in our testing program. The test was started on October 17, 1989 with the following loop parameters:

Coolant pH	= 5.
Average Heat Flux	= 18.7 MW/m ²
Coolant velocity	= 25.6 m/s
Inlet coolant temp	= 49.°C
Mid-spec coolant temp	= 69.°C
Inlet coolant pressure	= 3.7 MPa

About four hours into the test, the computer control system aborted the run for an as-yet-undetermined reason. After checking the DAS for potential causes, the loop was restarted (carefully!) the next morning without difficulty. The response of the system at this time implied that no profound change in the thickness or properties of the oxidation product had taken place. The experiment was continued until October 20, 1989, where after 58 hours of operation it was stopped with measured temperatures at the hot end of the specimen at about 480°C.

Calculations based on tear-sheet information are given in Figure 3, showing rapid increase in the film thickness particularly at Position 6 on the specimen (25mm from the coolant exit end). These preliminary results indicate that the heat flux in the hot end of the specimen exceeded 21 MW/m² near the end of the experiment. While not apparent from the rate curve, spallation had commenced at Position 6. Examination of this region at low magnification revealed the presence of several "eruptions" of the type found in CTESTS No.7 and No.10.

3. A letter report (REP to BHM, 10/10/89) addressed the "Probability and Consequences of Local Specimen Failure during Hot-Spot Test (presently set-up as CTEST No.17) in ANS Corrosion Test Loop". The conclusions of the inquiry were that:

- (1) with careful monitoring of the loop parameters, conditions are favorable for a routine, trouble-free experiment;
- (2) if pressure-drop and resistance indicators are not sufficiently sensitive, then breaching of the specimen may occur if the experiment were inadvertently allowed to run for too long;
- (3) catastrophic burning of the aluminum is extremely unlikely to occur, even in the event of partial or complete burn-through;
- (4) If the specimen were breached by a local melt-through, the safety system would quickly terminate the experiment without serious safety or environmental consequences;
- (5) If the breach of the specimen were virtually instantaneous, and resulted in a complete loss of electrical path, there would be a substantial arc. However, we feel that it should be localized to the area of the failure and contained by the specimen's stainless steel back-up plates.

4. The Pool Boiling Corrosion Experiment was reassembled during the month of October, and the data acquisition program was completed. A watchdog timer was installed between the PC

and the power supply which monitors the PC to ensure that the data acquisition/safety software is operating at all times during the test. If the timer detects that the system is not operating, it automatically shuts off the power supply.

An operating procedure is presently being prepared for the initial test. The shakedown test will use four thermocouples internal to the heater element and untreated demineralized water in the pool. This test will be used to ensure that unattended operation of the experiment can be accomplished. Heat flux levels during the test are expected to be approximately 0.5 MW/m^2 . (GLY)

Rep. 11/3/89
R.E. Pawel, 4500-S, T-32, MS-6156, 4-5138

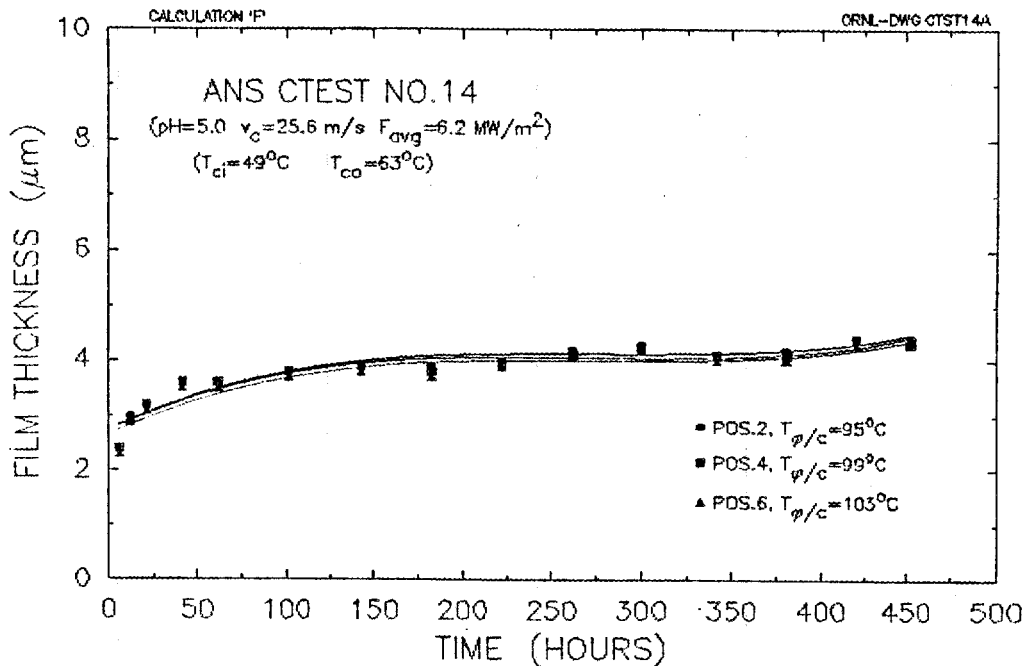


Figure 1. Calculated Film Growth for CTEST No.14

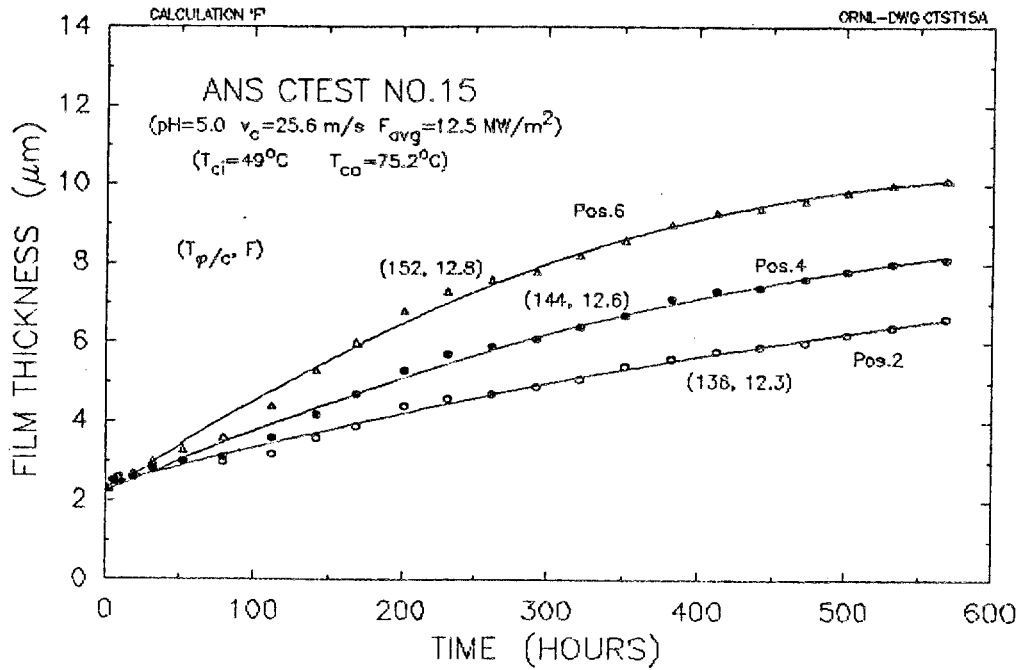


Figure 2. Calculated Film Growth for CTEST No.15

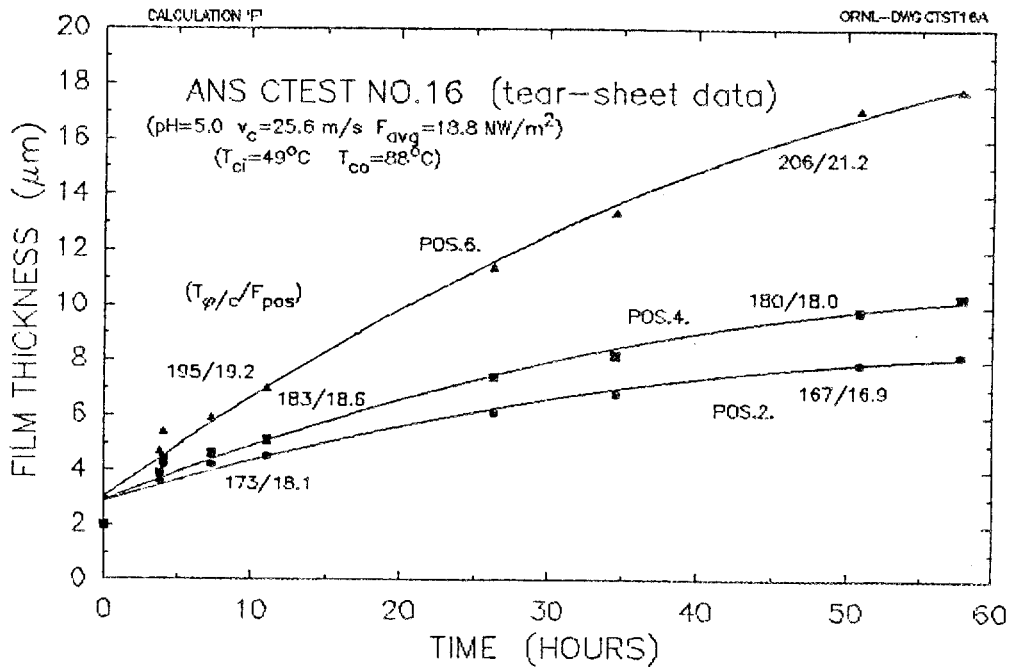


Figure 3. Calculated Film Growth for CTEST No.16 (tear-sheet data)

A Relationship, Under Certain Limited Operating Conditions,
Between Oxide Growth Rate and Inlet Temperature

J. A. Crabtree
B. H. Montgomery
R. E. Pawel
C. D. West
G. L. Yoder

Internal Correspondence

MARTIN MARIETTA ENERGY SYSTEMS, INC.

October 4, 1989

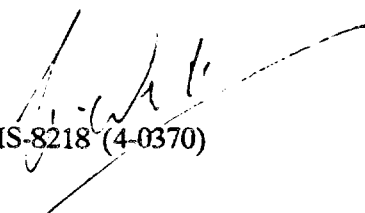
B. H. Montgomery, FEDC, MS-8218

A Still More Reductionist Slice of the Corrosion Loop Data

The corrosion loop data seem to establish that pH, inlet water temperature and bulk water temperature are major parameters influencing the oxide growth rate. Bulk temperature in particular may be only a surrogate for some underlying physical variable, such as interface temperature or the increase in water temperature above the inlet temperature (which presumably could significantly affect the solubility of some species present in the inlet water).

Other variables that may or may not affect the growth rate, but which seem in any case to be less sensitive, are heat flux, oxide thickness, and coolant velocity.

We now have lots of plots to help us to begin isolating the effects of different variables, and I wish to prepare yet another. Near to the inlet end of the specimen, the bulk temperature and the inlet temperature are nearly equal, i.e., they are not variables independent of each other. Near to the beginning of the cycle, the oxide thickness is nearly zero. Therefore a tabulation of the initial oxide growth rate measured at thermocouple 1 or 2 in each of the pH=5.0 runs would give us a data set in which some of the variables (specifically pH, oxide thickness, and the difference between bulk and inlet temperatures) do not in fact vary. If you agree, I should like to gather these data in the form of the attached table and perhaps as plots also.



C. D. West, FEDC, MS-8218 (4-0370)
Director, ANS Project

CDW:bab

Attachment:

cc/att: R. E. Pawel
G. L. Yoder
File - NoRC

Table: pH = 5.0 Growth Rates

Test No.	T _{in} , °C	Mw/m ² ^a	V _c , m/s	Initial Growth Rate ^b
11	39	11.9	19.2	
10	39	15.7	25.5	
8	43	11.7	25.4	
14	49	6.2	25.6	
15	49	12.4		
9	57	12.0	25.5	
13	67	10.6	27.8	
5	75	5.3	12.8	
7 ^c	80	11.6	24.2	

^aAverage

^bTime zero slope calculated from the fitted thickness vs time curve at thermocouple No. 2

^cInitial slope, where pH = 5, only

Plot

Initial growth rate vs inlet temp for 10-12 Mw/m² runs (11, 8, 15, 9, 13, 7)

CDW/10-04-87

Results presented in response to the memo (West to Montgomery, 10-4-89) are very interesting. Figure 1 plots only those points (from CT 7, 8, 9, 11, 13) for which the heat flux is almost the same (10.4-11.6 MW/m² - see table below). The points appear to lie on a good, straight line, shown in the figure, which is a least-squares fit. Here, then, is a limited but useful start to the correlations we need: for aluminum plates cooled by pH5 water flowing at ~20-30 m/s, the initial growth rate of oxide near the inlet is linearly dependent on inlet temperatures, in the range 40-80°C, with the numerical relationship given by rate of growth (micrometers/h) $\approx .0039 \times T_{\text{inlet}} (\text{°C}) - 0.154$. Inspection of the points suggests that an exponential may be an even better fit, and this will be tried in the future.

Moreover, the initial growth rates near the inlet do not correlate with the interface temperature, CT 11 having almost the highest interface temperature but the lowest growth rate.

Table 1. Conditions for pH 5, 10-12 MW/m² tests

Run no.	T _{inlet} ^b °C	Heat flux, ^a MW/m ²	V _{coolant} m/s	T _{bulk} ^a °C	T _{interface} ^a °C	Initial growth rate, μm/h
11	39	11.6	19.2	44.2	147.0	.00527
8	43	11.5	25.5	47.2	127.7	.01273
9	57	11.6	25.5	61.0	137.6	.00116
13	60.5 ^b	10.4	27.9	64.0	127.1	.06664
7	79	11.4	27.3	83.1	149.6	.16440

a

At TC 2 location.

b

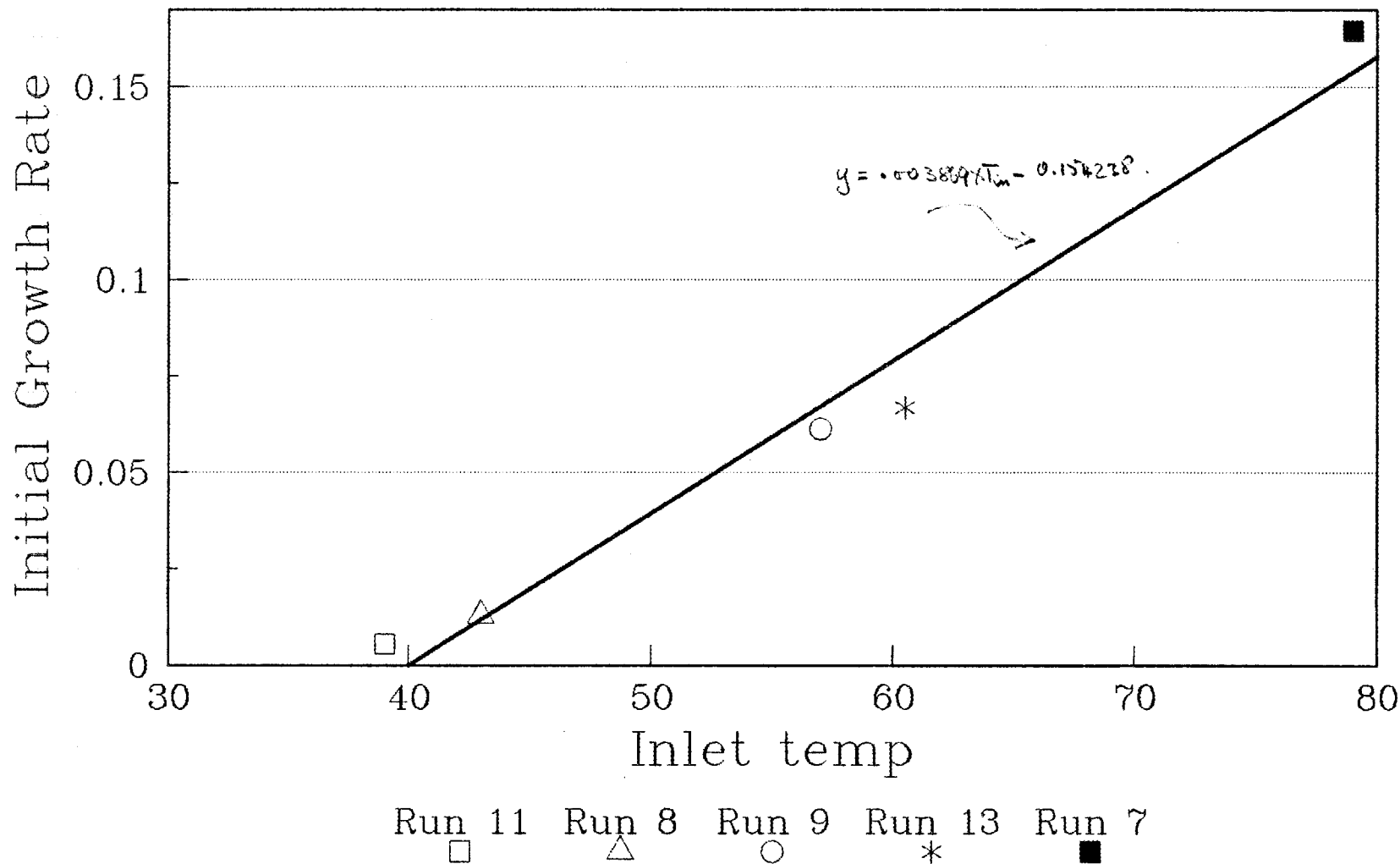
At beginning of test - later raised to 67°C.

In Fig. 2, the results from three other tests (CT 5, CT 10, and CT 14), that were carried out under different conditions, are plotted. For CT 10, all the conditions were similar to those used in deriving the straight line correlation, except the heat flux, which was higher. The oxide growth rate was also higher than the correlation. Similarly, for CT 14, with a lower heat flux, the oxide growth rate was also lower. For CT 5, the heat flux was again lower, and so was the coolant velocity, and so was the growth rate.

The results from CT 10 and CT 11 are also consistent with a sensitivity to heat flux and/or coolant velocity, or to some related variable such as metal temperature or oxide

FIGURE 1

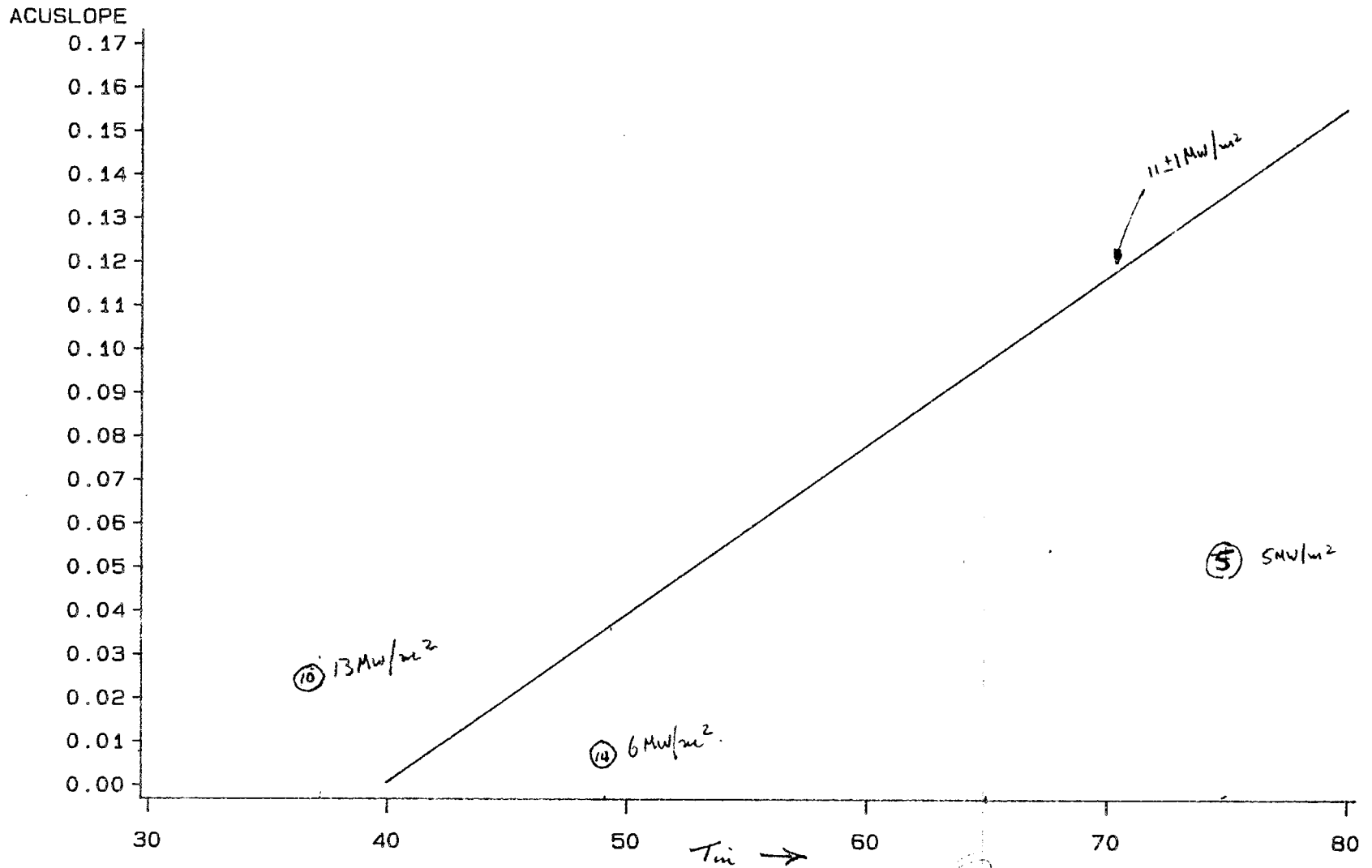
Initial Growth Rate vs Inlet Temperature for 10-12 Mw/m² Runs



IGRVSIT/JAJ

FIGURE 2

INITIAL GROWTH RATE VS. INLET TEMP.



temperature. These two tests had the same inlet temperature and very similar bulk temperature (at the TC 2 location). However, the growth rates - even near to the inlet and early in the cycle - were very different, as shown in Table 2. The factor four difference in growth rate is surprisingly large, and may reveal an undesirably high sensitivity to operating conditions.

Table 2. Initial growth rates and conditions in CT 5, 10, 14, and 11

Run no.	T_{inlet} °C	Heat flux, ^a MW/m ²	$V_{coolant}$ m/s	T_{bulk} ^a °C	$T_{interface}$ ^a °C	Initial growth rate, μm/h
5	75.5	5.2	12.9	78.8	136.7	.05453
14	38.1	5.7	25.7	40.3	83.6	.00803
10	37.5	13.1	25.6	42.2	135.5	.02363
11	38.7	11.6	19.2	44.2	147.0	.00527

^a

At the TC 2 location.

C. D. West/11-10-89

Internal Correspondence

MARTIN MARIETTA ENERGY SYSTEMS, INC.

November 10, 1989

J. A. Johnson

October Monthly Progress Report for Structural Analysis Activities on ANS

1. Flow Test of A Single Involute Epoxy Plate (R. L. Battiste, W. F. Swinson, and G. T. Yahr)

Preparation continued for a test to evaluate the structural response of an involute plate as water flows past on both sides through involute channels. The test plate is made from epoxy because the low modulus of elasticity of epoxy lowers the critical velocity. Data from these tests will provide important data for benchmarking the analytical methods that are used to design the involute fuel plates for ANS.

A pressure regulator was received and installed to reduce the pressure variations in the demineralized water supply which was earlier observed to fluctuate between 0.97 MPa and 1.65 MPa. The pressure regulator has reduced the pressure fluctuations to less than ± 0.1 MPa. This should be acceptable for the initial test.

Strain gages and lead wires were mounted on the epoxy test plate. Final assembly of the epoxy plate and the aluminum involute side plates into the test housing will be done next month in preparation for the test.

2. Studies to Support Conceptual Core Design Committee (G. T. Yahr and C. R. Luttrell)

A series of analyses were done to examine the effect increasing the inner hole size of the PS-2 core has on the maximum allowable flow velocity. The fueled volume, including the flow gaps, was held constant at 67.4-L and the fueled length of the fuel elements was held constant at 474 mm. The fueled annulus of the upper and lower elements and hence their cross-sectional areas were allowed to be different so that the collapse velocity was approximately the same. The involute plates were 1.27 mm thick and there was a 1.27 mm flow gap between plates. The involute generating radius was the inside radius of the fueled area.

Calculations were done for six different inner hole sizes. The results of the calculations are given in Table 1. The Miller method was used to calculate the collapse velocity for each of the elements. The maximum velocity was determined by multiplying Miller velocity

by 0.8 to account for intermittent welding of the involute fuel plates and dividing by a factor of safety of 1.5. The inside and outside radii listed in Table 1 are to the inside and outside of the fueled regions. Side plates are 7 mm thick; thus, the inside core diameter of the first case in Table 1 is 190 mm and the outside core diameter is 496 mm. As can be seen there are small differences in the velocities for the upper and lower fuel elements. The lower of the velocities for the upper and lower elements are plotted as a function of inside core diameter in Figure 1. The PS-2 design flow rate of 27.4 m/s is shown as a heavy horizontal line. This figure indicates that increasing the inside core diameter to 312 mm would provide a core that is not subject to collapse. This is an increase of 64 percent compared with the PS-2 inside core diameter of 190 mm. The corresponding increase in the outside diameter of the core would be from 496 mm for PS-2 to 562 mm; only a 13 percent increase.

3. Analytical Prediction of Involute Plate Hydraulic Instability (W. K. Sartory)

Exploration of a dynamic extension of the Miller-type flat-plate model of the involute instability problem is continuing. This model incorporates realistic boundary conditions at the channel entrance and exit to construct normal vibrational modes of the fluid-plate system. Numerical roundoff difficulties reported in the previous report have been overcome, and results that are interesting in two respects have been obtained.

First, the predicted instability threshold is around 1.8 to 2 times the Miller velocity. This is encouraging because experimental results of Swissaert seem to indicate stability above the Miller threshold, and because it might be helpful to the ANS design if both analytical and experimental evidence demonstrating stability well above the Miller velocity can be assembled. (As mentioned last month, some investigators have reported analytical findings that dynamic stability models predict instability far below the Miller velocity for disturbances of long wavelength. It appears the application of boundary conditions at the fluid entrance and exit eliminate such predictions.)

Second, the calculated mode shapes indicate that the deflection of the first marginally-stable mode is greatest at the plate inlet. It is known from experimental results that plate collapse occurs first at the inlet. Some investigators have proposed ad hoc models of lift at the plate inlet to account for this observation. It is encouraging that collapse at the inlet can be explained without such special-purpose models.

One approach to apply these flat plate results to involute plates is to artificially stiffen the flat plates based on finite-element involute deflection calculations, until the flat plates are as stiff as the involutes, and then to make the hydrodynamic stability calculations. Such stability calculations are planned.

J. A. Johnson
Page 3
November 10, 1989

Work is also beginning on a full involute plate model of the type described above.



G. T. Yahr, 9204-1, MS-8051 (4-0716)

GTY:tmp

Enclosure

cc: J. M. Corum
D. L. Selby
C. D. West

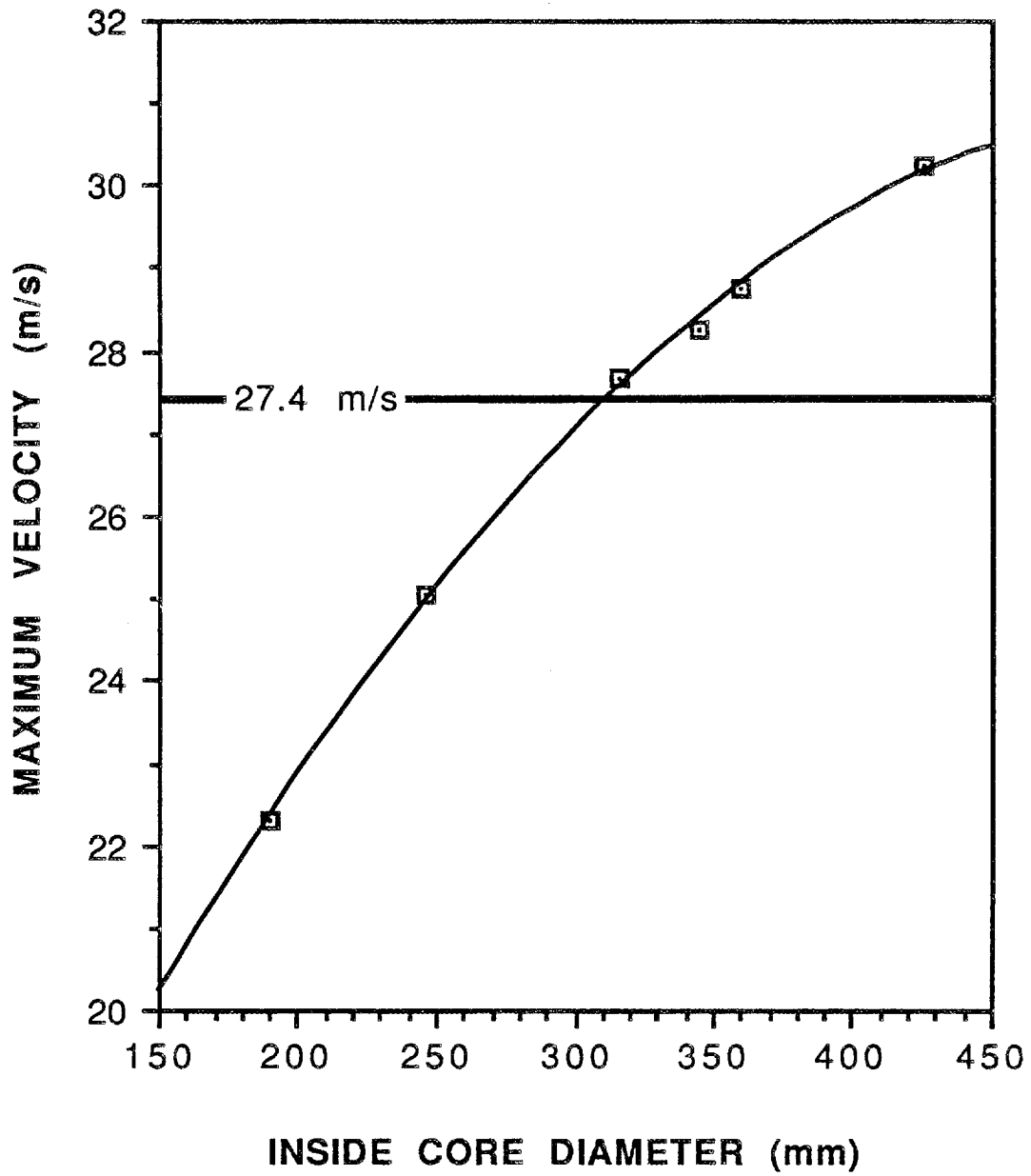


Figure 1. Maximum allowable flow velocity as a function of inside core diameter.

Table 1. Effect of increasing inside core diameter on the collapse velocity of ANS core.

Case Number	1	2	3	4	5	6
Lower Element						
Inside Radius (mm)	102	130	165	179	187	220
Outside Radius (mm)	169	191	219	230	237	264
Plate Span (mm)	89.01	75.31	62.84	58.27	56.69	48.40
Miller Velocity (m/s)	41.81	47.54	51.92	53.64	53.93	57.45
Maximum Velocity (m/s)	22.30	25.36	27.69	28.61	28.76	30.64
Upper Element						
Inside Radium (mm)	176	198	226	237	244	271
Outside Radius (mm)	241	255	275	284	289	312.5
Plate Span (mm)	77.00	65.20	54.31	51.66	49.15	44.68
Miller Velocity (m/s)	42.16	46.99	52.17	52.94	54.49	56.68
Maximum Velocity (m/s)	22.49	25.06	27.82	28.24	29.06	30.23
Inside Core Diameter (mm)	190	246	316	344	360	426
Outside Core Diameter (mm)	496	524	564	582	592	639

Internal Correspondence

MARTIN MARIETTA ENERGY SYSTEMS, INC.

November 10, 1989

J. A. Johnson, FEDC

ANS Cold Source Thermal-Hydraulics Progress Report, October, 1989

Fabrication of the cryogenic viewport assemblies has been resumed, with installation in the bath dewar expected soon.

New estimates of the liquid fraction are reported. The results are quite encouraging. Some unresolved and troublesome issues relating to the liquid fraction estimates are discussed.



T. L. Ryan

TLR:ldg

Attachment

Internal Correspondence

MARTIN MARIETTA ENERGY SYSTEMS, INC.

November 10, 1989

T. L. Ryan

ANS Monthly Progress Report, October, 1989

Thermal-Hydraulic Experimental Facilities

A visit was made to the Astronautics Group's Engineering Propulsion Laboratory in Littleton, CO, where we toured the National Aerospace Plane Slush Hydrogen Experimental Facility. We learned some things which will help in the ANS Cold Source R&D program, and are considering performing H₂/D₂ experiments at the EPL facility.

The fabrication and installation of the cryogenic viewport assemblies for the Characterization Test Article bath dewar had been delayed because of tolerance problems with tubing. Heavier-walled material was procured so that the critical parts could be accurately machined. The materials were received and fabrication activities have resumed. The results to date are quite good.

Thermal-Hydraulics Modelling

Efforts to accurately predict the pool liquid fraction have continued. The relevant figures were inadvertently deleted from the previous monthly report, so portions of last month's report are repeated herein.

Figures 1 thru 3 show the latest estimates of the liquid fraction (by volume). Figures 1 and 2 are calculations based on the model developed by Kazimi and Chen¹ (hereafter denoted as the KC model), and Figure 3 is based on a model developed by Ginsberg, Jones, and Chen² (hereafter called the GJC model). Each model assumes that heat is volumetrically deposited with spatially uniform heating density, that volumetric heating occurs only in the liquid phase, that the pool has a constant cross-section with an open top, and that the entire heat load is removed by vaporization. Some limitations of the KC model are discussed in last month's report. Many of them also apply to the GJC model. The GJC model is based on a more rigorous application of the two-phase flow drift flux model. Also, its authors compared it to a much larger body of data. I therefore believe it is the better model.

Referring to Figures 1 thru 3, some important points are evident. They include:

1. The KC model predicts a liquid fraction for the ANS cold source of $\sim 62\%$. This is based on a 0.42 m pool depth, hence a 0.26 m (0.42×0.62) collapsed liquid depth, at 0.15 MPa operating pressure. The GJC model predicts a $\sim 73\%$ liquid fraction for the 0.42 m pool depth.
2. The liquid fraction can be increased by elevating the operating pressure. For example, considering the 0.42 m deep pool at 0.30 MPa pressure, the KC model predicts a $\sim 68\%$ liquid fraction. Raising the operating pressure would, however, require structural and operational modifications which may prove unacceptable.
3. If the fluid properties and heating density are fixed, the liquid fraction depends only on collapsed liquid height, assuming that pool dimensions are large compared to bubble dimensions. Thus the pool's cross section does not affect the mean liquid fraction if the pool has straight, vertical sides (i.e., flow is one-dimensional).
4. The KC model predicts a liquid fraction for ILL with 5 kW total heat load and 0.38 m pool depth of $\sim 71\%$. The measured value is $\sim 80\%$. This yields $\sim 11\%$ error on liquid fraction, $\sim 45\%$ error on vapor fraction. The GJC model predicts $\sim 83\%$ liquid fraction, giving $\sim 4\%$ error on liquid fraction and $\sim 15\%$ error on vapor fraction. Geometry effects certainly introduce some error. I think that any adjustment for ILL's spherical geometry would lower the predicted liquid fraction.

A major difficulty with both models arises with respect to the two-phase flow regime. The KC model simply assumes that flow is churn-turbulent (C-T). The GJC model can be formulated for either bubbly or C-T flow; my calculations are based on C-T flow. The experimental and theoretical results have generally been presented with vapor fraction expressed as a function of dimensionless velocity (see Figure 4), where the dimensionless velocity is usually chosen to be the ratio of superficial vapor velocity at the pool surface to terminal bubble velocity in the bubble flow regime where bubble velocity is independent of bubble size.

Ginsberg, Jones, and Chen found that the transition from bubbly to C-T flow occurs when dimensionless velocity is in the range of 1 to 2. The ANS cold source will probably operate with a dimensionless velocity range of 0.5 to 1. Hence the GJC criteria says the cold source will operate in the bubbly flow regime. A quick glance at Figure 4 would suggest that if this is so, we have big problems, as the predicted vapor fractions in bubble flow are quite high. Fortunately, there exist a couple of caveats which may rescue us. First, the authors found that the C-T model actually correlates better with the bubbly flow experimental vapor fractions than does the bubbly flow model. Second, all the

experiments were done with water and some type of additive to enhance heating and/or flow visualization. In many cases, it was observed that as the impurity level increased, there was a tendency for the transition from bubbly to C-T flow to occur at higher dimensionless velocities; the bubbly flow seemed to get "locked" into a foamy regime which didn't trip to C-T flow as expected. The good news here is that impurities tend to effectively increase surface tension. If the bubbly to C-T flow transition dimensionless velocity happens to increase with surface tension, the transition velocity for cryogenics may be quite small, since they typically have very low surface tension (the surface tension of saturated H₂O is about 20 times that of saturated D₂ at 0.1 MPa).

Another troublesome issue regards the experimental results found by Kurtsman, Suvorov, and Ershler³. They observed a flow regime which they named the hydrodynamic boiling layer (HBL). They found bubble nucleation and growth to have negligible effect on the pool dynamics. Rather, they observed that much of the pool's lower section remained essentially single-phase liquid, and there was a layer of liquid-vapor mixture near the pool surface. At low power, the liquid superheat, the liquid velocity, and the two-phase mixture volume all exhibited periodic, or pulsed, behavior. At higher power, the periodic behavior gave way to steady state boiling, but still there was negligible effect by bubbles and the HBL apparently controlled the system dynamics. The natural convection (i.e., liquid velocity) was dramatically intensified by the presence of the two-phase layer. They reported that during pulsed boiling they observed the liquid velocity increasing from 0.01 m/s to 0.50 m/s or more. Neither the KC model nor the GJC model recognizes this flow regime; in fact it is hardly mentioned in the U.S. references that we have found. We are trying to analytically reproduce the reported results and to determine whether this phenomenon will affect the cold source.

In summary, the GJC model appears to yield good results, but there are several legitimate questions which must be answered in order to establish an acceptable level of confidence in the results. Some questions may only be answered experimentally.



Cliff Eberle

CCE:ldg

REFERENCES

1. M. S. Kazimi and J. C. Chen, Nucl. Sci. Engr., Vol. 65, p. 17 (1978).
2. T. Ginsberg, O. C. Jones, Jr., and J. C. Chen, ASME paper 79-HT-102, 1979.
3. E. D. Kurtzman, L. Ya. Suvorov, and B. V. Ershler, High Temp., Vol. 15, no. 5, p. 857 (1977).

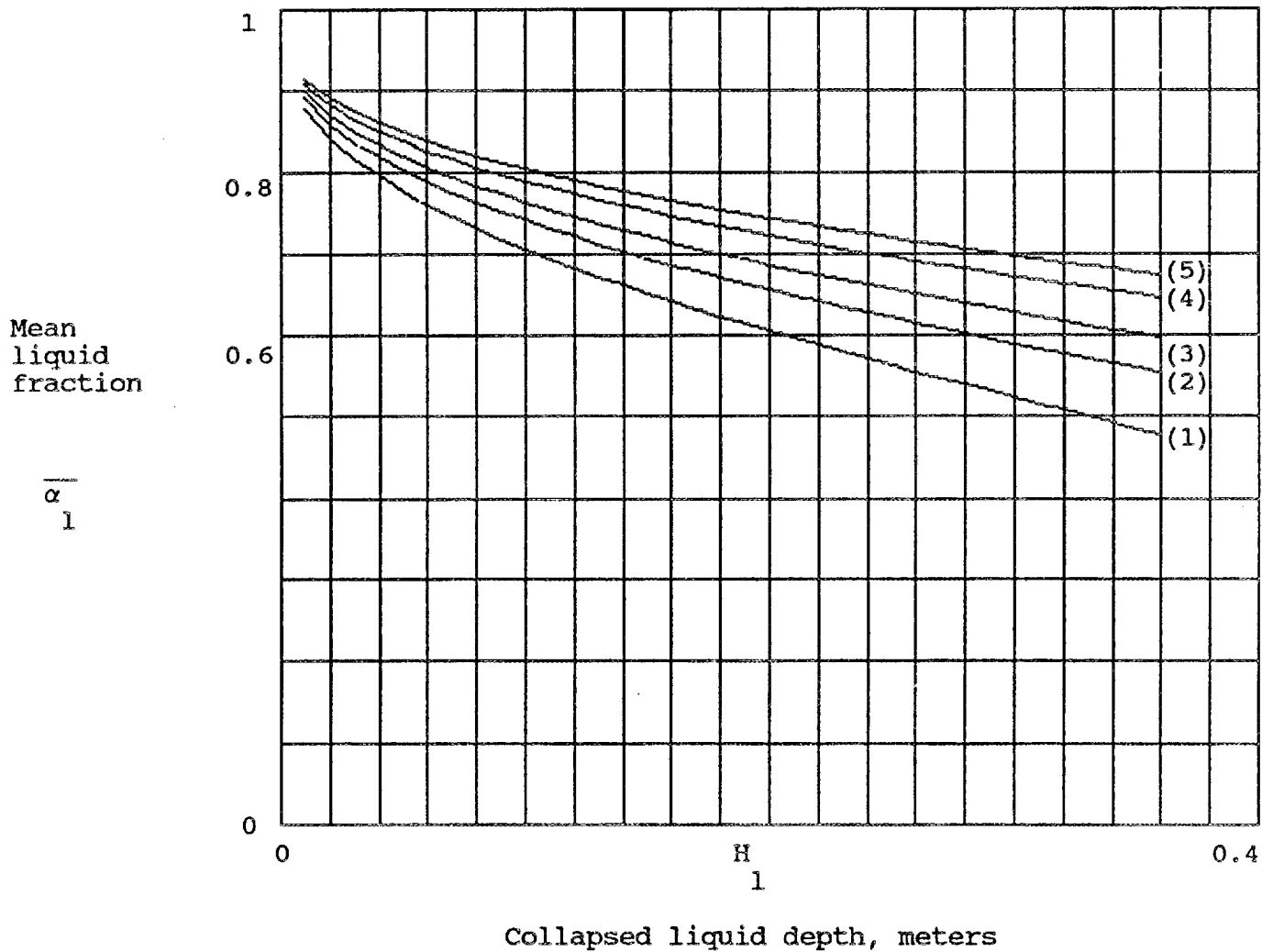


Figure 1. Calculated mean liquid fraction vs. collapsed liquid depth for a volume-heated, boiling LD2 pool with 0.42 kW/liter (equivalent to ANS baseline) heating density.

Key: (1) Pressure = 0.10 MPa
 (2) Pressure = 0.15 MPa
 (3) Pressure = 0.20 MPa
 (4) Pressure = 0.30 MPa
 (5) Pressure = 0.41 MPa

Note:

Pool depth := $\frac{H_1}{\bar{\alpha}_1}$

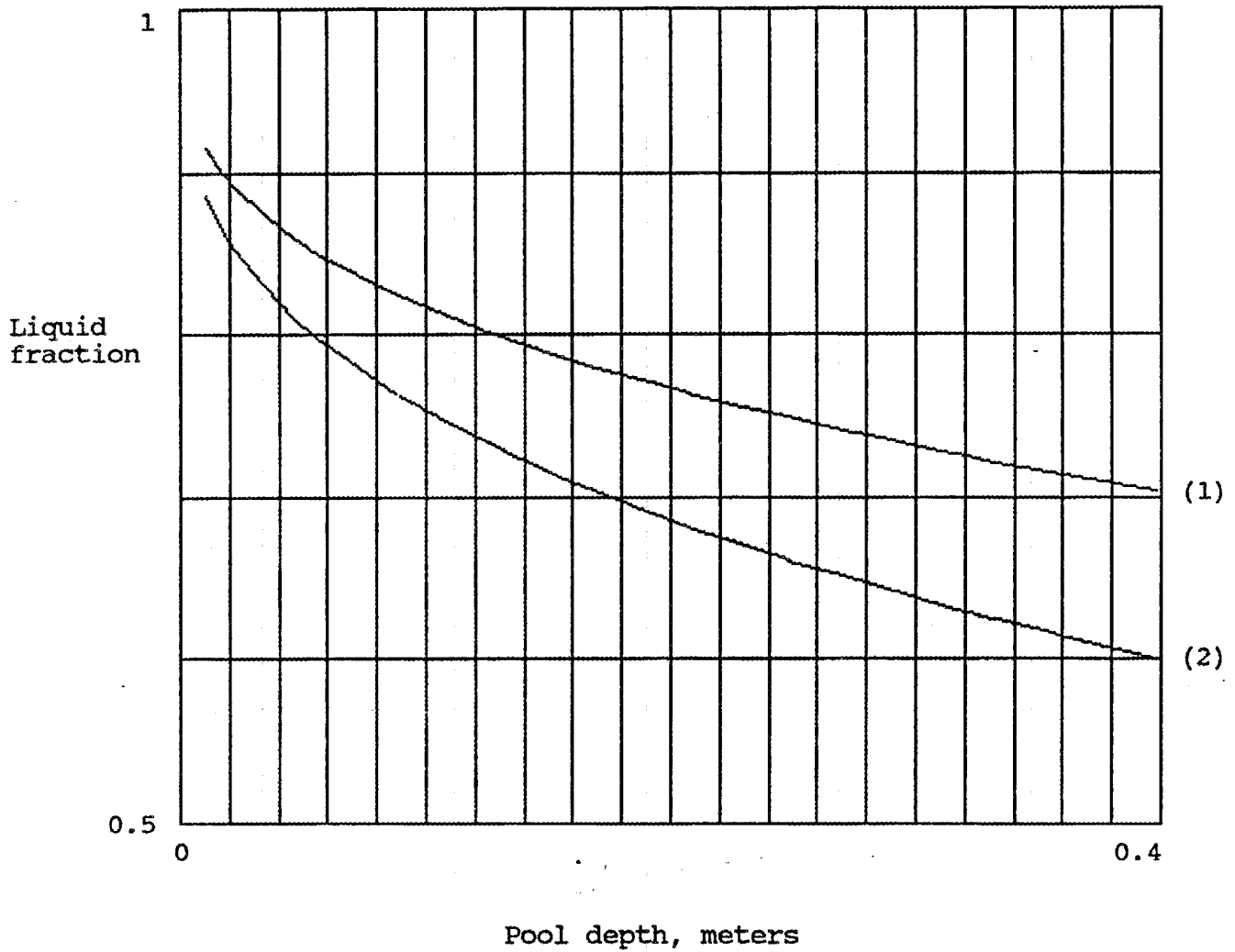


Figure 2. Calculated liquid fraction vs. pool depth for a volume-heated, boiling LD2 pool at 0.15 MPa pressure and 0.21 kW/liter heating density (ILL nominal conditions).

Key: (1) Mean liquid fraction
 (2) local liquid fraction

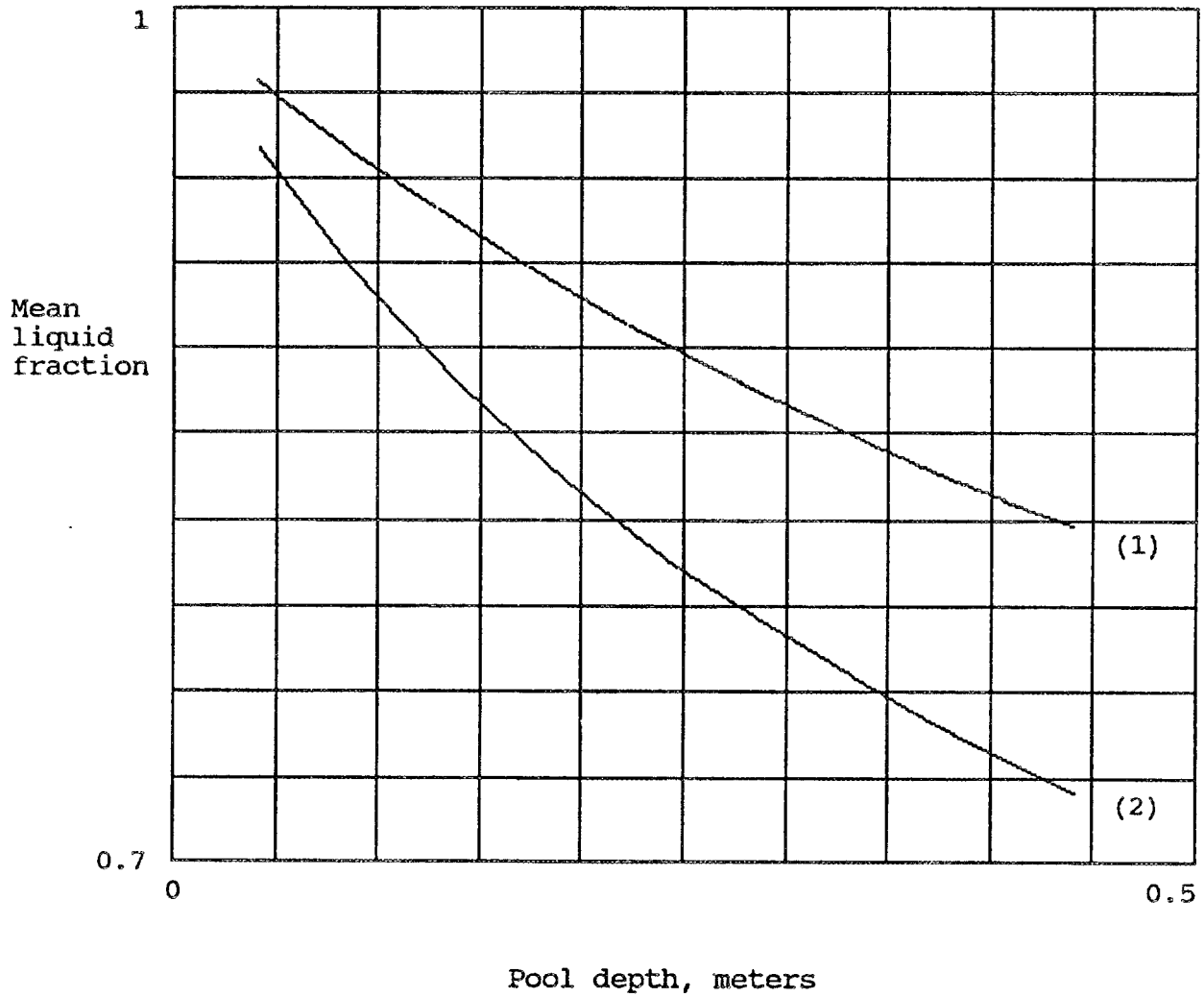


Figure 3. Calculated mean liquid fraction vs. pool depth for a volume-heated, boiling LD2 pool at 0.15 MPa pressure.

Key: (1) ILL heating density (0.21 kW/liter liquid)
 (2) ANS heating density (0.42 kW/liter liquid)

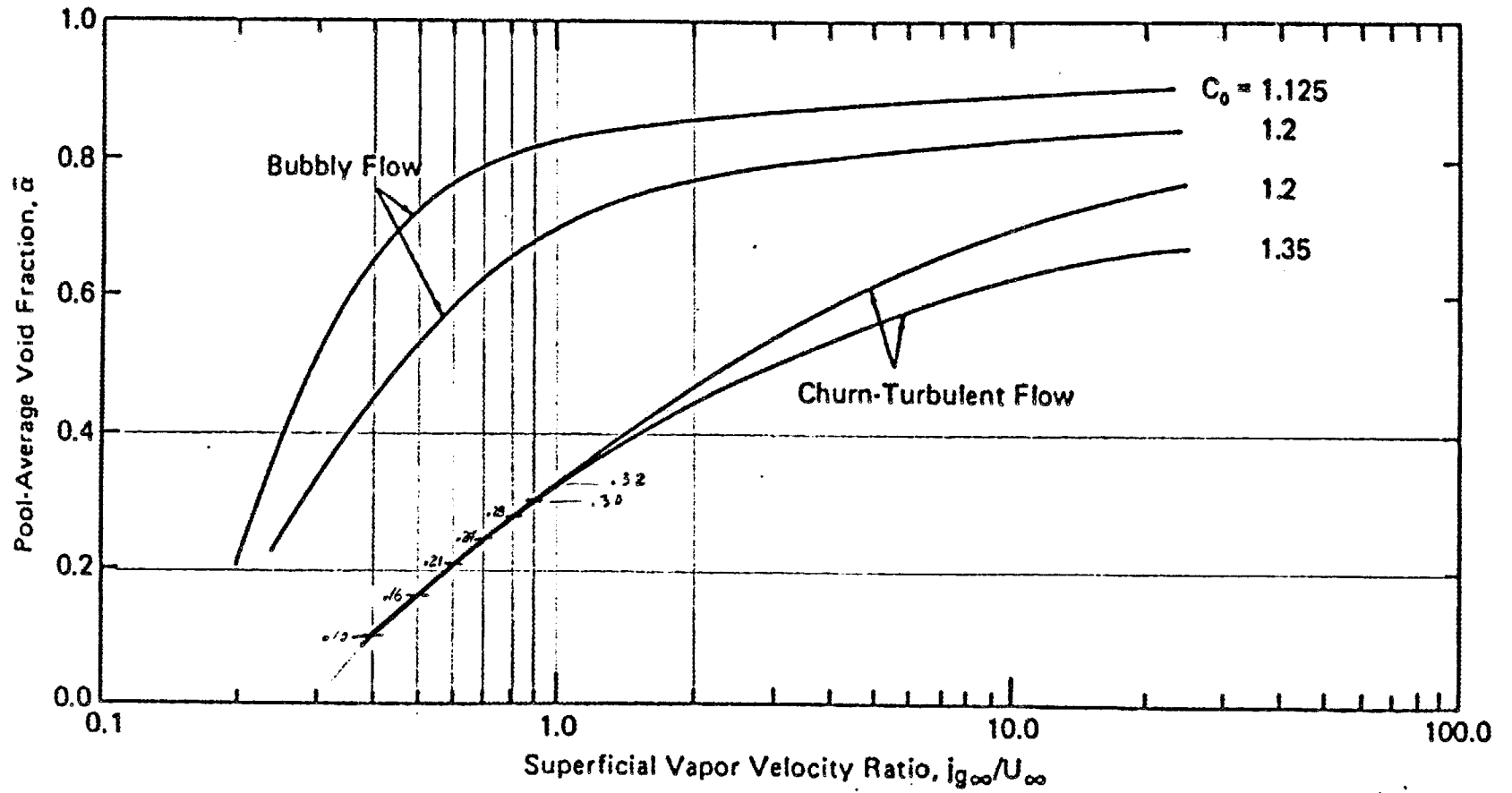


Fig. 4. Prediction of pool-average void fraction.

FROM REF. [2]

Design Calculations for the ANS Cold Source

R. A. Lillie

Two additional options were added to the two-dimensional cylindrical R-Z to R-Z boundary angular flux transformation coupling code DTD (Dort to Dort). These options consisted of 1) allowing a zero boundary flux along those portions of the coupling boundary which were outside of the original geometry and 2) allowing a condition of symmetry to exist (or not exist) at any Z plane in the original geometry. Previously, the angular flux at the closest mesh point in the original geometry had to be used to obtain the coupling boundary flux at all portions of the coupling boundary which were outside of the original geometry and symmetry had to exist at the $Z = 0$ plane in the original geometry. With the elimination of these restrictions, the boundary angular fluxes needed for the ongoing analysis of the thermal neutron beam tubes can now be obtained directly from the transformation code.

Calculations were also performed to complete the verification of the version¹ of DTD which allowed full angular rotation of one cylindrical geometry relative to another since this version will be needed for the verticle cold source beam tubes. (It will also be needed fairly soon for the analysis of the off axis no-line-of-sight thermal neutron beam tubes). Previously, this version of the code had successfully compiled and reproduced boundary angular fluxes for the default case, i. e., the coupled geometries are at right angles. As a result of these calculations, the code logic was greatly simplified and the angles of rotation were redefined. The original two euler angles of rotation were replaced with a polar angle and azimuthal angle of rotation as these angles are much easier to visualize. Unfortunately, the most up to date source deck of the version of DTD allowing full angular rotation (along with a massive amount of binary data) was destroyed on Oct. 27, 1989 when the account at LLL under which most of the cold source neutronics calculations were carried out was released.

Finally, a corrected copy of Table 9 appearing in last month's progress report² is included. The currents with no cavity present (column 4 in Table 9) were low by a factor of 6.28319. This factor was inadvertently left out in the conversion from angular leakage to current.

References

1. R. A. Lillie, April 1989 ANS Monthly Progress Report, Attachment 14.
2. R. A. Lillie, September 1989 ANS Monthly Progress Report, to be published.

Table 9. Calculated Gains in Neutron Current into a Neutron Guide Tube per unit Wavelength for varying Cavity and Neutron Guide Tube Radii

Cold source distance from Reactor centerline = 748 mm,
Cold Source diameter = 380 mm,
Cavity length = 190 mm

Neutron Energy Group	Lower Wavelength (nm)	Guide Tube Radius (mm)	Current (Neut./s/mm/m ²)		Gain				
			(no cavity)	59.4	Cavity Radius (mm)	71.3	83.1	95.0	106.9
15	1.65-2 ^a	47.5	8.80+14	3.14	3.40	3.48	3.48	3.47	
16	3.27-2	(82.4) ^c	1.36+15	2.53	2.73	2.80	2.80	2.80	
17	6.17-2		1.23+16	2.21	2.40	2.46	2.47	2.47	
18	1.28-1		1.94+16	1.47	1.57	1.62	1.62	1.62	
19	2.86-1		1.45+16	1.47	1.55	1.56	1.53	1.50	
20	5.02-1		3.56+15	1.61	1.67	1.67	1.62	1.55	
21	9.81-1 ^b		2.72+13	1.87	1.93	1.93	1.83	1.75	
15	1.65-2	59.4	8.86+14	2.81	3.15	3.33	3.38	3.38	
16	3.27-2	(94.3)	1.38+15	2.32	2.51	2.68	2.73	2.71	
17	6.17-2		1.24+16	2.07	2.25	2.38	2.42	2.42	
18	1.28-1		1.99+16	1.39	1.46	1.52	1.55	1.55	
19	2.86-1		1.50+16	1.37	1.41	1.43	1.44	1.40	
20	5.02-1		3.68+15	1.48	1.52	1.53	1.51	1.46	
21	9.81-1		2.84+13	1.68	1.73	1.74	1.71	1.63	
15	1.65-2	71.3	8.98+14	2.50	2.87	3.08	3.22	3.25	
16	3.27-2	(106.2)	1.41+15	2.07	2.33	2.48	2.60	2.63	
17	6.17-2		1.28+16	1.88	2.08	2.22	2.33	2.36	
18	1.28-1		1.99+16	1.35	1.41	1.46	1.52	1.54	
19	2.86-1		1.49+16	1.32	1.37	1.39	1.40	1.40	
20	5.02-1		3.68+15	1.40	1.45	1.48	1.48	1.44	
21	9.81-1		2.81+13	1.59	1.68	1.69	1.66	1.62	
15	1.65-2	83.1	9.11+14	2.20	2.60	2.90	3.05	3.17	
16	3.27-2	(118.0)	1.43+15	1.86	2.15	2.35	2.49	2.59	
17	6.17-2		1.30+16	1.71	1.94	2.12	2.22	2.33	
18	1.28-1		2.00+16	1.30	1.39	1.44	1.49	1.53	
19	2.86-1		1.49+16	1.26	1.33	1.37	1.38	1.38	
20	5.02-1		3.68+15	1.31	1.41	1.44	1.44	1.43	
21	9.81-1		2.81+13	1.45	1.58	1.64	1.63	1.60	

^a1.65-2 read as 1.65x10⁻².

^bUpper wavelength of group 21 is 9.05 nm.

^cValues in parenthesis are cavity radii needed for full illumination of neutron guide tube entrance with 2 deg. maximum deflection angle.

Internal Correspondence

MARTIN MARIETTA ENERGY SYSTEMS, INC.

November 5, 1989

M R McBee

WBS 1.1.9: Monthly Progress Report on Neutron Science Tasks for October, 1989**1. Detector Shielding (J. F. Carew, BNL)**

The ANISN detector shielding calculations have been completed. The calculations were carried out in two steps: (1) the calculation of the neutron spectrum incident on the detector shield, and (2) the determination of the energy-dependent attenuation of the polyethylene/B₄C shield. In the first step, a 69-group P-3 ANISN model of the HFBR, from the core out through the biological shield, was constructed and the neutron spectrum leaking from (1) the biological shield, (2) a typical monochromator, and (3) the beam were calculated. A neutron spectrum measured at the H-9 beam port was also obtained. Using these input spectra, the energy-dependent attenuation of the detector shield was computed using a 69-group ANISN model. The detector neutron count rate is given in Fig. 1 for an assumed HFBR H-9 measured spectrum. The group-wise attenuation (detector absorptions per incident neutron) for the biological shield leakage spectrum (the hardest spectrum) and the H-9 measured spectrum (the softest spectrum) are given in Figs. 2 and 3, respectively. It is seen that the attenuation is relatively weak at high energies ($E > 1$ MeV), and is strong at intermediate energies ($1 \text{ eV} < E < 1 \text{ MeV}$) due to the slowing down in the shield. The thermal peak is due to the buildup of slowed neutrons and may be further reduced by increasing the ¹⁰B loading.

A substantial sensitivity of the detector response was observed with respect to (1) the shield polyethylene thickness (a factor of about 25 decrease for a 50% increase in thickness), (2) the incident neutron spectrum (a factor of about 100 increase when the biological shield leakage spectrum replaces the H-9 measured spectrum), and (3) the B₄C region thickness (a factor of about 10 increase for a 100% reduction in thickness). It is also noteworthy that about 80% of the incident neutrons which entered the shielding leaked out of the system before being absorbed by the shield or the detector.

These results have been summarized in a BNL memorandum which will be issued shortly.

M R McBee
November 5, 1989
Page 2

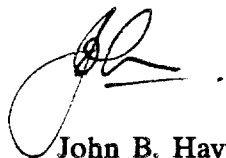
2. Neutron Polarizer Development (H. A. Mook, Solid State Division)

The stacked silicon wafer supermirror polarizer being developed (see February, 1989 Monthly Progress Report) has been selected for a 1989 R&D-100 award by *Research and Development* Magazine, which annually lists the top 100 R&D innovations in the USA.

3. New Value Reported for the Neutron Lifetime

A new value for the neutron lifetime, which is the worst-known fundamental physical constant, is reported in the August 7, 1989 issue of *Physical Review Letters* by a team from French, British and American laboratories working at ILL, Grenoble. Walter Mampe *et al.* measured the lifetime by counting the ultracold neutrons remaining in a fluid-walled bottle as a function of the duration of storage. Neutron losses caused by imperfect wall reflections were eliminated by varying the volume-to-surface ratio of the bottle. The result obtained for the neutron β -decay lifetime is 887.6 ± 3 s. While this is the most accurate measurement to date, there is still substantial room for improvement, when compared with the precision typically expected for undamental values. Such improvement largely depends on a higher flux source of ultracold neutrons (such as the ANS).

4. The seventh issue of **TRans** is appended.



John B. Hayter, FEDC, MS-8218 (6-9300)

JBH:jh

FIGURE 1

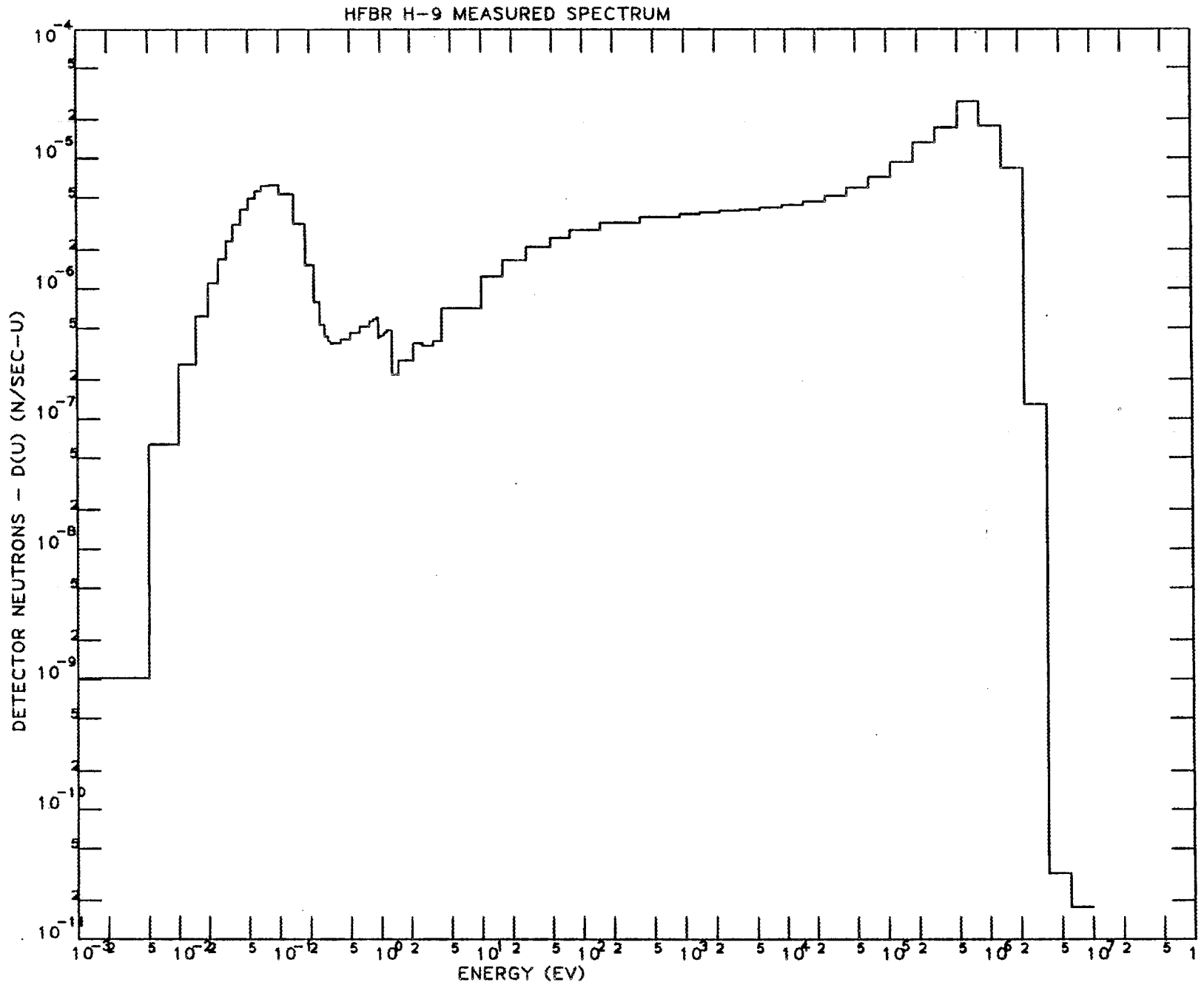


FIGURE 2

HFBR BIOLOGICAL SHIELD LEAKAGE SPECTRUM

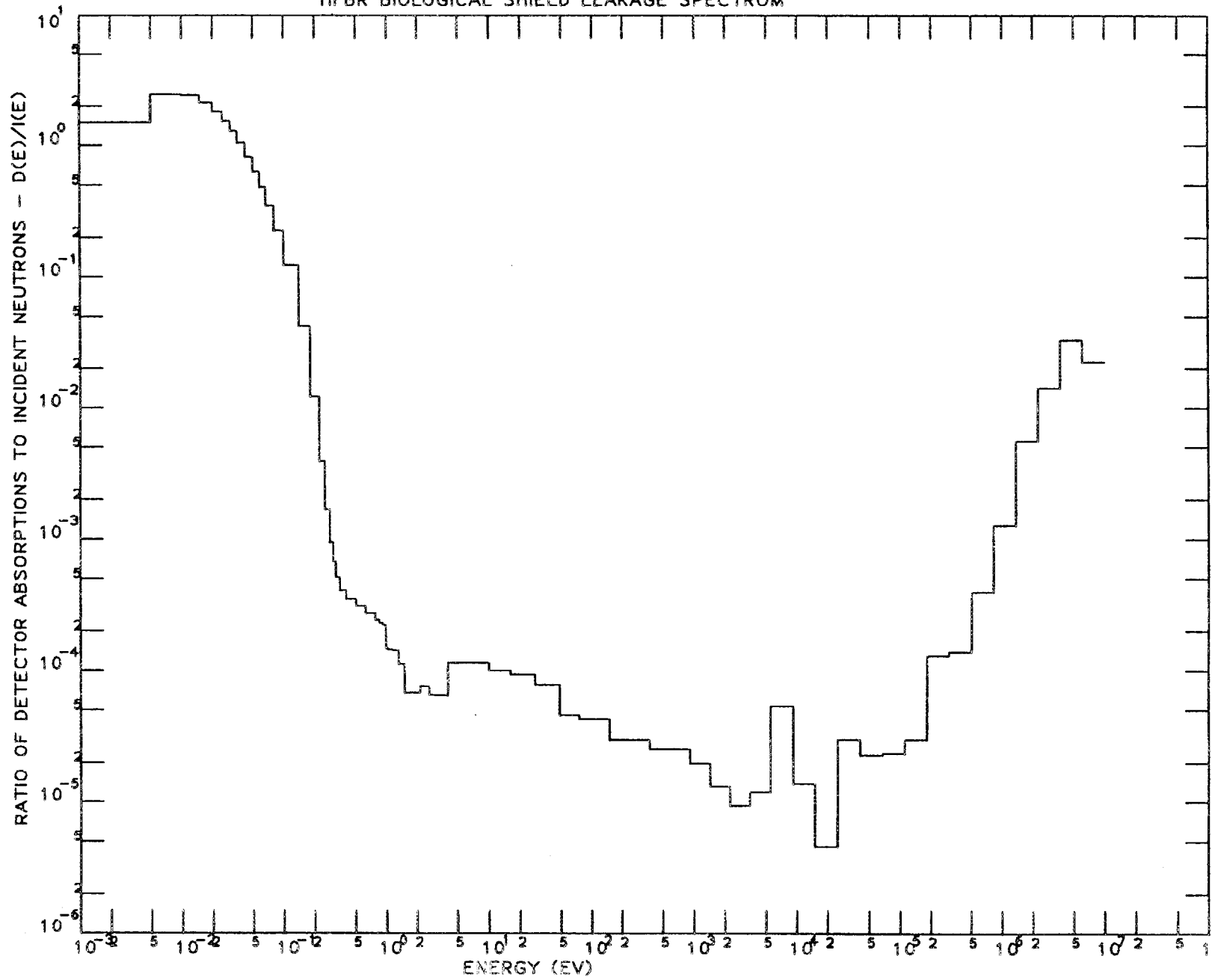
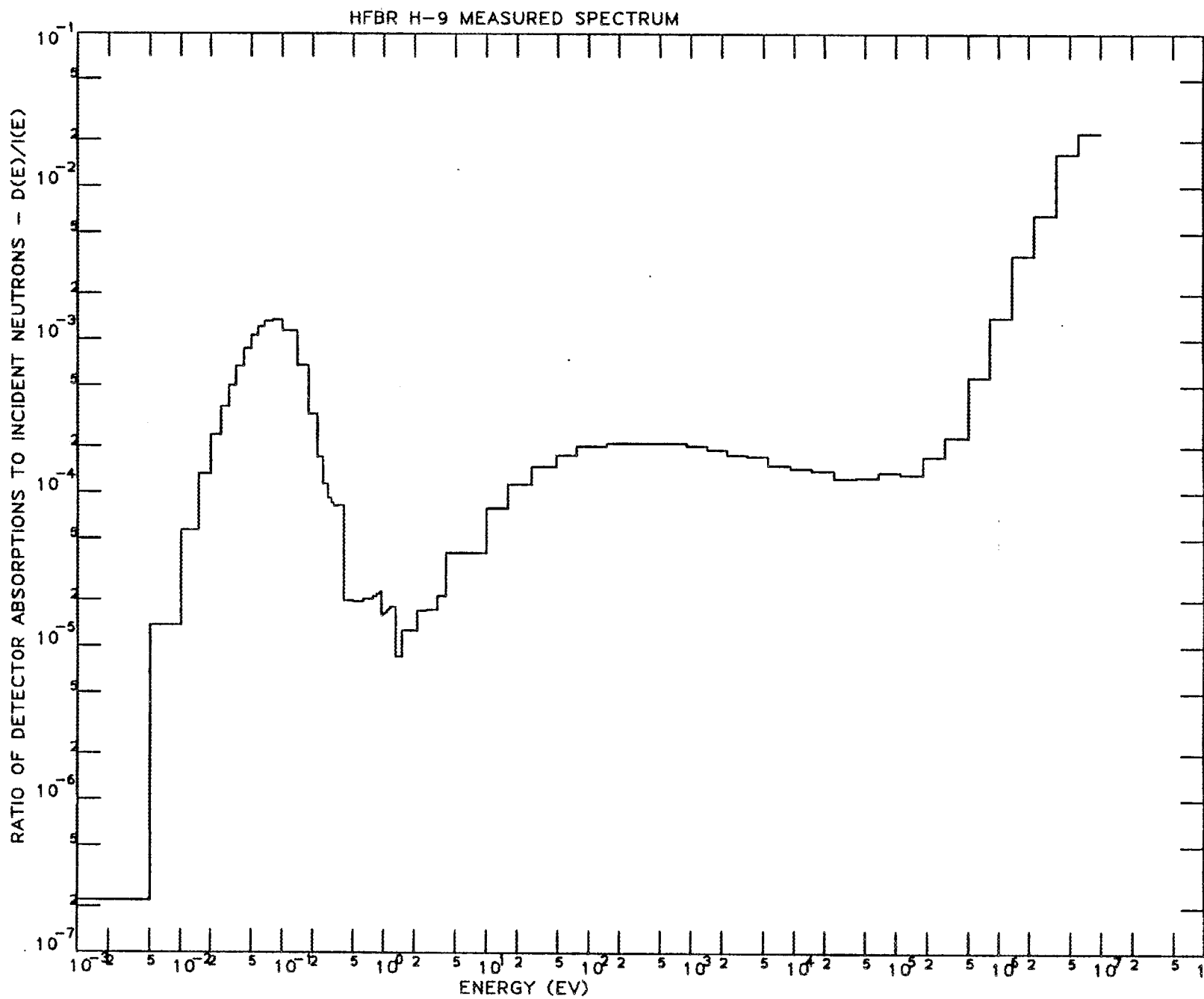


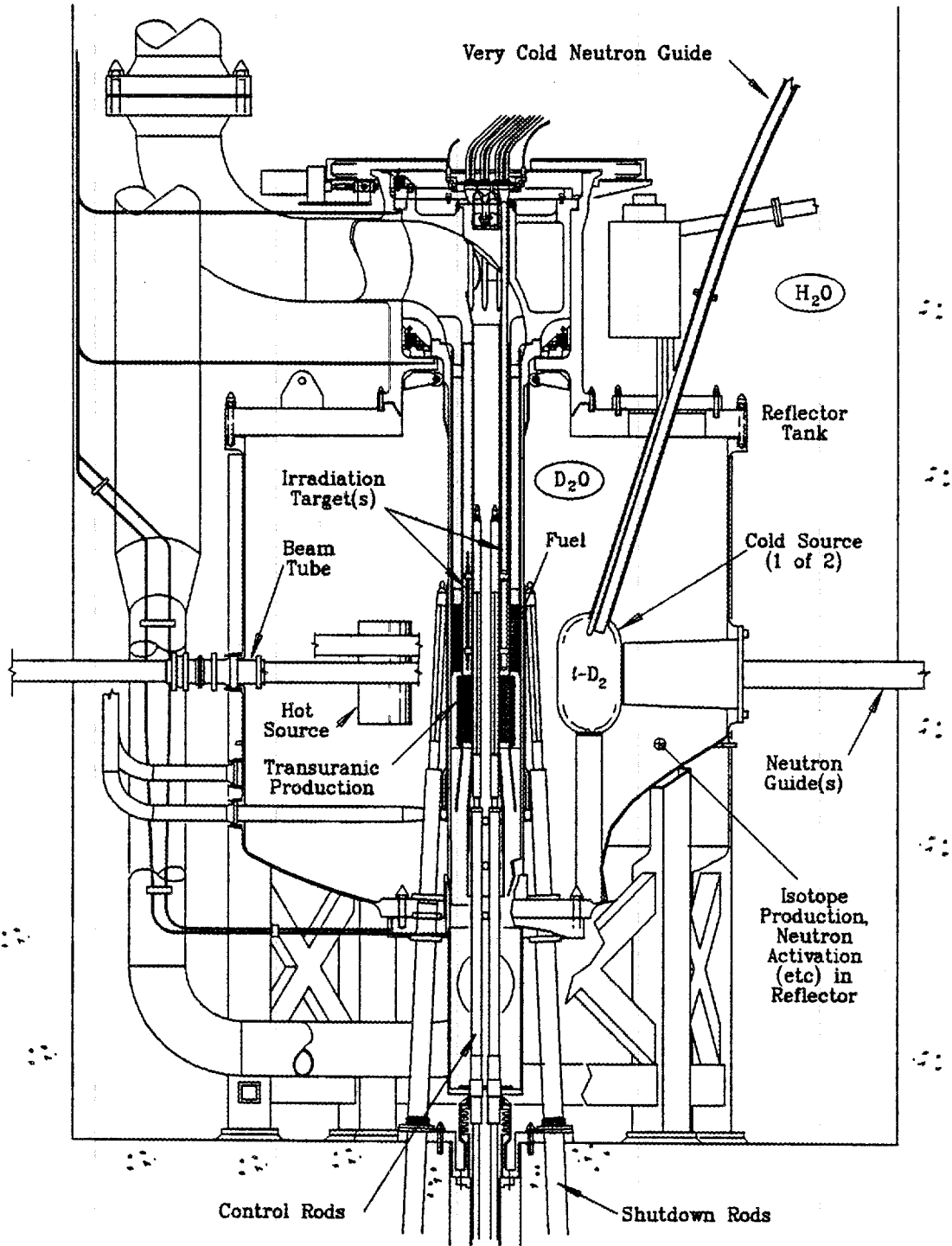
FIGURE 3



TOPICAL REPORTS ON THE ADVANCED NEUTRON SOURCE

no 7, september 1989

ANS Reactor Assembly



ANS Reactor Assembly

The key elements of the reactor assembly are shown in the drawing overleaf. The two-element split core (described in *TRans* no 2) is mounted in the core pressure boundary tube (CPBT) which passes vertically through the center of the 3.5 m diameter heavy water reflector tank. The entire assembly is mounted at the bottom of the light water reactor pool, as shown in the last *TRans*.

The reactor core is cooled by a heavy water primary coolant loop, with coolant *upflow* through the CPBT. The choice of upflow slightly complicates the reflector tank mounting, but provides a very desirable added safety feature, since it ensures an immediate transition to natural convection cooling (without any time delay for flow reversal) in the unlikely event of rupture of the primary circuit at a point which forestalls compensation by the independent backup circuit. (It should be noted that the normally low probability of major pipe rupture is being further reduced by designing for leak-before-break, with continual leak monitoring.)

The reactor is controlled by four hafnium control rods in the central core channel. Each rod is provided with an independent scram mechanism, and any three of the four are able to shut down the reactor. A second, independent, shutdown mechanism is provided by eight shutdown rods placed outside the CPBT. Each rod is again provided with an independent scram mechanism, and any seven of the rods are sufficient for total shutdown. Thus the reactor may be shut down, even if there is total failure of one complete set of independent scram mechanisms and partial failure of the other.

There are six major types of experimental facilities in the reactor assembly. Inside the CPBT, materials irradiation takes place in either instrumented or uninstrumented capsules placed inside the upper fuel element, while transuranium elements are produced in targets just outside the lower fuel element. These positions, which are chosen to provide appropriate fast and epithermal neutron spectra, have minimal effect (<2%) on the fluxes at the other experimental positions in the heavy water reflector tank.

Neutron beams are extracted from the reflector by beam tubes which penetrate either into the peak thermal flux position (about 400 mm from the core centerline), or terminate at the graphite hot source at the reflector tank wall. The hot source is one of two types of spectral converter which are placed in the reflector to tailor beam energies for specific applications; conversion to sub-thermal energies is accomplished by two liquid-D₂ cold sources. Cold neutrons are transported by horizontal neutron guides into a neutron guide hall adjacent to the containment building, or by slant guides to the second floor beam room (see issues 3-5 of *TRans*).

The large volume of high thermal flux available in the reflector tank is well suited to isotope production and analytical chemistry operations. To accommodate these activities, various experiment holes and rabbit tubes penetrate the top of the reflector tank. Seven vertical and two slant holes will provide thermal fluxes ranging from 4×10^{18} to 7.5×10^{19} m⁻².s⁻¹ for isotope production; these holes will be complemented by four hydraulic rabbit tubes in the flux range 2 to 8×10^{19} m⁻².s⁻¹. The in-tank experimental facilities are completed by three pneumatic rabbit tubes for thermal activation analysis; these and the other analytical chemistry facilities will be described next month.

. . .

Next issue: *Materials Analysis Facilities*

TRans is edited by

John B. Hayter
Oak Ridge National Laboratory
FEDC
PO Box 2009
Oak Ridge, TN 37831-8218

Oak Ridge National Laboratory is operated by Martin Marietta Energy Systems, Inc., under Contract No. DE-AC05-84OR21400 with the United States Department of Energy.

Internal Correspondence

MARTIN MARIETTA ENERGY SYSTEMS, INC.

November 8, 1989

R.G. Alsmiller, Jr.

ANS Progress Report for the Month of October 1989

Energy and Angular Dependent of Particle Fluxes in a Radial Beam Tube

The work reported here is a continuation of the work initiated by Dr. Takeo Nishigori, Osaka University. Using the particle fluxes throughout the reflector region generated by Dr. Nishigori for the intermediate reference core E3 at BOC, a DORT calculation has been carried out to determine the transport of particles in a cylindrical radial beam tube (see Fig. 1). The code DTDMAX developed by R. A. Lillie was used to obtain a boundary energy and angular source (see Fig. 1) that could be used in conjunction with DORT to obtain the energy and angular dependent fluxes of neutrons and gamma rays at various positions in the beam tube. To adequately treat the particle streaming in the beam tube, a highly biased quadrature containing 315 directions was used in the DORT calculations. For comparative purposes, calculations were carried out with the beam tube both present and absent.

In Fig. 2, the angular flux of thermal (energy ≤ 3 ev) neutrons in the beam tube at a fixed radius and various z coordinates is shown as a function of angle. The angular flux becomes progressively more forward at position along the beam tube away from the reactor. In Fig. 3, the angular flux of thermal neutrons near the exit of the beam tube for several radial values is shown as a function of angle. Results for the fast neutron flux and the gamma ray flux similar to those shown in Figs. 2 and 3 are in preparation.

In Table 1, the scalar flux of neutrons and gamma rays in various energy ranges is shown at the three positions: a, b, c, indicated in Fig. 1. Results are shown both with the beam tube present and absent. The thermal flux of neutrons at position c is very large when the beam tube is present compared to the case of no beam tube. This increase of the fluxes near the exit of the beam tube requires further consideration. The thermal flux at position a without the beam tube is slightly higher than the flux at this position with the beam tube. The position of the beam tube with respect to the peak in the thermal flux has not as yet been optimized. The ratio at position b, the exit of the beam tube, of the flux of neutrons with energy ≤ 3 ev to the flux of neutrons with energies between 100 kev and 20 Mev is approximately 72 and the ratio of the flux of neutrons with energy ≤ 3 ev to the flux of gamma rays with energies between 10 kev and 20 Mev is 0.8. Results similar to that shown in Table 1 but based on the angular fluxes in the vicinity of zero degrees is in preparation.

As soon as the calculations for the radial beam tube are completed, calculation for a tangential beam tube will be initiated.

M. Hayashi
M. Hayashi, 6025, MS-6363 (4-3174)
Kyoto University

cc: T. Nishigori
R. A. Lillie

Table 1. Scalar flux calculated by DORT boundary source (n/m²/sec)

	position*	with beam tube	without beam tube
neutron (6.4 Mev - 20 Mev)	a	6.14×10^{15}	5.90×10^{15}
	b	1.80×10^{12}	7.81×10^{-1}
	c	8.52×10^7	3.89×10^{-1}
neutron (100 kev - 20 Mev)	a	2.72×10^{17}	2.86×10^{17}
	b	4.25×10^{13}	8.93
	c	9.72×10^9	2.32
neutron (3 ev - 20 Mev)	a	3.35×10^{18}	3.96×10^{18}
	b	3.15×10^{14}	2.15×10^1
	c	3.43×10^{10}	4.26
neutron (1×10^{-5} ev - 3 ev)	a	5.76×10^{19}	7.17×10^{19}
	b	3.07×10^{15}	1.13×10^2
	c	6.85×10^{11}	1.14×10^1
gamma ray (10 kev - 20 Mev)	a	3.21×10^{19}	3.54×10^{19}
	b	3.99×10^{15}	1.63×10^8
	c	2.82×10^{12}	7.24×10^7
gamma ray (8 Mev - 20 Mev)	a	1.75×10^{15}	1.72×10^{15}
	b	4.91×10^{11}	3.70×10^5
	c	9.64×10^9	2.55×10^5
gamma ray (300 kev - 400 kev)	a	1.71×10^{18}	1.70×10^{18}
	b	2.72×10^{14}	9.24×10^6
	c	1.71×10^{11}	3.36×10^6

*a: r = 0.562cm, z = 15.5cm

b: r = 0.562cm, z = 524.1cm

c: r = 33.124cm, z = 524.1cm

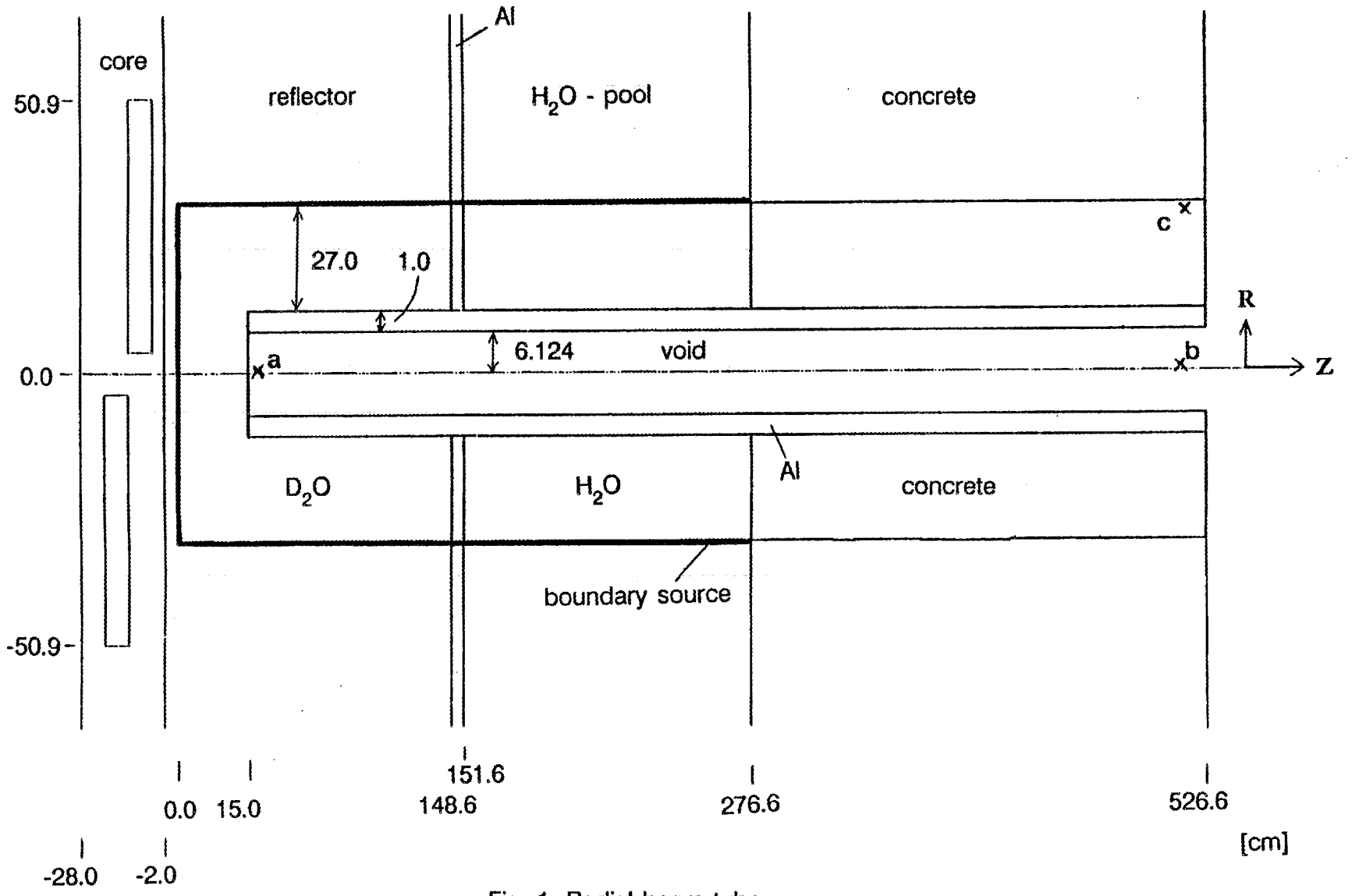
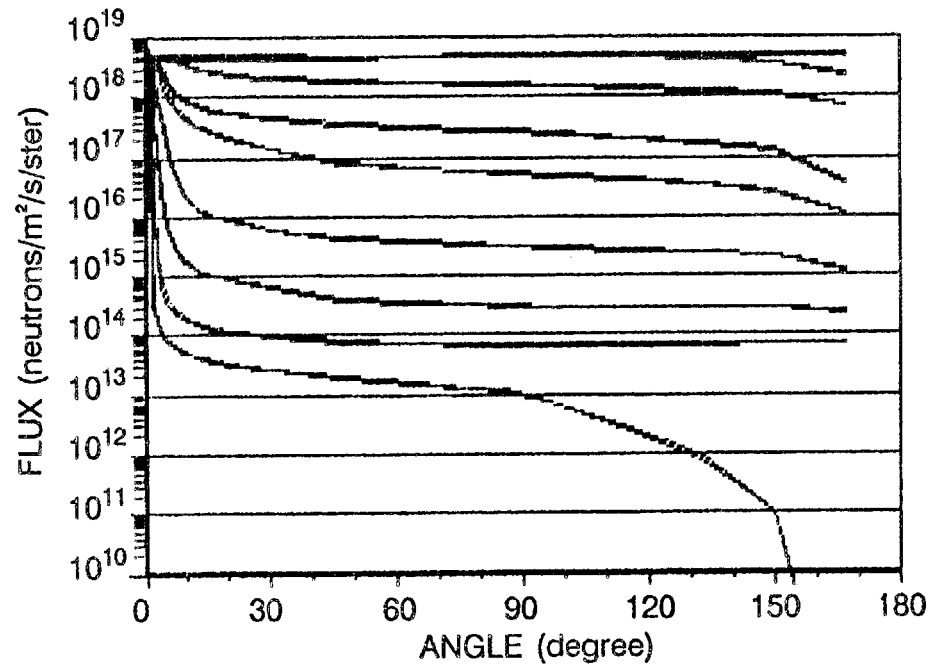


Fig. 1. Radial beam tube

Fig. 2. DORT Thermal Neutron Angular Flux
along Beam Tube Axis (BOC)

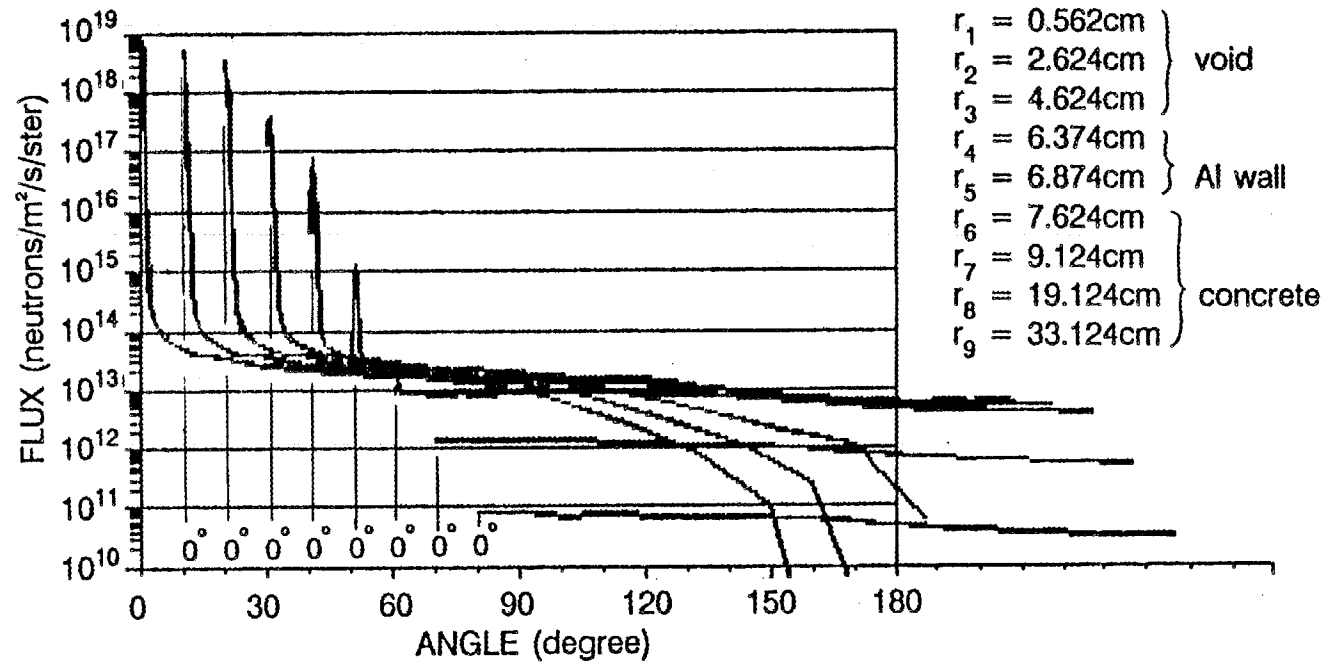


$r = 0.562\text{cm}$

- $z_1 = 1.0\text{cm}$
- $z_2 = 16.5\text{cm}$
- $z_3 = 73.85\text{cm}$
- $z_4 = 138.85\text{cm}$
- $z_5 = 164.6\text{cm}$
- $z_6 = 224.1\text{cm}$
- $z_7 = 289.1\text{cm}$
- $z_8 = 389.1\text{cm}$
- $z_9 = 524.1\text{cm}$

Fig. 3. DORT Thermal Neutron Angular Flux
at Beam Tube Exit (BOC)

$z = 524.1\text{cm}$



November 13, 1989

September 1989 Progress Report

TASK 1.1.12. INSTRUMENTATION AND CONTROLS

Principal investigators:

- M. Abu-Shehadeh
- J. L. Anderson
- B. Damiano
- J. E. Hardy
- M. Ibn-Khayat
- J. March-Leuba
- L. C. Oakes

Progress to Date

Work continues in the areas of control rod requirements, control and plant protection systems definition, and dynamic modeling. We continue our efforts in the RS2 committee to define and document the conceptual configuration of the reactivity control systems. A draft final report for the RS2 task has been issued for comments. The task should be finalized during November. We are also cooperating in Tasks BOP 1a and BOP 1b helping define the reactor cooling system under normal and abnormal conditions. As part of these tasks, we have performed several dynamic model runs to study the behavior of the ANS reactor under transient conditions, including loss of main circulation pumps and small breaks leading to depressurization.

Dynamic model calculations have also been performed to define expected power overshoots and their corresponding reduction in critical power ratio (CPR) following reactivity steps. The results are presented in Table 1 and Figs 1 and 2, and correspond to calculations using the old (43 L) split core reactivity coefficients (-43.3 cents/%_void in the core coolant region). Model used is IC/ANS/M/89-1, with parameter set IC/ANS/P/90-2. The steady state CPR has been calculated at the plant protection system limiting setpoints to show the effect on the core thermohydraulics of slow transients that do not trip the reactor. The CPR is the ratio of critical heat flux to actual heat flux; as such, CPRs lower than 1.0 indicate a condition where departure from nuclear boiling (DNB) is likely.

The effect of coolant inertia has been accounted for in the model with some degree of approximation by localizing all the inertia of the coolant circuit at the pump location. The relative locations of the leak and the accumulator can be modelled approximately by changing the inertance (ratio of length to flow area, L/A). Figures 3 through 6 show the relative effect of the coolant inertia on flow rate and core outlet pressure for a core inlet and core outlet 150 mm (6 inch) break. It can be observed that the coolant inertia reduces the core flow for about 100 ms while the coolant between the accumulator and the break is accelerated. The larger the L/A ratio is, the larger the inertia and the larger the flow reduction through the core is.

Figure 7 presents the effect of coolant inertia on a transition from full flow to pony motor flow in the presence of a 150 mm break at the core inlet. The main effect of the inertia term is to increase the coolant and fuel-surface temperatures for the initial 100 ms. Following the scram, the slow part of the transient behaves similarly to the non-inertia transient.

A new heat transfer correlation has been included in the model. This correlation takes into account the transition to laminar flow, where heat transfer is lower. The effect of this reduction in heat transfer coefficient is seen in Fig. 8 as an abrupt increase in wall temperature 400 s into the transient.

Table 1. Calculated response to reactivity steps.

Reactivity (\$)	Max_Neutron_Flux (Relative)	Max_Heat_Power (MW)	Min_CPR
0	1.000	326.5	1.278
0.5	1.255	381.2	0.972
1.0	1.450	429.6	0.770
1.5	1.825	497.5	0.545

Table 2. Steady state critical power ratios

Condition	CPR*
Nominal	1.278
Power +15% (402.5 MW_fission)	1.001
Pressure -20% (2.96 MPa_inlet)	0.98
Flow -20% (2196 Kg/s_@pump)	1.049
Inlet temp +10% (53.7 °C)	1.224
Nominal Power, Pressure-20%, Flow-20% Inlet temp +10%	0.81

* CPR = Critical power ratio

HEAT POWER vs FISSION POWER REACTIVITY STEP, 30ms DELAY

IC/ANS/F/90-7

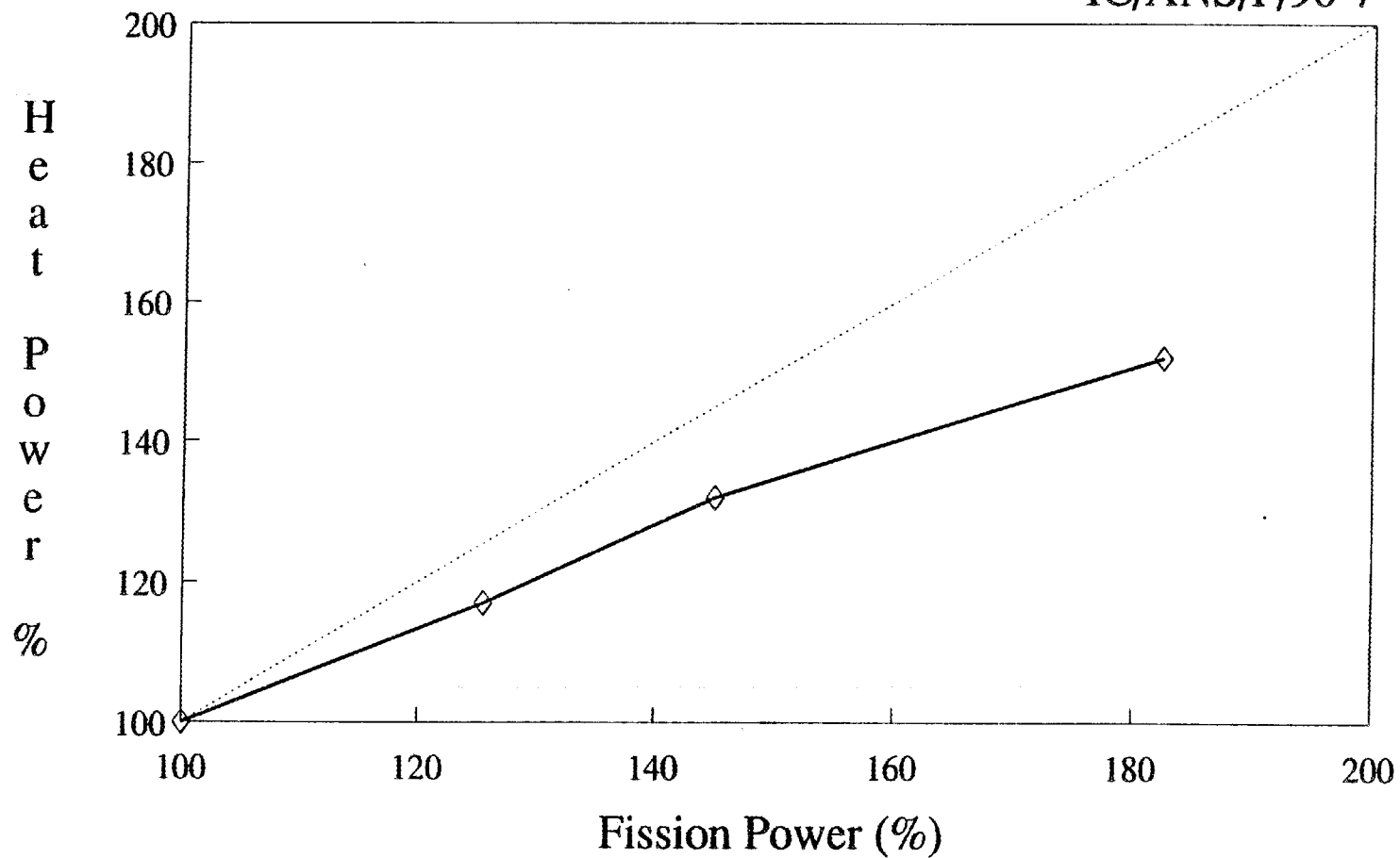


Fig. 1. Heat Power (i.e., power deposited in channel coolant) versus fission power following reactivity steps of different magnitudes. Scram is assumed with a 30 ms delay.

CPR vs REACTIVITY STEP 30ms SCRAM DELAY

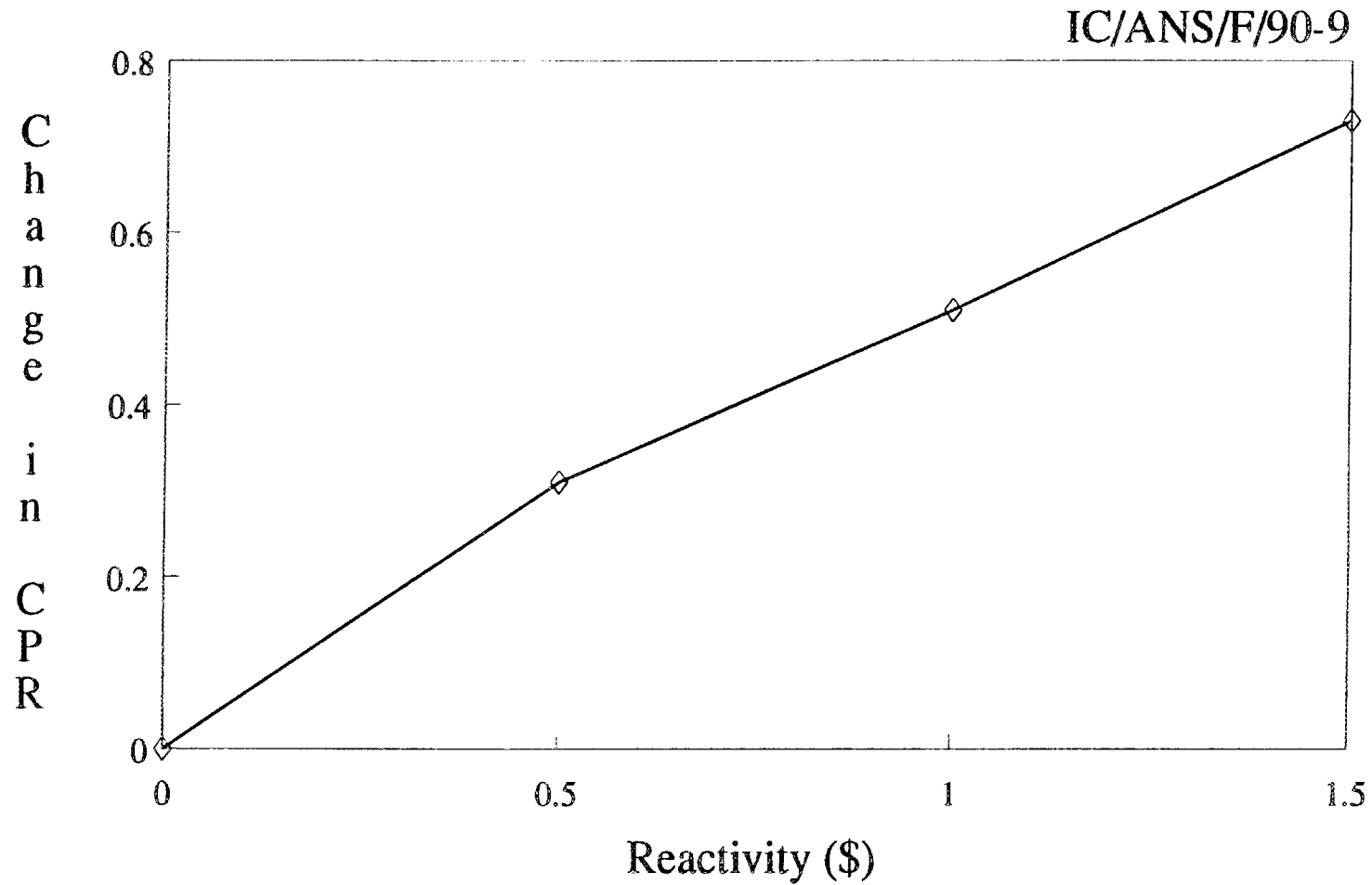


Fig. 2. Reduction in critical power ratio (CPR) following a reactivity step.

150 mm Break @ Core Inlet

Effect of loop inertia

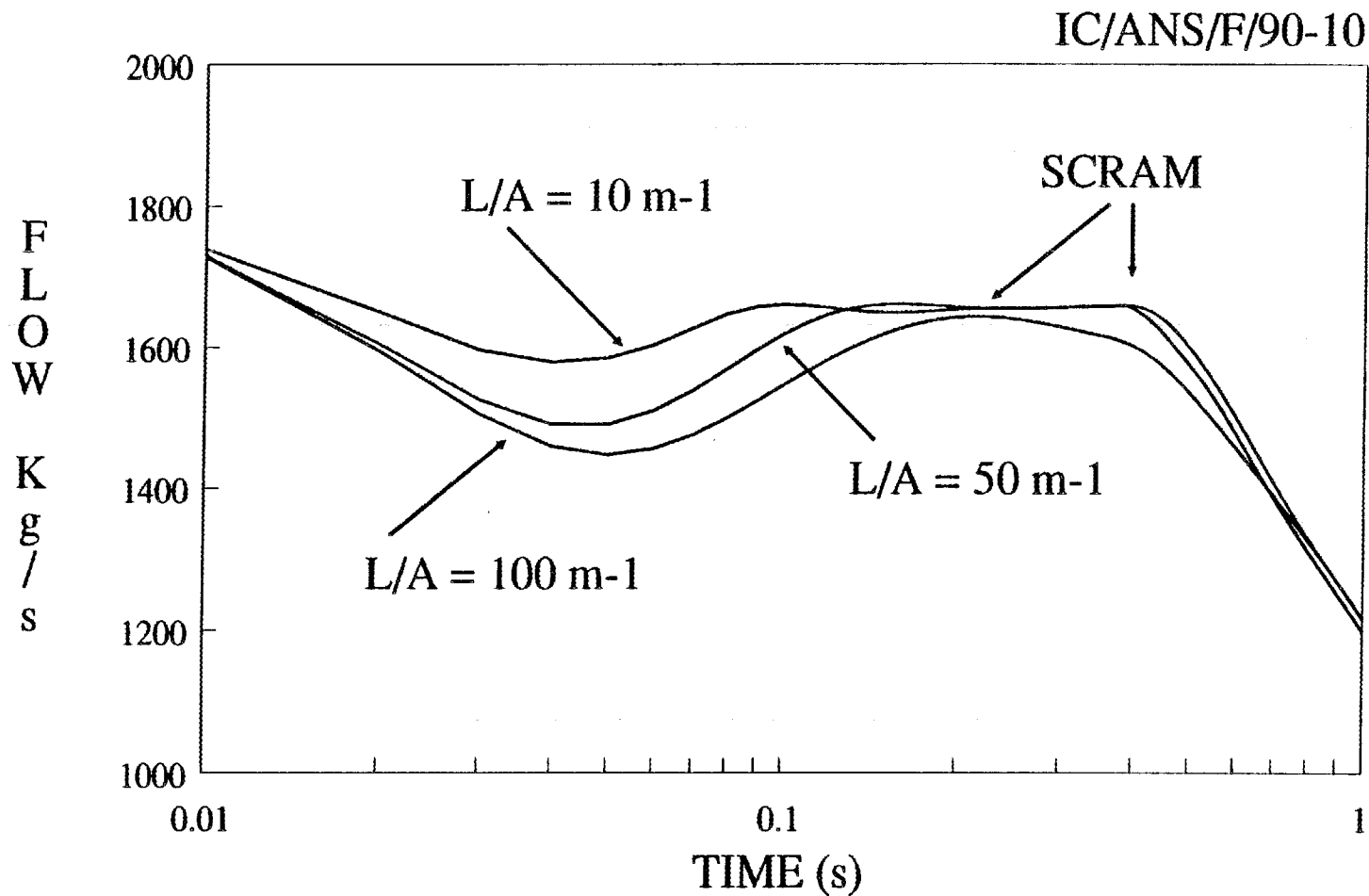


Fig. 3. Core flow following a 150 mm (3 inch) break at the core inlet.

150 mm Break @ Core Inlet

Effect of loop inertia

IC/ANS/F/90-11

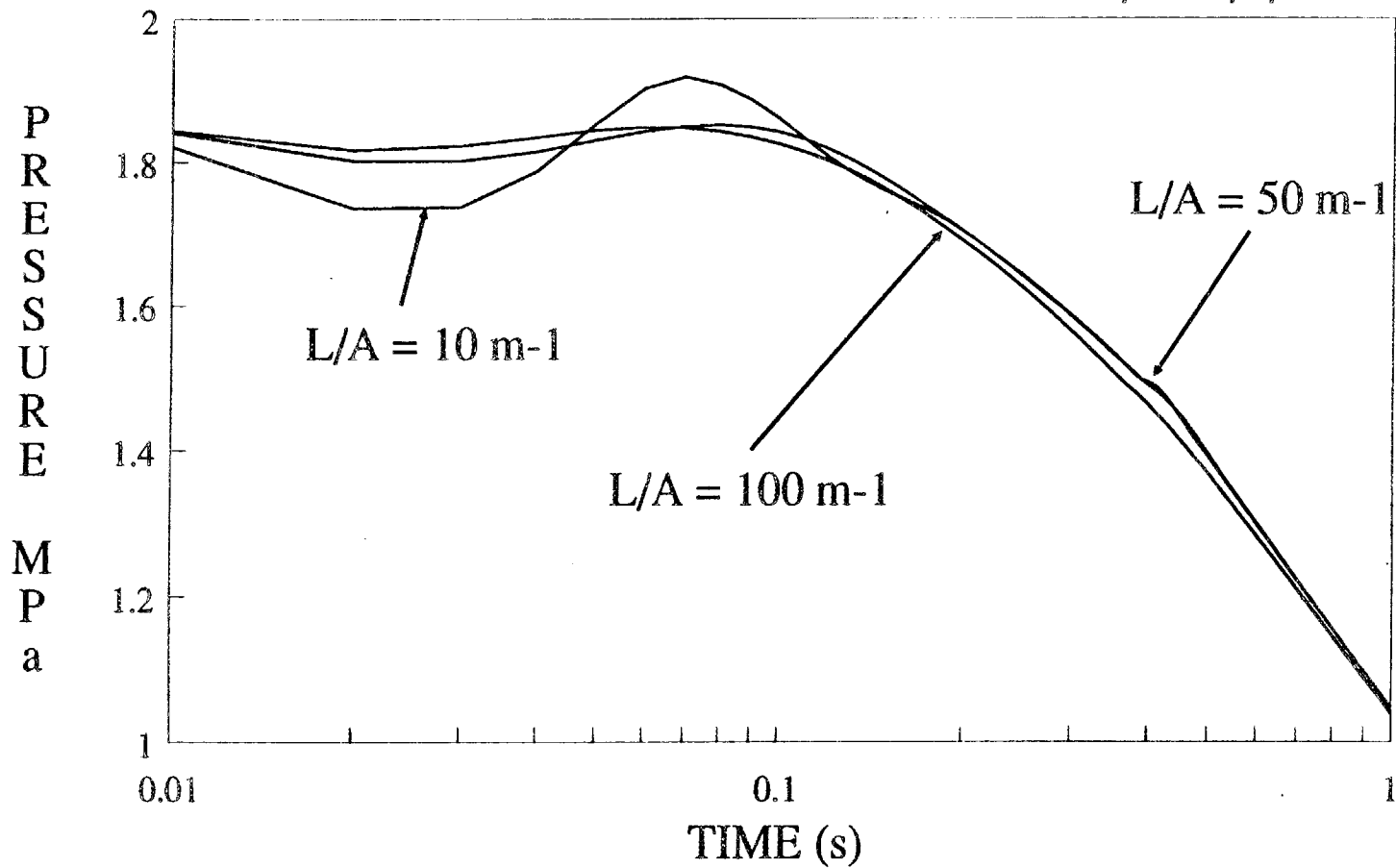


Fig. 4. Core outlet pressure following a 150 mm (3 inch) break at the core inlet.

150 mm Break @ Core Outlet Effect of loop inertia

IC/ANS/F/90-13

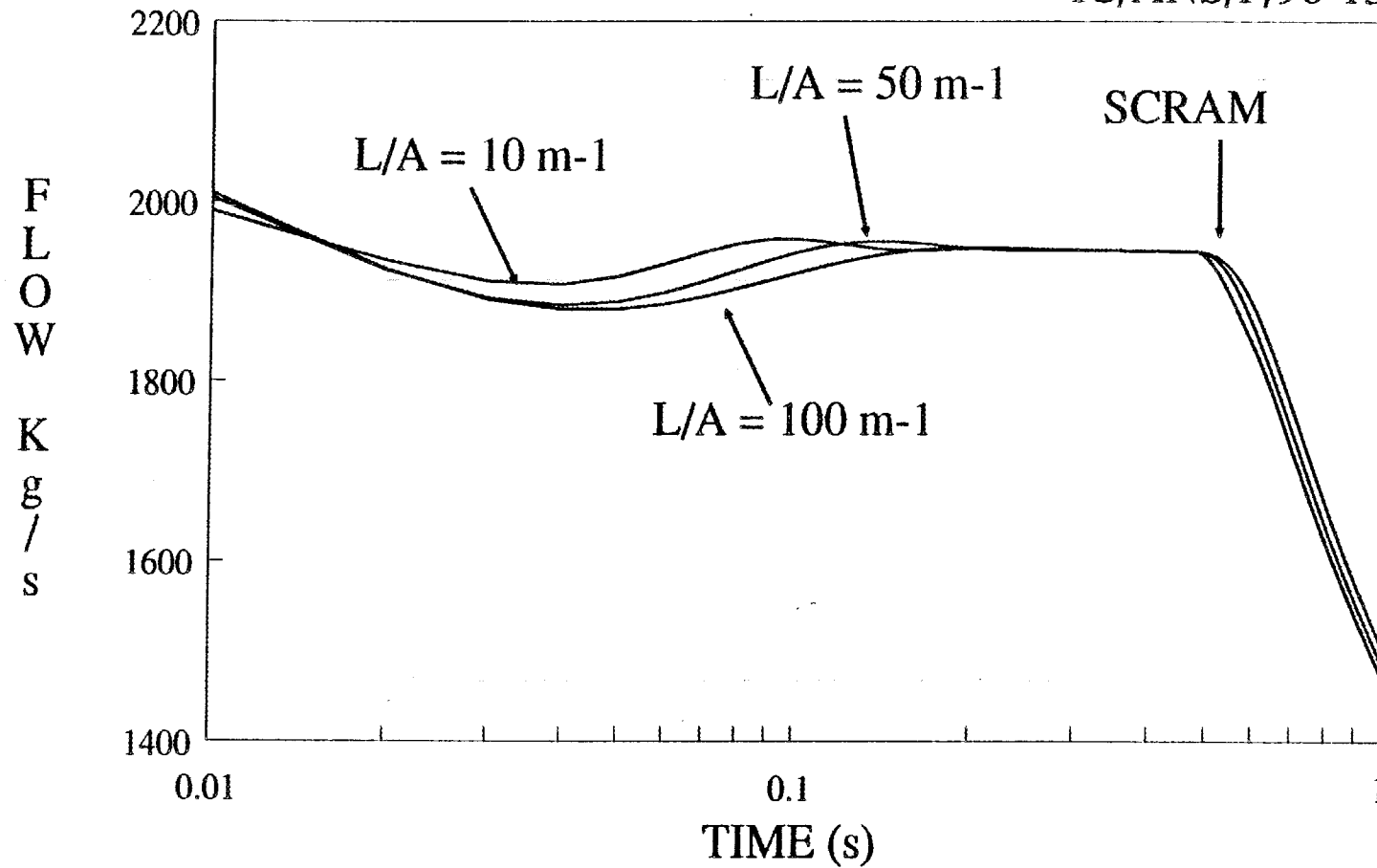


Fig. 5. Core flow following a 150 mm (3 inch) break at the core outlet.

150 mm Break @ Core Outlet

Effect of loop inertia

IC/ANS/F/90-14

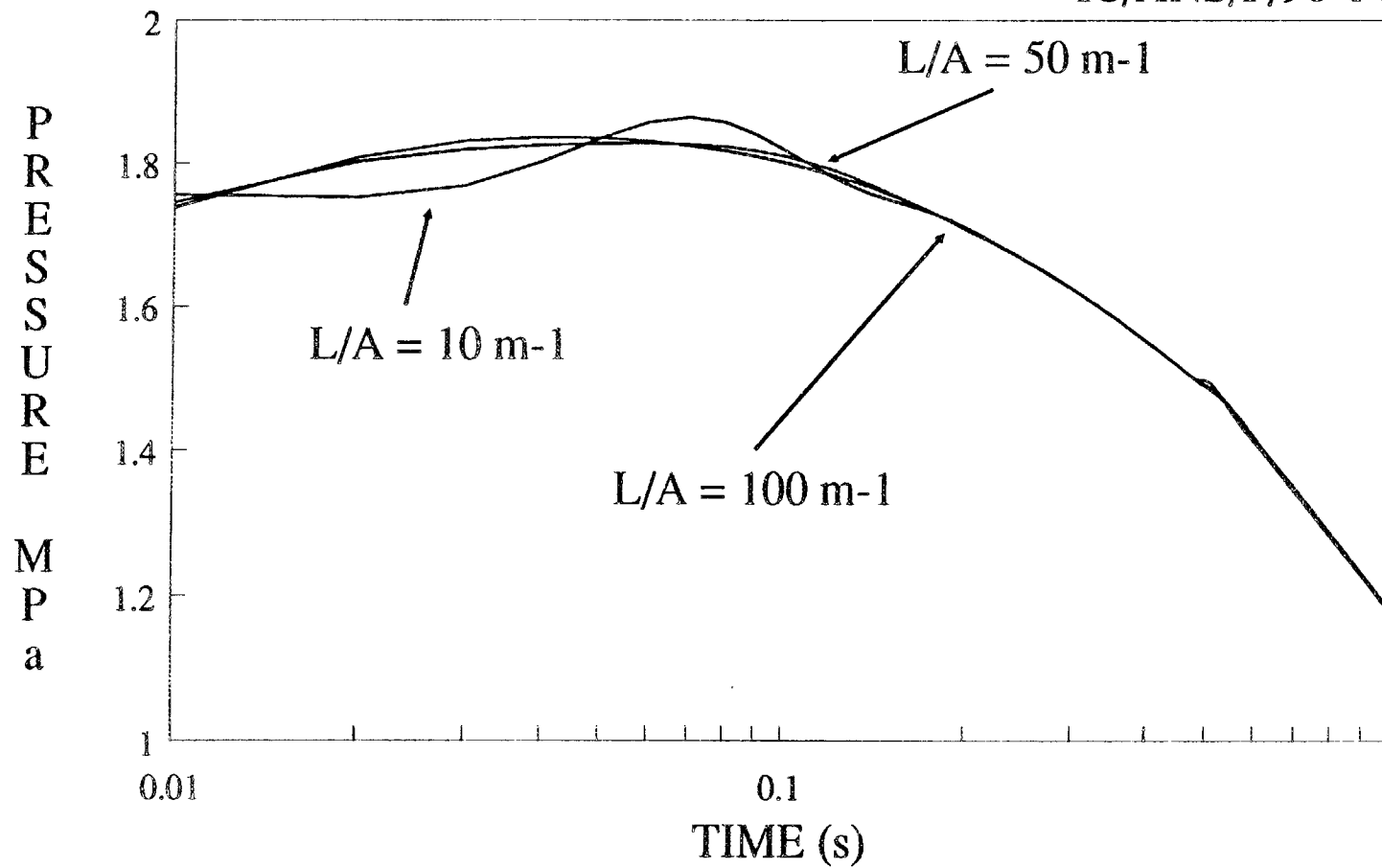


Fig. 6. Core outlet pressure following a 150 mm (3 inch) break at the core outlet.

150 mm Break @ Core Inlet

Pony Motors Active. $L/A = 50 \text{ m}^{-1}$

IC/ANS/F/90-16

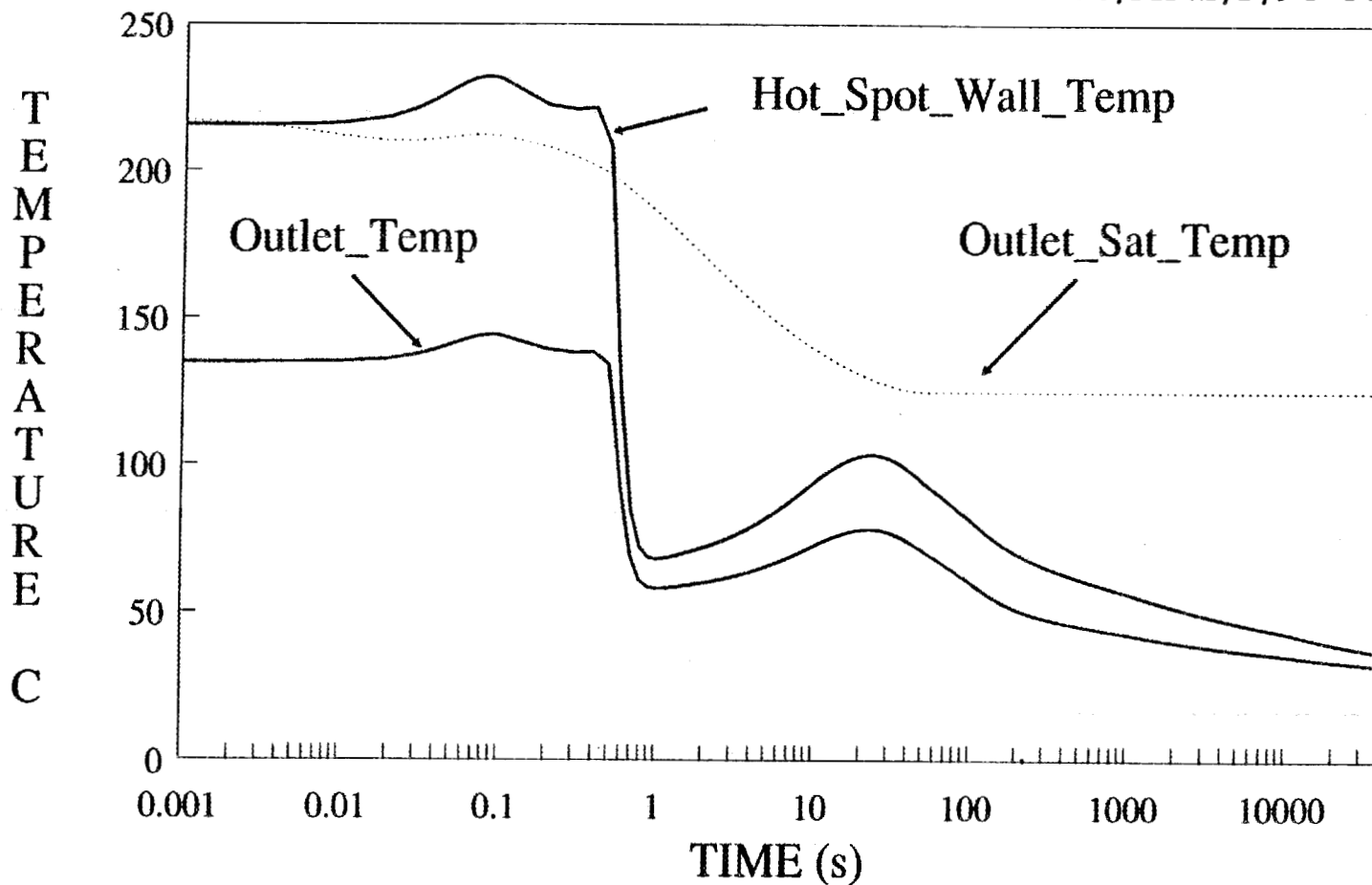


Fig. 7. Hot-spot-wall temperature and hot-channel-coolant outlet temperature following a 150 mm (3 inch) break at the core inlet. Scram occurs on low flow and pumps are tripped to pony motor flow.

BOP Task-1b TEST_CASE-1

IC/ANS/F/90-6

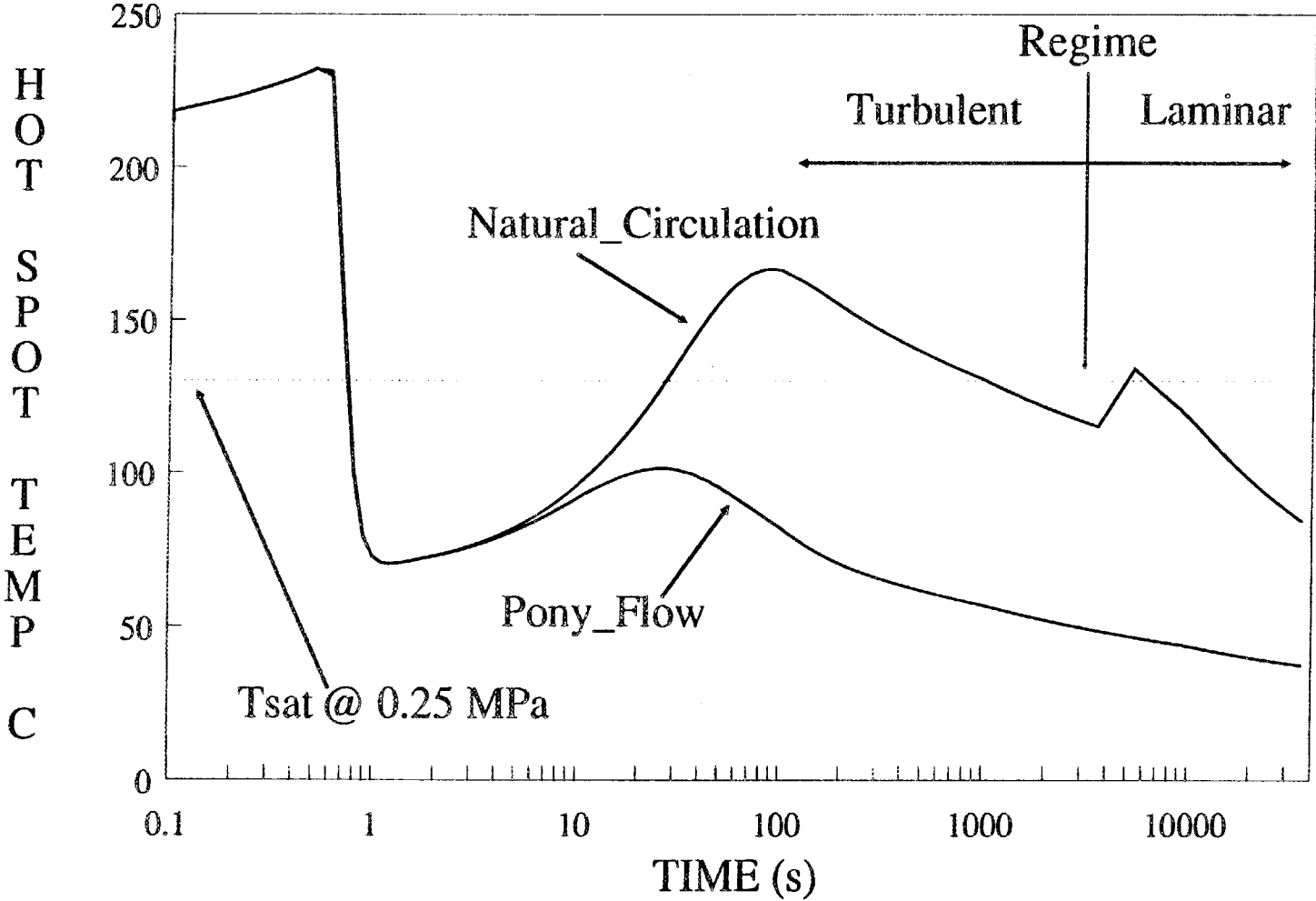


Fig. 8. Transition to natural circulation or pony flow from nominal conditions. Natural circulation conditions result in transition to laminar flow and an increase in wall temperature

ANS Project Safety Activities - October 1989

The major activities of the month included transient and steady-state thermal-hydraulics analysis, severe accident analysis, and probabilistic risk assessment.

J. R. Buchanan, W. E. Kohn, M. D. Muhlheim, and E. G. Silver of the ORNL Engineering Technology Division's Nuclear Operations Analysis Center (NOAC) met with ANS Project personnel to present various activities that NOAC could pursue under ANS FY 1990 funding to further develop the documentation of ANS regulatory safety goals and criteria. The proposed activities include the development of an automated data base of all applicable regulations and guides, the review of the Electric Power Research Institute Advanced Light Water Reactor requirements document for possible applicability to the ANS, and the completion of the ANS Reference Documentation List (RDL), which is currently in draft form. At the meeting it was determined that funding limitations would most likely preclude any work on the first two items, but that some funding might be available to pursue the third item-- completion of the ANS RDL (the ANS FY 1990 budget is, at this writing, still tentative). Even if extensive funding were available, the development of an automated data base of standards, regulations and guides would have to be planned in coordination with the highly similar effort that has been initiated in the Engineering Technology Division by the New Production Reactor Project. The desirability of some provision for on-call assistance in the identification and interpretation of applicable regulations was also discussed.

Transient thermal-hydraulic accident analysis, WBS 1.2.3.2, activities (see G. L. Yoder's report, attached) included further activities aimed toward successful execution on the ORNL CRAY computer of the RELAP5 model of the ANS reactor. Version 4B1 of RELAP5-MOD2.5 was successfully installed on the ORNL Cray last month, but the "ANS updates" (special code modifications for ANS geometry and flow conditions) were not compatible with this version. This difficulty has, with the support of INEL personnel, been fixed, and RELAP activities are presently concentrating on verifying that identical input produces the same output on both the ORNL and INEL computers.

INEL activities in support of the ANS RELAP5 model development and analysis resumed in mid-October after a two week hiatus due the depletion of the FY89 funds. INEL personnel provided assistance to ORNL in getting the ANS RELAP5 model running on the ORNL computers. In addition, INEL code development personnel have initiated corrective action to solve the post-departure-from-nucleate boiling (i.e., film boiling) heat transfer problem previously identified in the medium and large pipe break calculations.

PRA activities at BNL, WBS 1.2.3.4 (report attached) included review and modification of the final reports of the two major FY 1989 PRA activities: the scoping study of dominant severe fuel damage risk initiators, and the large pipe break risk study. PRA activity at BNL during early FY 1990 will be at a low level until after completion of major design options studies that are currently under way at ORNL.

The severe accident issues characterization task, WBS 1.2.3.5 activities included the continuation of the two scoping studies currently in progress: one on core melting, relocation and fission product release for ANS severe accident sequences and the other on hypothetical core-concrete interactions resulting from severe accidents. Dr. Taleyarkhan's report is attached.

The paper "The Advanced Neutron Source Safety Approach and Plans", written by R. M. Harrington, was presented on October 24, 1989 at the International Symposium on Research Reactor Safety, Operations and Modifications by F. J. Peretz. Dr. Taleyarkhan presented a paper "Large Break Loss of Coolant Accident Analysis for the High Flux Isotope Reactor, " at a poster session on the same day. The conference provided a good forum for the exchange of useful information. Several very interesting papers were presented by Japanese and one interesting one by the French:

(1) "JRR-3 Cold Neutron Source Facility H2-O2 Explosion Safety Proof Testing," by Takehiko Hibi et al., (Japan Atomic Research Institute (JAERI), Japan).

(2) "Further Data of Silicide Fuel for the LEU Conversion of MTR," by M. Saito et al., (JAERI, Japan)

(3) "Prise En Compte D'Un Accident De Reactivite Dans Le Dimensionnement Des Reacteurs De Recherche," by H. Abou Yehia et al. (ISPN, Centre d'Etudes Nucleaires de Fontenay-Aux-Roses, France).

The French paper describes a study of reactivity excursion initiated steam explosion for research reactors, and is being translated at ORNL. The Japanese work on accident testing of silicide fuels could be of direct benefit to the ANS. Dr. Taleyarkhan is pursuing a direct contact with M. Saito to discuss cooperation and possible sharing of data.



R. M. Harrington
FEDC (MS-8218), 574-1062 (FTS 624-1062)

Internal Correspondence

MARTIN MARIETTA ENERGY SYSTEMS, INC.

November 13, 1989

R. M. Harrington
J. A. Johnson

ANS Transient Thermal Analysis Task Monthly Progress Report for October 1989

During the month of October, it was discovered that the version of RELAP5 which we received, and the ANS updates were not compatible. A second RELAP5 version and update package were received and installed. In addition, a correction was made to the D₂O properties package which is now available for use with the code. Presently, two versions of RELAP5 4B1 are installed on the Martin Marietta Energy Systems CRAY X-MP; a version without the ANS specific changes and a version which includes changes requested specifically for analysis of ANS transients.

RELAP5 Model Development and Review (N. C. J. Chen)

I attended a UNICOS training session during the month of October to familiarize myself with the recently instituted operating system for the CRAY.

While corrections were being made to combine RELAP5 with the ANS updates, a test run with the standard RELAP5 version was made to ensure that the code will operate on the Martin Marietta Energy Systems, Inc. CRAY. This test run was a steady state run using a modification of the ANS15 input file supplied by Don Fletcher. For this run, H₂O was used as the coolant. Although results are not particularly significant for ANS analyses, the code did execute successfully on the CRAY.

Decay Heat Removal (N. C. J. Chen, G. L. Yoder)

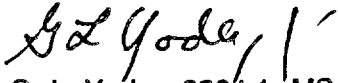
Some spot checks of the March-Leuba ANS dynamic model were made and findings reported in the September 1989 monthly. The case reviewed was decay heat removal with main circulation pump coast down to natural circulation conditions. The assessment focused on correlations used in different flow regions, hot channel coolant exit temperatures, and hot spot wall temperatures.

Continued efforts were made this month to provide thermal limit calculations under the same transient conditions. Three limits were calculated: incipient boiling using Bergles and Rohsenow, onset of net vapor generation by Saha-Zuber, and critical heat flux by Gambill. The computed results at three time steps after reactor scram were listed in Table 1 with decay heat included.

The results show that incipient boiling heat flux is smaller than the heat flux for the onset of net vapor generation which in turn is less than the critical heat flux. At a time of 36,000 seconds, $q''(\text{CHF}) \approx 2 q''(\text{ONVG}) \approx 4 q''(\text{IB})$. Note that decay heat stays below that of ONVG

R. M. Harrington
J. A. Johnson
Page 2
November 13, 1989

at larger times but not at time equal 120 seconds where decay heat exceeds $q''(\text{ONVG})$. Also, the predicted exit coolant temperatures were close to saturation both at ONVG and CHF conditions.



G. L. Yoder, 9204-1, MS-8045 (4-5282)

GLY:beh

Attachment

cc: N. C. J. Chen
W. G. Craddick
W. R. Gambill
D. G. Morris
A. E. Ruggles
C. D. West

TABLE 1

Time T = 120 seconds
(turbulent flow; Petukhov correlation)

	Incipient Boiling	Onset of net vapor generation	Critical Heat Flux	Decay Heat
$q''(\text{Mw/m}^{**2})$	0.067	0.15		0.17
T_e (°C)	88	118		

Time T = 3600 seconds
(transition flow; best estimate)

	Incipient Boiling	Onset of net vapor generation	Critical Heat Flux	Decay Heat
$q''(\text{Mw/m}^{**2})$	0.054	0.11		0.062
T_e (°C)	86	119		

Time T = 36000 seconds
(laminar flow; $Nu = 6$)

	Incipient Boiling	Onset of net vapor generation	Critical Heat Flux	Decay Heat
$q''(\text{Mw/m}^{**2})$	0.029	0.068	0.165	0.021
T_e (°C)	79	120	121	

MONTHLY HIGHLIGHTS FOR OCTOBER 1989

Probabilistic Risk Assessment for ANS

BNL Principal Investigator: R. Fullwood (FTS 666-2180)

ORNL Project Manager: M. Harrington (FTS 624 1062)

The report "Event Tree Analysis for the ANS Conceptual Design" has been completed but has been delayed by the BNL review process. The results are as reported in the September progress report.

During this month the report, "Preliminary Large LOCA Assessments Based on the Preconceptual Design of the Advanced Neutron Source for Oak Ridge National Laboratory" was revised to address and include the ORNL review comments. In the process of this revision, two errors were discovered in estimating the threshold of leak detectability. The revisions indicate that the D₂O inventory balance method can detect leaks greater than about 4 ltr/min with current primary coolant letdown rates. This suggests reconsideration of the need for 400 - 800 ltr/min letdown rates. If this rate was reduced, leak detection by this method which is effective for submerged leaks improves accordingly. If leaks are submerged, it is estimated that a 4 ltr/min leak can be detected after 12 hours by measuring the tritium increase in the reactor pool. Tritium detection in air is by far the most sensitive method but is not believed to be effective for submerged leaks.

This report is now in BNL review to be published as a BNL technical report.

ANS SEVERE ACCIDENT ANALYSIS PROGRAM REPORT
(October 1989)

Program Manager: R. P. Taleyarkhan
Principal Investigators: C. R. Hyman
R. P. Taleyarkhan

Several areas in the ANS Severe Accident Analysis Program were addressed during October 1989. The results of these investigations and efforts are highlighted below.

Characterization of Melt Progression and Fission Product Release Issues for the ANS

(R. P. Taleyarkhan)

During October efforts continued to characterize severe accident issues in relation to core melting, relocation, and fission product release for the ANS. Various aspects of these phenomena are being investigated. It should be noted that these issues have widespread implications on ANS safety and design. Important areas such as determination of the source term, basemat penetration, generation of steam explosions, formulation of accident management/mitigation strategies, and the magnitude and timing of radioactivity release to the environment are directly impacted. Due to the scoping nature of these evaluations, conservative approaches have often been adopted. Conclusions derived from such analyses are thus not to be considered in a definitive sense. The results of these investigations will be documented as an issue paper in a format similar to that developed for the issue paper, "Steam Explosion Related Safety Concerns for the ANS."

Scoping evaluations initiated during August for ANS conditions were completed. The mathematical modeling approach developed for evaluation of rate-dependent volatile fission product release from UAl fuels was reviewed by R. Lorenz.

ANS SEVERE ACCIDENT ANALYSIS PROGRAM REPORT
(October 1989)

His comments have been implemented in the modeling approach. Additional information recently obtained specifically on fission product release from U_3Si_2/Al fuels will also be incorporated. Other efforts during October concentrated on documentation aspects, with a draft report slated for completion early in November.

Characterization of Core Debris / Concrete Interactions for the ANS (C. R. Hyman)

During October work continued on the evaluation of the potential impact of molten core/concrete interactions (MCCI) for hypothesized severe accidents for the ANS. This study has a direct bearing on important severe accident areas such as basemat penetration, release of noncondensable and combustible gases, deflagration and/or detonation of gases, and containment overpressurization. The results of this study are currently being documented.

Reports, Papers, and Publications

A technical paper describing the mathematical models for rate dependent fission product release from $U-Al$ fuels is under preparation for presentation at the next American Nuclear Society conference.

The completed report on the ANS steam explosion issue paper is currently going through the final editing stage by the ORNL editorial staff. The ANS Project Office will publish the edited report as an ORNL/TM report.

Meetings & Trips

R. P. Taleyarkhan presented a paper entitled "Large Break Loss-Of-Coolant-

ANS SEVERE ACCIDENT ANALYSIS PROGRAM REPORT
(October 1989)

Accident Analysis of the High Flux Isotope Reactor," at the International Atomic Energy Agency Meeting on Research Reactor Safety, Design, and Operation. The meeting was held at the Chalk River Nuclear Laboratory, Canada, from 23 to 27, October 1989.

Internal Correspondence

MARTIN MARIETTA ENERGY SYSTEMS, INC.

November 8, 1989

J. A. Johnson

October Monthly Progress Report for ANS Project Quality Assurance Activities**WBS-1.2.5.1 Program Development**

The ANS Quality Assurance Plan has been revised to address comments from DOE-ORO and to reflect recent ORNL organizational changes. The QA Plan revisions were mainly to include additional detail on the control elements and do not require any substantial changes in the ANS QA Program.

WBS-1.2.5.2 Program Monitoring

The response to ANS Surveillance Report ANS-SURV-89-001 dated September 25, 1989, was reviewed and found to be acceptable. This surveillance was closed by letter from L. M. Jordan to C. D. West dated October 9, 1989.

A Key Activity Review of the PS-2 Reference Core Development has been initiated. The review team consists of technical and quality experts who will review major assumptions, decisions, calculations and available documentation to confirm the conclusions reached by the PS-2 Committee. Any identified process deficiencies will be corrected in the ongoing Conceptual Core Design effort.

WBS-1.2.5.3 Project Support

A presentation was made to E. J. Bjoro of DOE-EH on the status of implementing the ANS QA Program on October 12, 1989. His trip report dated October 23, 1989, indicated that the "Lessons learned" in the RRD were being applied directly to the ANS Project. He further observed that the controls and methodologies of the quality program were being phased in at the appropriate project phases and that the recognition by line management of the quality responsibility was obvious.

Training was conducted for 25 ANS Managers and Task Leaders on the recently implemented ANS Commitment and Action Tracking System. Training was conducted during scheduled bi-weekly meetings and covered using the system and the responsibilities of participating individuals.

J. A. Johnson
Page 2
November 8, 1989



M. L. Gildner, FEDC, MS-8218 (6-5476)



L. M. Jordan, 9201-3, MS-8063 (6-3711)

cc: R. E. Fenstermaker
P. E. Melroy
C. D. West

Internal Correspondence

MARTIN MARIETTA ENERGY SYSTEMS, INC.

November 6, 1989

J. A. Johnson

October Monthly Progress Report for Design Activities on the Advanced Neutron SourceGeneral

Some budget uncertainties remain, as the impacts of Gramm-Rudman have yet to be defined, and the Laboratory does not yet have a complete financial plan. Questions on overhead rates at ORNL also complicate the allocation of manhours for a given amount. However, work orders have been revised based on a FY-90 funding level of \$9 million, and assumed Laboratory and Engineering manhour rates.

Two papers were presented at the International Atomic Energy Agency Symposium on Research Reactor Safety, Operations and Modifications, at Chalk River, Ontario. The paper "Advanced Neutron Source - Designing to Meet the Needs of the User Community", by F. J. Peretz, was presented on October 26, and the paper "The Advanced Neutron Source Safety Approach and Plans", by R. M. Harrington, was also presented by Peretz on October 24. The Symposium was well attended by representatives from research institutes throughout the world. Particularly useful contacts were made with personnel from the Institute Laue-Langevin, Grenoble, France; the PIK research reactor project, Leningrad, USSR; and the Maple-X and Advanced Maple reactor projects at Chalk River and Whiteshell, Canada. Extended synopses of all papers and preprints of selected talks are available from F. J. Peretz; a full publication of all papers will be available soon.

Final planning for the trip to the Institute Laue-Langevin, the ORPHEE reactor in Saclay, and the Julich reactor is now underway. This trip will take place from November 7 through 16.

WBS 1.2, Project Support

Contingency plans are being generated in the event that the three year design-only line item is not supported in FY-91. Funding profiles are being developed for operating funds in FY-91, and a design-only line item following that year. Various profiles have been developed, ranging from providing an equivalent amount of operating funds in FY-91 as would be provided by the line item, to various reduced funding profiles with schedule slippage. Direction from ORNL management is to generate contingency plans, while continuing to base the main project plan on pursuing support of the design-only line item for FY-91.

No progress has been made on identifying a selection official for the architect-engineer contract, because of the transition from Energy Research to Nuclear Energy, and the uncertainties of the design-only line item.

WBS 1.3, Reactor Systems

A review of the mechanical concept for the reflector tank has begun, with an initial focus on the structural integrity of the tank itself. In particular, attention is being given to whether a thick flat head is the best approach, or whether an ellipsoidal dished head is preferable. The flat head was initially selected to simplify penetrations into the top of the reflector. Although penetrations in a dished head may be slightly more complicated, a dished head may be significantly thinner, and thus lighter and easier to cool. Loads for the reflector tank assembly, including the load created by the primary system pressure with a slip-joint attachment for the core pressure boundary tube, are being reviewed to estimate deflections in the tank structure. Attention is also being given to cooling of the beam tubes penetrating the side of the vessel, and to the support structure for the vessel, which also serves as the support for the entire reactor assembly. These issues are discussed more fully in Charles Queen's report.

A final draft of the design task RS-2 report, documenting the selection approach for the control drive configuration, has been circulated for comments. This report presents a flow chart showing options considered, and the selected options, and then provides text to more fully explain the rationale for selecting the approach taken. This report will be issued after comments are received; it is expected that the report will be reviewed and revised periodically as the project evolves.

WBS 1.4, Experiment Systems

Twenty interface drawings have been prepared to define the location and space requirements for the irradiation facilities in the reflector tank. These facilities include two slant irradiation facilities, which correspond to the RB* positions in the HFIR, four hydraulic rabbit tubes for transplutonium production in a high-epithermal flux and for irradiation of various targets near the peak thermal flux region, three pneumatic rabbit tubes further out in the reflector tank for activation analysis, and seven isotopes production facilities at the outer edge of the reflector tank. Most of these facilities are shown on the attached figure. The drawing package is now being prepared for comment issue under transmittal. Attention on the irradiation facilities will now shift to the impact on the flux profiles in the reflector tank, to establish whether this array of facilities is acceptable. Design work will shift to definition of hot cell facilities and unloading stations needed to support the irradiation facilities.

WBS 1.5 and WBS 1.6, Balance of Plant

A major workshop on the requirements for site and facility development was held by the architectural team on October 18 and 19. This workshop culminated an effort to have all project participants and interfacing ORNL support functions establish their needs. Representatives from each experiment team, each design discipline, and the major ORNL support functions made presentations at the workshop. The architectural team is now correlating the input from the workshop, and will begin to develop the requirements for reviewing the design of the site and facilities.

Considerable progress has been made in establishing the basis for development of the revised reactor cooling system. A series of meetings have been held to define the fundamental options for flowsheets, physical arrangements, heat sinks, approaches to pressurization, etc. which can be considered in developing a new design. Studies have also been initiated to establish reliability and availability associated with various numbers of parallel loops. At the same time, the validation of

analytical tools for evaluation of cooling circuits is nearly complete, and lists of transient initiators and corresponding success criteria have been developed. Attention is now shifting to developing a few candidate circuit design concepts for more detailed evaluation. Once some preliminary analyses have been completed, a major workshop will be held to discuss the possible options, and to define the characteristics of the cooling system to be used as the basis for conceptual design.

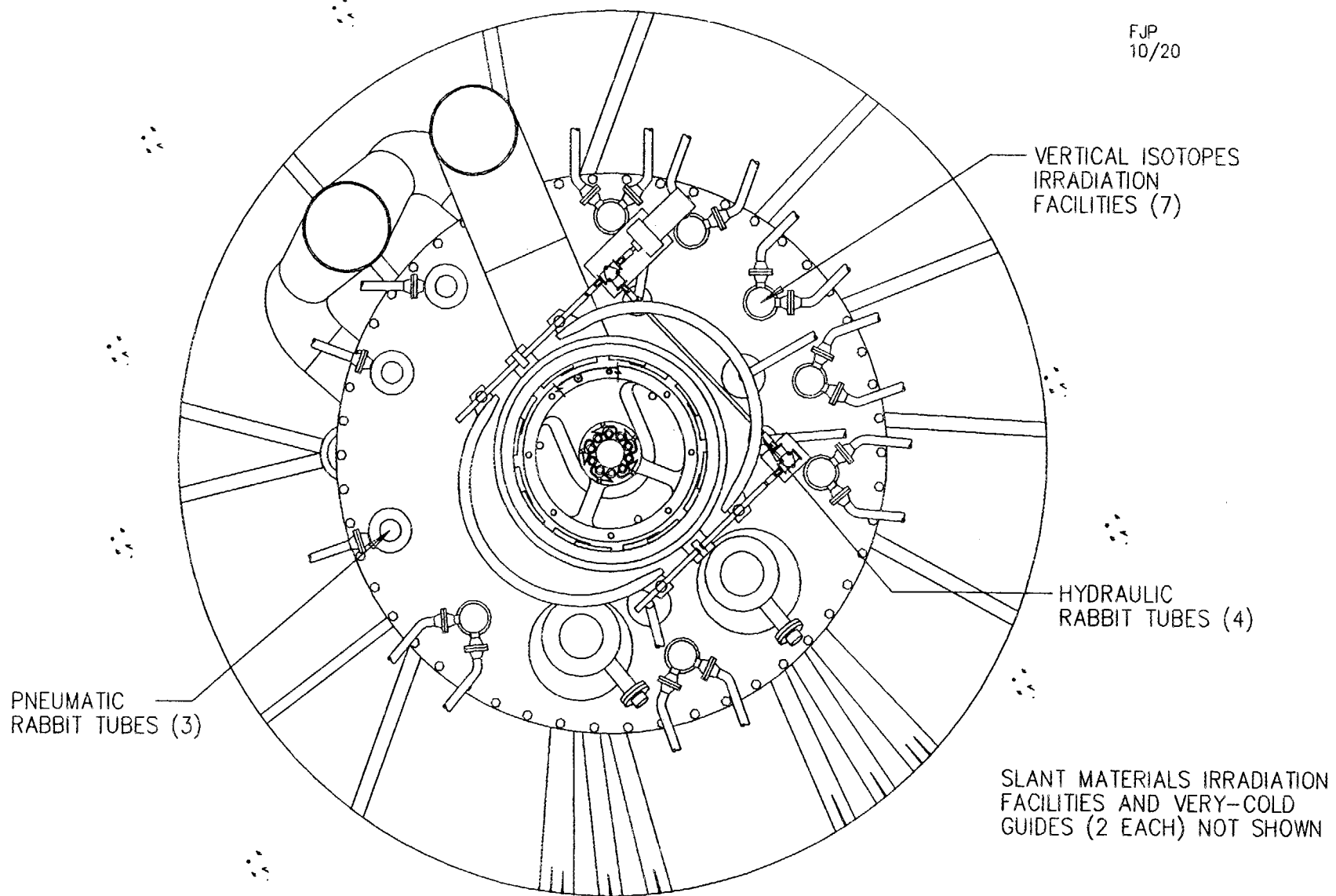
A meeting covering the containment design and operation at the Institute Laue-Langevin reactor, and the security role of the containment structure, was held on November 2. This meeting is a continuation of the BOP-2 task on containment design. Progress on this task has been slow as a result of manpower constraints, but will pick up at the end of the calendar year.



F. J. Peretz, FEDC (6-5516)

cc: R. O. Barnett
R. M. Beckers
H. C. Beeson
R. A. Brown
D. D. Cannon
R. M. Canon
W. W. Chance
R. O. Daugherty
L. J. Degenhardt
J. R. Dixon
C. P. Frew
R. W. Glass
C. L. Hahs
R. L. Johnson
G. F. Kalb
B. S. Maxon
C. S. Meadors
T. J. McManamy
G. R. McNutt
R. Miller
H. R. Payne
W. H. Power
C. C. Queen
W. R. Reed
T. L. Ryan
J. P. Schubert
J. L. Snyder
P. B. Thompson
B. D. Warnick

FJP
10/20



Internal Correspondence

October 3, 1989

MARTIN MARIETTA ENERGY SYSTEMS, INC.
TE-89-42J.A. Johnson
F.J. PeretzANS Reactor Systems Design Monthly Report

Work has continued on special study task RS 1a and RS 1b identified to focus on the core pressure boundary tube (CPBT) seals and to explore alternate approaches to remote refueling. Four basic approaches were identified for sealing the CPBT and a number of possible configurations were generated for each approach. The different approaches are: a) flange seals at both the top and the bottom of the CPBT, b) a flange seal at the top of the CPBT and a radial seal at the bottom of the CPBT (which will permit thermal expansion), c) a flange seal at the top and a labyrinth seal at the bottom utilizing the flow thru the labyrinth seal to cool the components in the reflector vessel d) the CPBT would become an integral part of the fuel element assembly and would employ one of the other three sealing arrangements. A preliminary design requirements document has been generated and transmitted for comment. The different seal configurations were presented in task team status meetings. In the future there will be a workshop with independent participants to review the different approaches and, hopefully, to generate other configurations. The requirements document will then be used to evaluate the different configurations in an effort to establish a baseline configuration.

Work has continued on evaluating the different sealing options. The leakage through labyrinth seals for different number of lands was calculated using the following relationship:

$$\Delta P = \frac{1}{2} \rho V^2 \cdot \left[1 + \frac{n \cdot f \cdot L}{2 \cdot b} + .5 + (n - 1) \right]$$

Where :

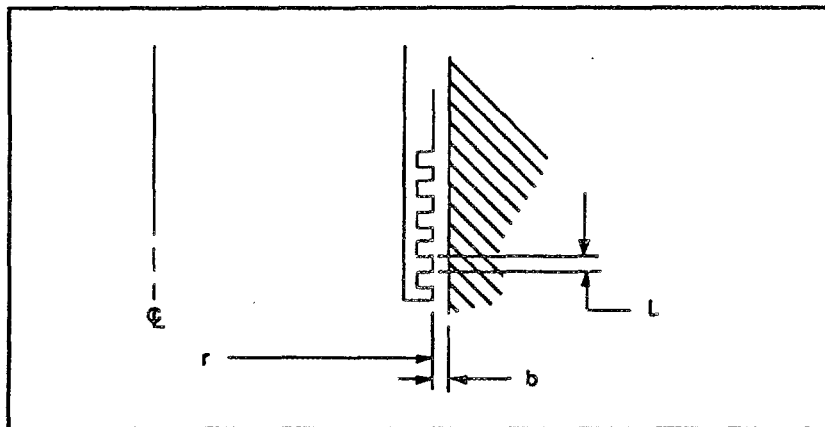
 ΔP = pressure drop, $\frac{N}{m^2}$ ρ = density of fluid, $\frac{kg}{m^3}$ V = velocity, $\frac{m}{s}$ n = number of lands b = radial clearance, m L = width of land, m f = friction factor, $\approx .316 Re^{-.25}$

$$Re = \frac{\rho V D_H}{\mu}$$

$$D_H = 2(r + b) - 2r$$

$$D_H = 2b$$

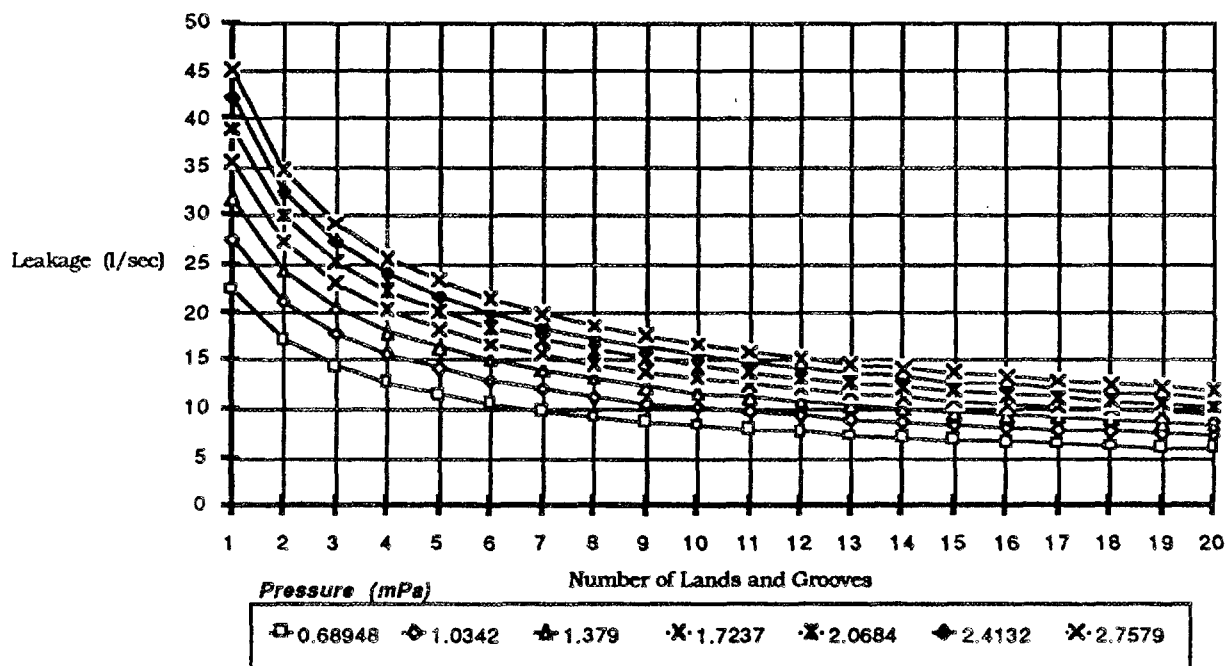
 μ = kinematic viscosity, $\frac{Ns}{m^2}$



Schematic of labyrinth seal arrangement

The results of looking at a number of different pressure drops and numbers of lands are shown in the graph below.

Characteristics of Labrynth Seals



Before we can really assess whether this is a viable option a number of questions concerning safety, ASME code acceptability, etc. will have to be addressed.

The second task RS1b has generated several approaches to refueling. One approach is a completely self-contained refueling machine (see Fig. 1 attached); and the other is an arrangement that combines long handled tools and manipulators working through a heavy water stack (see Fig. 2 attached). Both of these approaches are being developed to a point that the advantages and disadvantages of each can be better understood.

October 3, 1989
J.A. Johnson
F.J. Peretz

A package of interface drawings showing component placement and size have been transmitted for comment. These drawings will be used to establish space availability in the areas immediately in and around the reflector vessel.

No significant changes have been made in the control rod drives (inner and outer) but additional work has been done to refine the conceptual design. A method to operate the scram indicator switch for both inner and outer rods has been devised; upper stabilizing guides for the inner rods have been added to the conceptual design drawings and the high pressure bellows will be replaced with pipe and a low pressure bellows.

Fission and Ionization Chambers will be located outside the reflector tank and near the core midplane. A method of changing their radial position with respect to the core, using ball screw mechanical drives, has been shown on the conceptual design drawings; but changes will be made to provide a more compact drive unit. These can be either manual or motor driven from a remote location.



C.C. Queen Jr., 9201-3, MS 8068

cc C.W. Alexander, 7920, MS 6384
J. L. Anderson, 3500, MS 6008
B. Damiano, 3500, MS 6010
J. R. Dixon, 1000, MS 6332
W. R. Gambill, 1000, MS 6363
S. R. Greene, 9104-1, MS8057
R. M. Harrington, FEDC, MS 8218
T. J. McManamy, 9204-1, MS 8055
J. March-Leuba, 3500, MS 6010
B. S. Maxon, 9105, MS 8040
B. H. Montgomery, FEDC, MS 8218
L. C. Oakes, 3500, MS 6009
H. R. Payne, 9201-3, MS 8068
H. Reutler, FEDC, MS 8218
T. L. Ryan, 9204-1, MS8055
D. L. Selby, FEDC, MS 8218
R. P. Taleyarkhan, 9104-1, MS 8057
P. B. Thompson, 9105, MS 8040
K. R. Thoms, 9108, MS 8087
C. D. West, FEDC, MS 8218
G. T. Yahr, 9204-1, MS 8051
R. B. Zimmerman, 9201-3, MS 8068

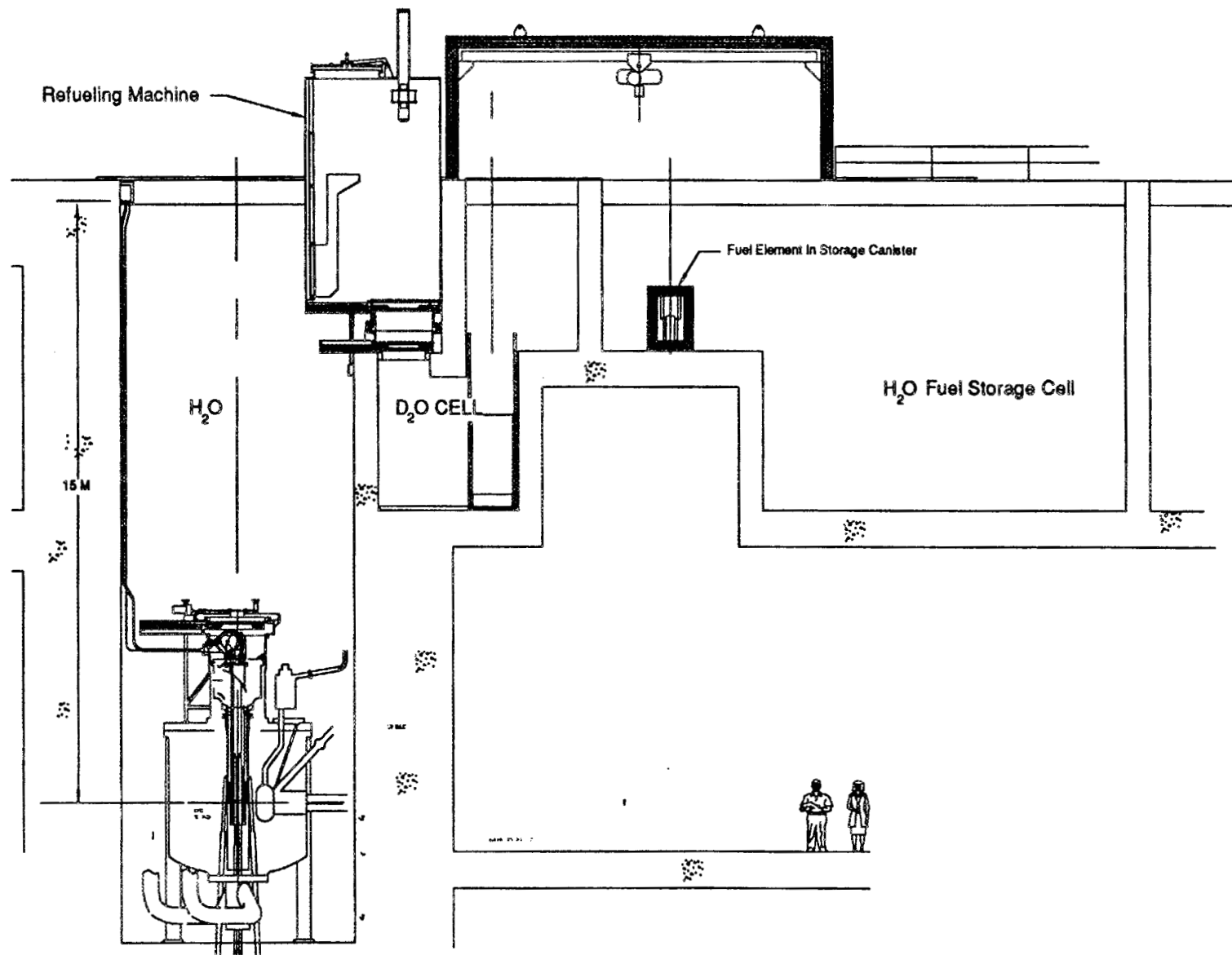


Fig. 1 Refueling machine shown Docked with Transfer Cell

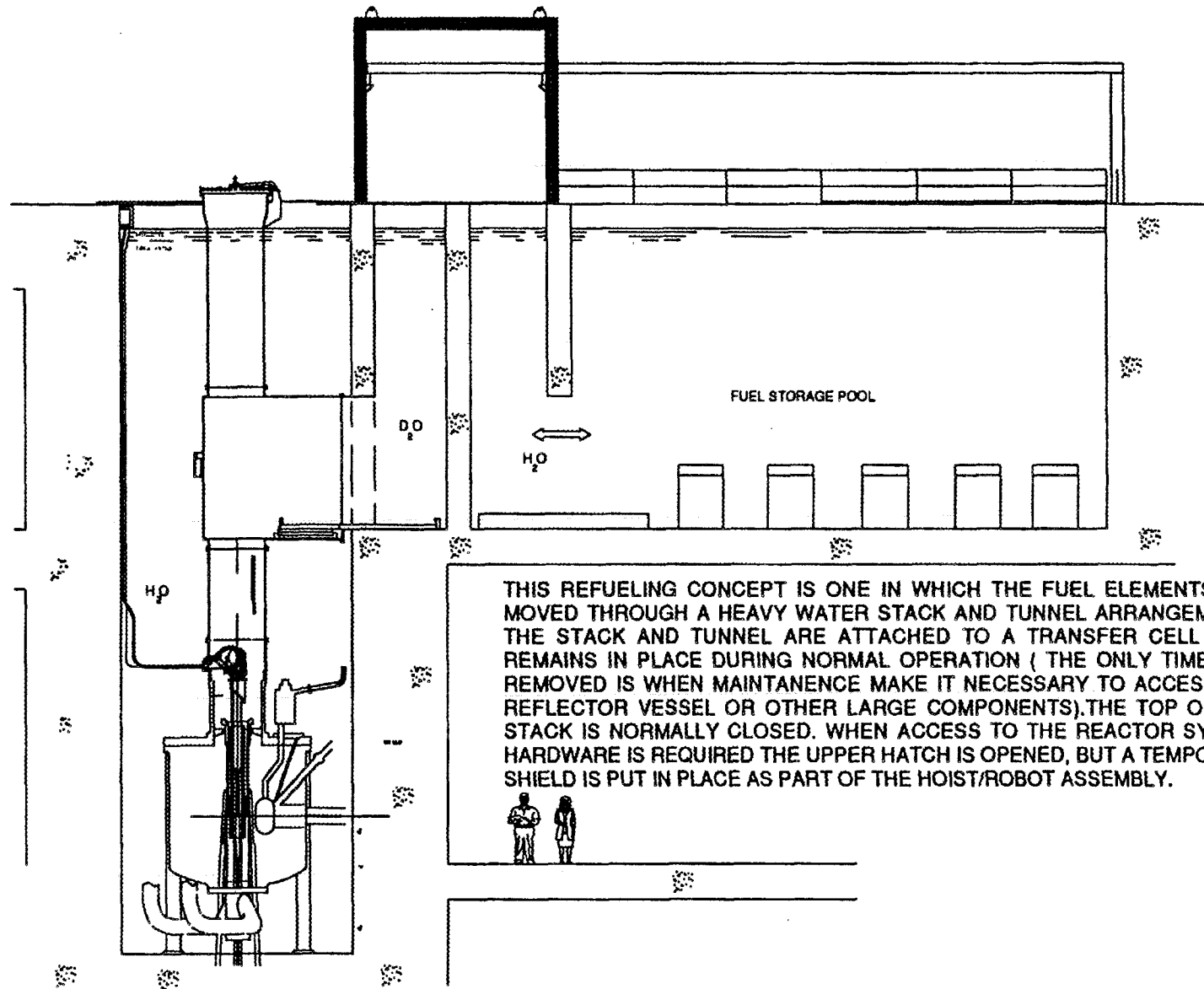


Fig. 2 Refueling Tunnel Concept

Internal Correspondence

MARTIN MARIETTA ENERGY SYSTEMS, INC.

November 17, 1989

J. A. Johnson

Advanced Neutron Source Monthly Progress Report for October 1989, "Site and Facility Planning - BOP-3"

The Balance of Plant Task 3, "Site and Facility Planning" was formed in June 1989.

The purpose of this task is to 1) provide an opportunity for dialogue between all the disciplines involved in the ANS design; 2) identify and review users (scientists) management, operation and maintenance criteria; 3) resolve conflicts; and 4) establish a framework for developing conceptual design.

The planning and design of the ANS facility involves a large number of experts from both the design end (Engineering, for example) and the client (users, operators, and management). The issues considered by each of the disciplines are numerous and have strong implications on decisions made by other disciplines which are likely to create conflicts or strongly affect the design process. These issues have to do with different systems to different system interactions, as well as systems-to-people, people-to-people, systems-to-experiments, etc., and ANS and its relationship to ORNL support systems.

The site and facility effort will be carried out through both the conceptual and developmental design stage and will:

- collect criteria from the different disciplines, review those criteria, and analyze their impact on the general building concept;
- identify conflicts among the criteria and/or questions concerning them;
- create a dialogue among all disciplines that will result in resolution of some of those conflicts;
- translate the information into a matrix of relationships and into space requirements;
- prepare criteria for the A-E.

A major milestone of conceptual design criteria identification was culminated in the ANS Site and Facility Planning Workshop, which was held in the Fusion Engineering Design Center on October 18-19, 1989. Over 30 presentations covering ANS planning issues were presented and grouped into three major categories.

J. A. Johnson
Page 2
November 17, 1989

The Users/Clients Session was moderated by J. B. Hayter and included issues such as operation and maintenance of the future facilities and aspects that could contribute to a high degree of efficiency through the design process. This included discussions on delivery, service, climate control, cranes, monorails, elevations, noise levels, air pads, food, lodging and transportation. Pool facilities, reactor, and user requirements were presented by Chemistry, Physics, Materials Analysis, Materials Irradiation, Hot Cells, Technical Support, and Experiment Systems personnel. Types of spaces required, including but not limited to offices (for permanent staff and visitors), library, auditorium, document storage, mechanical-cryogenic and electronic shops, sample prep labs, chem and biochem labs, clean storage at and away from instruments, active sample storage and monitoring, experiment staging areas at instruments, and instruments were also discussed. ALARA was mentioned as a primary consideration along with the need for user-friendly access. Safety issues including proper training, access control, alarms, and automation will no doubt affect the design of the ANS.

The General Support and Site Issues Session was moderated by W. W. Chance and focused on Industrial Hygiene and Safety monitoring and its integration with ORNL's overall plan. Security, fire protection, and emergency preparedness discussions were both general and site specific. Another issue discussed at this session was laboratory commitment to upgrade its support facilities in order to be able to accommodate the increasing load once ANS is in operation - for example, maintenance shops and a user liaison office.

The Systems Issues Session, chaired by F. J. Peretz, included presentations by engineers who design the piping, electrical, instruments and controls, process, reactor and cooling systems. Like all the other sessions, it provided a needed opportunity for information exchange, a dialogue that for many of us led to a better understanding of the scope of the designs as well as identifying those areas needing close cooperation between the different disciplines working on ANS.

Summaries of each of these sessions were prepared for presentation in a joint meeting between all categories. Those presentations were followed by open discussions.

Many technical issues were discussed, but some technical choices require policy decisions, and they include:

- Maintenance shops - is the lab going to support ANS by upgrading the existing facility?
- Guide hall - is it going to be located as laboratory or containment?

J. A. Johnson
Page 3
November 17, 1989

- On-site lodging and user-friendly access
- Size of auditorium
- Road access
- Helium recovery
- Toilets inside the primary containment
- Biochemical facilities depend on different classes of experiments

Approximately 65 people attended the meeting, with each receiving a handout containing highlights of the presentations. Some of the summaries were received by our office too late to be included in the handout, and they will be mailed later.

We are now in the process of sorting out the material and hope to include it in the first draft of a conceptual design criteria document within the next few months.

H. B. Shapira
H. B. Shapira, FEDC, MS-8218 (4-2042)

HBS:kfr

cc: C. D. West

Internal Distribution

1. C. W. Alexander
2. R. G. Alsmiller
3. J. L. Anderson
4. B. R. Appleton
5. Y. Y. Azmy
6. J. R. Buchanan
7. N. C. J. Chen
8. G. L. Copeland
9. F. C. Difilippo
10. J. R. Dixon
11. H. L. Dodds
12. F. F. Dyer
13. W. W. Engle
14. R. E. Fenstermaker
15. W. R. Gambill
16. R. K. Genung
17. M. L. Gildner
18. H. A. Glovier
19. R. M. Harrington
20. J. B. Hayter
21. D. T. Ingersoll
22. J. A. Johnson
23. L. M. Jordan
24. R. A. Lillie
25. B. S. Maxon
26. R. Miller
27. B. H. Montgomery
28. R. M. Moon
29. F. R. Mynatt
30. R. K. Nanstad
31. L. C. Oakes
32. R. E. Pawel
33. F. J. Peretz
34. R. T. Primm, III
35. C. C. Queen
36. J. S. Rayside
37. H. Reutler
38. A. E. Ruggles
39. T. L. Ryan
40. D. L. Selby
41. H. B. Shapira
42. W. D. Shults
43. R. P. Taleyarkhan
44. P. B. Thompson
45. K. R. Thoms
46. D. B. Trauger
47. R. E. Uhrig
48. C. D. West
49. M. K. Wilkinson
50. G. T. Yahr
51. G. L. Yoder
52. A. Zucker
53. Laboratory Records (RC)

External Distribution

54. C. W. Burger, Energy Programs, U.S. Department of Energy, Oak Ridge Operations, P. O. Box 2001, Oak Ridge, TN 37831-2001.
55. R. F. Domagala, RERTR Program, Argonne National Laboratory, 9700 South Cass Avenue, Argonne, IL 60439.
56. B. Chalmers Frazer, Materials Sciences Division, U.S. Department of Energy, Germantown, ER-132, Washington, D.C. 20545.
57. Ralph Fullwood, Brookhaven National Laboratory, Upton, NY 11973.
58. J. A. Lake, Manager, Nuclear Engineering and Reactor Design, Idaho National Engineering Laboratory, P. O. Box 1625, Idaho Falls, ID 83415.
59. John Marks, Research and Test Reactor Fuel Elements, Babcock and Wilcox Co., P. O. Box 785, Lynchburg, VA 24505.

60. Robert J. Neuhold, U.S. Department of Energy, Germantown, NE-472, Washington, DC 20545.
61. John M. Ryskamp, Idaho National Engineering Laboratory, P. O. Box 1625, Idaho Falls, ID 83415.
62. J. L. Snelgrove, Coordinator, Engineering Applications, RERTR Program, Argonne National Laboratory, 9700 South Cass Avenue, Argonne, IL 60439.
63. Iran Thomas, Director, Materials Science Division, Office of Energy Research, U.S. Department of Energy, Germantown, ER-13, Washington, D.C. 20545.
64. R. P. Wadkins, Idaho National Engineering Laboratory, P. O. Box 1625, Idaho Falls, ID 84515.
65. D. K. Wilfert, Energy Programs, U.S. Department of Energy, Oak Ridge Operations, P. O. Box 2001, Oak Ridge, TN 37831.
66. R. J. Willard, U.S. Department of Energy, Oak Ridge Operations, P. O. Box 2001, Oak Ridge, TN 37831.